



Aalborg Universitet

AALBORG UNIVERSITY  
DENMARK

## Model-Based Control of a Ballast-Stabilized Floating Wind Turbine Exposed to Wind and Waves

Christiansen, Søren

*Publication date:*  
2013

*Document Version*  
Early version, also known as pre-print

[Link to publication from Aalborg University](#)

*Citation for published version (APA):*  
Christiansen, S. (2013). *Model-Based Control of a Ballast-Stabilized Floating Wind Turbine Exposed to Wind and Waves*.

### General rights

Copyright and moral rights for the publications made accessible in the public portal are retained by the authors and/or other copyright owners and it is a condition of accessing publications that users recognise and abide by the legal requirements associated with these rights.

- Users may download and print one copy of any publication from the public portal for the purpose of private study or research.
- You may not further distribute the material or use it for any profit-making activity or commercial gain
- You may freely distribute the URL identifying the publication in the public portal -

### Take down policy

If you believe that this document breaches copyright please contact us at [vbn@aub.aau.dk](mailto:vbn@aub.aau.dk) providing details, and we will remove access to the work immediately and investigate your claim.

Søren Christiansen

*Model-Based Control of a Ballast-Stabilized  
Floating Wind Turbine Exposed to Wind and  
Waves*



**AALBORG UNIVERSITY**  
DENMARK

PhD thesis:

Model-Based Control of a Ballast-Stabilized Floating Wind Turbine  
Exposed to Wind and Waves

PhD student:

Søren Christiansen

Supervisor:

Professor Thomas Bak  
Associate professor Torben Knudsen

List of publications:

- Paper A: S. Christiansen, T. Knudsen, & T. Bak, Optimal Control of a Ballast-Stabilized Floating Wind Turbine, IEEE Multi-Conference on Systems and Control, 2011
- Paper B: S. Christiansen, T. Bak, & T. Knudsen, Damping Wind and Wave Loads on a Floating Wind Turbine, IEEE Transactions on Control Systems Technology – submitted, 2012
- Paper C: S. Christiansen, T. Bak, & T. Knudsen, Minimum Thrust Load Control for Floating Wind Turbine, IEEE Multi-Conference on Systems and Control, 2012
- Paper D: S. Christiansen, T. Knudsen, & T. Bak, Extended On-shore Control of a Floating Wind Turbine with Wave Disturbance Reduction, The Science of Making Torque from Wind, 2012
- Paper E: S. Christiansen, S. M. Tabatabaeipour, T. Bak & T. Knudsen, Wave Disturbance Reduction of a Floating Wind Turbine Using a Reference Model-based Predictive Control, American Control Conference – submitted, 2013

January 2013

Copyright 2012–2013 © Søren Christiansen

This thesis has been submitted for assessment in partial fulfillment of the PhD degree. The thesis is based on the submitted or published scientific papers which are listed above. Parts of the papers are used directly or indirectly in the extended summary of the thesis. As part of the assessment, co-author statements have been made available to the assessment committee and are also available at the Faculty. The thesis is not in its present form acceptable for open publication but only in limited and closed circulation as copyright may not be ensured.

# | Contents

<b>Contents</b>	<b>III</b>
<b>Preface</b>	<b>V</b>
<b>Abstract</b>	<b>VII</b>
<b>Synopsis</b>	<b>IX</b>
<b>1 Introduction</b>	<b>1</b>
1.1 Motivation . . . . .	1
1.2 State-of-the-Art and Background . . . . .	5
1.3 Outline of the Thesis . . . . .	11
<b>2 Methodology</b>	<b>13</b>
2.1 Reduced Order Model of a Floating Wind Turbine . . . . .	13
2.2 Fatigue and Damage Equivalent Loads . . . . .	19
2.3 FAST and Simulation . . . . .	22
<b>3 Summary of Contributions</b>	<b>27</b>
3.1 Linear Time-Varying Control Model . . . . .	28
3.2 Gain-Scheduled LQR control . . . . .	28
3.3 Extended Onshore Control . . . . .	29
3.4 Reference Model-based Predictive Control . . . . .	29
3.5 Paper Contributions . . . . .	30
<b>4 Conclusion</b>	<b>33</b>
4.1 Future Work . . . . .	34
<b>References</b>	<b>37</b>
<b>Contributions</b>	<b>43</b>
<b>Paper A: Optimal Control of a Ballast-Stabilized Floating Wind Turbine</b>	<b>45</b>
1 Introduction . . . . .	47
2 Methods . . . . .	49
3 Experimental Setup . . . . .	52
4 Results . . . . .	54

# CONTENTS

---

5	Discussion . . . . .	56
6	Conclusion . . . . .	59
	References . . . . .	59
<b>Paper B: Damping Wind and Wave Loads on a Floating Wind Turbine</b>		<b>61</b>
1	Introduction . . . . .	63
2	Methods . . . . .	64
3	Environmental Setup . . . . .	73
4	Results . . . . .	74
5	Discussion . . . . .	74
6	Conclusion . . . . .	78
7	Acknowledgment . . . . .	79
	References . . . . .	79
<b>Paper C: Minimum Thrust Load Control for Floating Wind Turbine</b>		<b>81</b>
1	Introduction . . . . .	83
2	Methods . . . . .	84
3	Experimental Setup . . . . .	90
4	Results . . . . .	91
5	Discussion . . . . .	92
6	Conclusion . . . . .	95
7	Acknowledgment . . . . .	95
	References . . . . .	95
<b>Paper D: Extended Onshore Control of a Floating Wind Turbine with Wave Disturbance Reduction</b>		<b>97</b>
1	Introduction . . . . .	99
2	Methods . . . . .	100
3	Experimental Setup . . . . .	104
4	Results . . . . .	105
5	Discussion . . . . .	107
6	Conclusion . . . . .	108
7	Acknowledgment . . . . .	109
	References . . . . .	109
<b>Paper E: Wave Disturbance Reduction of a Floating Wind Turbine Using a Reference Model-based Predictive Control</b>		<b>111</b>
1	Introduction . . . . .	113
2	Methods . . . . .	115
3	Experimental Setup . . . . .	119
4	Results . . . . .	120
5	Discussion . . . . .	121
6	Conclusion . . . . .	123
7	Acknowledgment . . . . .	123
	References . . . . .	123

# | Preface and Acknowledgments

This PhD thesis is submitted as a collection of papers in partial fulfillment of the requirements for the degree of Doctor of Philosophy in Automation and Control at the Department of Electronic Systems, Aalborg University, Denmark. This work has been carried out from December 2009 to January 2013 under the supervision of Professor Thomas Bak and Associate Professor Torben Knudsen.

I would like to thank my supervisors for their support, engagement, and helpful discussions throughout the project. I am deeply thankful to them.

I would also like to thank the Norwegian Centre for Offshore Wind Energy (NORCOWE) for financial support under grant 193821/S60 from Research Council of Norway (RCN). Another thanks goes to the colleagues and partner at NORCOWE who made this work possible.

At Automation and Control, I would like to thank my colleagues for interesting discussions and for contributing to a comfortable and social work environment.

I would like to thank Doctor Karl A. Stol from the Department of Mechanical Engineering, who kindly hosted my stay abroad at Auckland University, New Zealand in 2010. During my stay, Karl and his wife made my family and I feel welcome with their warm hospitality.

I would also like to thank my family for their understanding and encouragement, and especially my wife and children for their love and presence.



# | Abstract

The wind turbine is a commercial product which is competing against other sources of energy, such as coal and gas. This competition drives a constant development to reduce costs and improve efficiency in order to reduce the total cost of the energy. Its reliability has increased since the first wind turbines were installed, which has led to the deployment of wind turbines in remoter and harsher environments. Experiences from the oil and gas industry in offshore installations and foundations has allowed wind power installations offshore where the wind is stronger. The average offshore wind speed is typically 20% greater than onshore. The turbulence is also lower, which potentially prolongs the turbine's lifetime from 25 years to 30 years. Furthermore, issues related to noise and visual impact are reduced.

Wind power installations based on, e.g., monopile foundations are economically only feasible for shallow water depths below 30 meters. Other concepts of foundations, such as the jacket and tripod, have been designed for water depths in the range of 25–50 meters. The latest offshore development is the floating wind turbine, for water depths beyond 50 meters. It is not yet clear if the additional cost necessitated by a floating structure can be offset by its benefits, such as access to deeper waters and the possibility of assembly in protected waters before towing to and being moored at the desired location. A floating wind turbine is subject to not only aerodynamics and wind induced loads, but also to hydrodynamics and wave induced loads. In contrast to a bottom fixed wind turbine, the floating structure, the hydrodynamics and the loads change the dynamic behaviour of a floating wind turbine. The wave motion causes the platform to pitch forward, which results in an increase of the relative wind speed, and with a conventional pitch control system the blades will pitch to feather and decrease the rotor thrust. The result is an exacerbation of the platform's motion. In control terms, conventional pitch control introduces a negative damping term resulting in larger motion and loads.

This work addresses the control of a floating spar buoy wind turbine, and focuses on the impact of the additional platform dynamics. A time varying control model is presented based on the wind speed and wave frequency. Estimates of the wind speed and wave frequency are used as scheduling variables in a gain scheduled linear quadratic controller to improve the electrical power production while reducing fatigue. The wind speed is estimated using an extended Kalman filter and the wave frequency, by an auto-regressive filter.

To address the problem of negative damped fore-aft tower motion, additional control loops are suggested which stabilize the response of the onshore controller and reduce the impact of the wave induced loads. This research is then extended to model predictive control, to further address wave disturbances. A dynamic model of the undisturbed closed-loop system is used as a reference for the disturbed system within a framework



## CONTENTS

---

based on model predictive control.

In the context of control engineering, the dynamics and disturbances of a floating wind turbine have been identified and modelled. The objectives of maximizing the production of electrical power and minimizing fatigue have been reached by using advanced methods of estimation and control.

# | Synopsis

Vindmøllen er et kommercielt produkt, der konkurrerer med andre energikilder, som kul og gas. Denne konkurrence driver en konstant udvikling mod at reducere omkostningerne og forbedre effektiviteten med henblik på at reducere de samlede omkostninger til energi. Pålideligheden er steget siden de første møller blev installeret, hvilket har ført til opførelse af vindmøller i mere fjerntliggende og barske miljøer. Erfaringer fra olie og gas industrien i offshoreanlæg og fundamenter, har gjort det muligt at installere vindmøller offshore, hvor vinden er stærkere. Den gennemsnitlige offshore vindhastighed er typisk 20 % større end onshore. Turbulensen er også lavere, hvilket potentielt set forlænger vindmøllelevetiden fra 25 år til 30 år. Desuden er gener i forbindelse med støj og visuel indtryk reduceret.

Vindmøller baseret på f.eks. monopælfundamenter kan økonomisk kun lade sig gøre på lave vanddybder under 30 meter. Andre koncepter af fundamenter, såsom jackets og tripods er designet til vanddybder i intervallet fra 25 til 50 meter. Den seneste offshore udvikling er den flydende vindmølle til vanddybder over 50 meter. Det er endnu ikke klart, om de ekstra omkostninger nødvendiggjort af en flydende struktur kan opvejes af fordelene, såsom adgang til dybere vande, og muligheden for montage i beskyttede farvande inden bugsering til og forøgning ved det ønskede sted. En flydende vindmølle er ikke kun påvirket af aerodynamik og vind inducerede belastninger, men den er også genstand for hydrodynamik og bølge inducerede belastninger. I modsætning til den bundfæstet vindmølle, ændrer den flydende struktur, hydrodynamikken og belastningerne den dynamiske opførelse af en flydende vindmølle. Bølgebevægelsen får platformen til at pitch fremad, hvilket resulterer i en forøgelse af den relative vindhastighed, og med et konventionel pitch kontrolsystem, vil vingerne pitch-to-feather, og reducere rotor thrusten. Resultatet er en forværring af platformens bevægelse. I kontrol termer, introducerer konventionel pitch kontrol et negativt dæmpnings bidrag som resulterer i stor bevægelse og belastninger.

Dette projekt adresserer kontrol af en flydende spar buoy vindmølle og fokuserer på indvirkningen af den ekstra platform dynamik. En tidsvarierende kontrol model præsenteres baseret på vindhastigheden og bølgefrequensen. Estimer af vindhastigheden og bølgefrequensen anvendes som schedulerings variable i en gain scheduleret lineær kvadratisk regulator til at forbedre den elektriske produktion, mens fatigue mindskes. Vindhastigheden estimeres med et extended Kalman filter og bølgefrequensen med et auto-regressiv filter.

For at løse problemet med negativ dæmpet tårn bevægelser, forslås der yderligere reguleringsløsninger til at stabiliserer responsen af en konventionel regulator og mindske virkningerne af bølgedrevne belastninger. Dette er udvidet til model prædiktiv kontrol til at behandle bølge forstyrrelser yderligere. En dynamisk model af det uforstyrrede lukket

## CONTENTS

---

sløjfe systemet bruges som reference til det forstyrrede systemet i en struktur baseret p model prædiktiv kontrol.

I forbindelse med reguleringsteknik er dynamikken og forstyrrelser af en flydende vindmølle blevet identificeret og modelleret. Målsætninger for maksimeret elektrisk produktion og minimeret fatigue, er nået ved hjælp af avancerede metoder til estimation og kontrol.

# 1 | Introduction

This chapter describes trends for wind turbines and the motivation for the current work. The properties of a floating wind turbine are introduced and control issues are described regarding the new freedoms of the application. An overview of the background and the state of the art is presented, followed by an outline of the thesis.

## 1.1 Motivation

The idea of extracting energy from the wind is not new. It has been traced back to the time of the first sailing boat, where the trust from the wind was used for propulsion of the craft. In agriculture, the wind was used to pump water from wells to fields and cattle, and for grinding grain. Here, the wind energy was transformed into torque by means of a spinning rotor and a shaft. In recent time, the torque from the wind has found a new application, where the same principle of a spinning rotor is used to produce torque and thus electrical power in a wind turbine setup.

Today, the wind turbine is a commercial product which is competing against other sources of energy, such as gas and coal. This competition has driven a constantly developing design and optimization process aiming at reducing costs and improving efficiency in order to reduce the total cost of the energy. Partly as a response to this, the size of wind turbines has increased from kilowatts to multi megawatts. This trend is supported in [UpWind, 2011], which shows that wind turbines are feasible even at 20 MW with rotor diameters of 252 meters.

Reliability has increased since the first inland prototypes were installed, which has lead to the deployment of wind turbines in remoter and harsher environments. Experience from the oil and gas industry in offshore installations and foundations has allowed the wind turbine to go offshore, where the wind is stronger. In [Association, 2012], an analysis shows that offshore wind farms are being built further from the coast and in deeper waters. Since 2011, the average offshore wind farm water depth has increased from 22.8 meters to 25.3 meters, and the distance to shore has increased from 23.4 km to 33.2 km.

In [Shikha et al., 2003], the advantages of siting wind turbines offshore are analysed. The average offshore wind speed is typically 20% greater than onshore. The ambient turbulence is less, which prolongs the turbine's lifetime. Furthermore, issues related to noise and visual impact are reduced.

Depending on the water depth, a variety of foundations have been used, as presented in Figure 1.1. From an economic point of view, the deep water foundations are the most ex-

persive in Figure 1.1, however, the expected wind speeds are higher and thus the expected electrical power production is higher. The monopile foundation is a popular example of offshore deployment. However, this foundation is economically limited to shallow water depths below 30 meters. Other concepts of foundations, such as the jacket and tripod, are designed for water depths in the range of 25–50 meters.

Another aspect and motivation for installations in deeper waters is the globally limited extent of shallow water. Furthermore, the consumers of the electrical power must be within a reasonable range of the wind turbines to avoid considerable loss due to power transmission. To provide significant offshore wind energy to some large population areas, e.g., on the east coast of the US or around Japan, installations at deep waters are required.

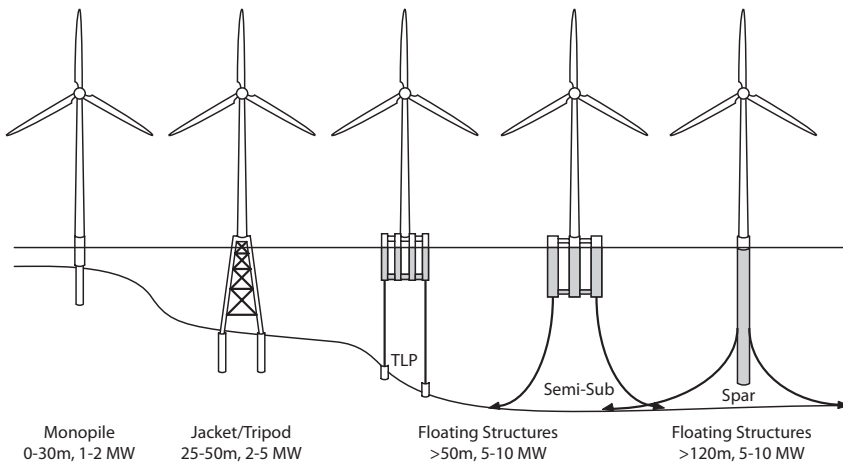


Figure 1.1: Offshore wind turbine foundations.

The latest offshore development is the floating wind turbine. The floating foundation exists in several shapes. In Figure 1.1 we present three different types: the tension legs platform (TLP), the semi-submersible, and the spar buoy. In 2009, the Hywind Demo was deployed, which was the first full scale floating wind turbine. It was based on a spar buoy foundation as shown in Figure 1.2(a). The spar buoy is kept in place with catenary mooring and drag embedded anchors. Later in 2011, the Windfloat was deployed, based on a semi-submersible foundation as shown in Figure 1.2(b). A floating wind turbine is subject not only to aerodynamics and wind induced loads, but also hydrodynamics and wave induced loads. The floating structure, the hydrodynamics and the loads change the fundamental dynamic behaviour of the floating wind turbine system compared to an onshore or bottom fixed turbine.

These dynamics and loads are crucial for the life time of the wind turbine, and must hence be taken in to consideration during the design of the control system. A conventional wind turbine controller is designed to produce a steady electrical power output, at a controller bandwidth slow enough not to excite structural oscillations. However, for a floating wind turbine, the dynamics of the structure are relatively slow. In this case, the bandwidth of the conventional wind turbine controller is fast enough to excite the structure, and this causes instability and damaging structural oscillations. This is referred to



Figure 1.2: Examples of floating wind turbines. The Hywind Demo (a) is a 2.3 MW Siemens wind turbine mounted on a spar buoy foundation. The Windfloat (b) is a 2 MW Vestas wind turbine mounted on a semi-submersible foundation.

as negative damped oscillations in fore–aft motion, and this must be addressed such that the lifetime of the total structure does not suffer.

## Objectives

As the thrust force from the wind pushes the wind turbine backward, a conventional on-shore controller experiences a decrease in the relative wind speed. Thus, the blade pitch angle is reduced, causing an increase in the thrust force. As the wind turbine moves forward, a conventional controller experiences an increase in relative wind speed. Thus, the blades pitch to feather, causing a decrease in the thrust force. This phenomenon is true for both bottom fixed and floating wind turbines, but due to the freedom of a floating structure and the wave induced oscillations, the phenomenon is exaggerated for a floating turbine. For a bottom fixed turbine, the bandwidth of the pitch system is designed to avoid this phenomena. Negative damping occurs when a controller, designed for an bottom fixed wind turbine, is applied to a floating wind turbine, without modifying the controller. The difference between the fore–aft natural frequency of a bottom fixed tower and that of a floating spar buoy is approximately a factor of ten, [Larsen and Hanson, 2007]. This changes the dynamic response and causes negative damping in fore–aft of the platform. Furthermore, a floating wind turbine is exposed to disturbances from both wind turbulence and incident waves. Consequently, the system experience an increase in the loads, a reduction in the wind turbine fatigue lifetime, and thus an increase in the cost of the energy.

The problems addressed in this dissertation are hence as follows: I) that conventional wind turbine control systems, designed for bottom fixed wind turbines, induce negative damped oscillations on a floating wind turbine, which causes power oscillations and reduces the fatigue lifetime, and II) as a consequence of the induced floating foundation, the dynamic response to both wind and wave loads causes exaggerated oscillations of the structure and thus a reduction in fatigue lifetime.

To address these problems, methods based on system identification, process estima-

tion, and model-based control are combined and the significance of the results are validated with respect to power performance, actuator wear, and structural fatigue, by means of damage equivalent loads.

The objectives are specified in the following:

1. A dynamic model of a floating wind turbine which relates the dynamics of the structure to the dynamics and loads of the wind and waves. The model formulation is suitable for model-based control and capable of modelling nonlinearities over a range of wind and wave operational conditions.
2. A model-based control system to optimize the production of power and to reduce the fatigue on the structures and actuators, while taking the nonlinear dynamics and disturbances of the wind and waves into account.
3. A strategy to extend the conventional onshore control from bottom fixed to floating wind turbines, while avoiding negative damped oscillations. A floating wind turbine, including a conventional onshore controller, is stabilized without redesigning the entire control system.
4. Model-based disturbance control to accommodate the predictive loads induced by incident waves to reduce the fatigue on the structures based on dynamic estimations of the process and references.

## Scope

The industrial prototypes presented in Figure 1.2 are examples of wind turbines where the control systems have been designed to accommodate the negative damping in fore-aft. These industrial controllers are classified, and thus the relevant research and development are not publicly available. However, since Statoil is a partner in NORCOWE, there exists a unique opportunity to address practical control issues related to the Hywind Demo, where Statoil can provide insight and possibly measurements from the Hywind Demo. Since this work is funded by NORCOWE, there is a mutual interest among the partners involved, in addressing research topics related to the concepts of floating wind turbines. This dissertation is hence focussed on a floating structure similar to the ballast-stabilized Hywind Demo.

Experimental work on the Hywind Demo has not been possible, and the work presented here has hence been limited to simulations of such systems. The scope for simulation has, in collaboration with the NORCOWE partners, been limited to the high fidelity code FAST ([Jonkman, 2010b]) by NREL which simulates an upscaled version of the Hywind Demo. This code is well documented and recognized in [Passon et al., 2007].

Thus the scope of this thesis is as follows:

- The research on control systems should address the Hywind Demo or similar wind turbines based on a ballast-stabilized platform of the spar buoy type.
- Collaborate with Statoil to identify interesting key performance indexes and the weighting between these on the Hywind Demo.

- The suggested solutions and control systems should be computationally feasible on practical applications, based on available or measurable data on a commercial wind turbine.
- The response of the floating wind turbine is simulated using the FAST high fidelity codes for a ballast-stabilized spar buoy wind turbine.
- No changes are applied to the simulations of the ballast-stabilized spar buoy wind turbine in relation to actuators and the structure.

## 1.2 State-of-the-Art and Background

The wind turbines is an application which has the interest of a broad audience of engineers and economists who see a potential in wind energy. Over the years, this interest has consolidated the research in wind energy as a strong and independent research area. Built on existing research, the floating wind turbine has emerged, which is a new and promising application to reach new water depths. The literature shows that the design and deployment of floating foundations has drawn the attention of new research areas to the wind energy area, such as marine and ocean engineering. The contributions from these areas are research in hydrodynamics and structural dynamics. These contributions are necessary to complete the basic understanding of the floating wind turbine. However, the current floating wind turbines are still only prototypes of future hopefully cost competitive installations. To determine the current progress on floating wind turbine, state of the art of their control methods will be presented.

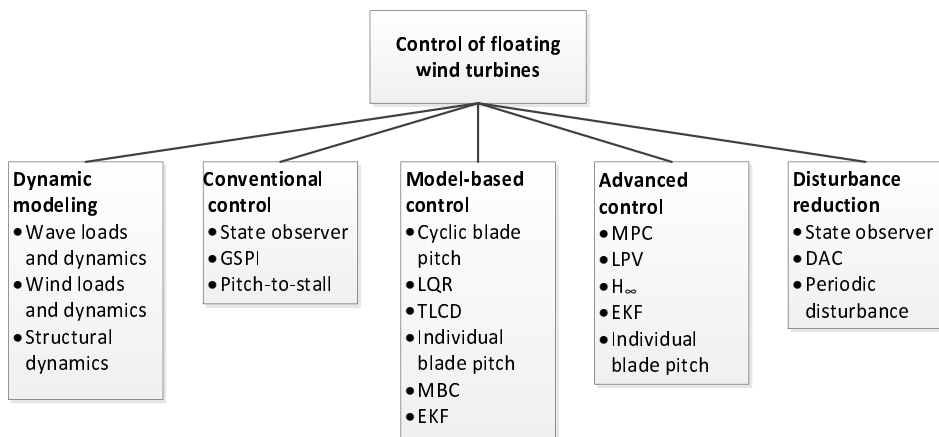


Figure 1.3: Sketch of state of the art methods for the control for floating wind turbines divided into topics (bold).

In the context of control engineering, an overview of the state of the art is presented in Figure 1.3. This figure illustrates how the state of the art can be divided into five topics (bold), based on their complexity and objectives. Under each topic a list of methods (bullet points) is presented which relates to the topic, and where some methods relates to



multiple topics. The topic of Dynamic modeling is presented because it is a prerequisite in model-based control. The state of the art for the control is divided into three topics, where Conventional control represents simple controllers, Model-based control represents controllers based on modeling and Advanced control represents the most complex controllers. The topic Disturbance reduction represents means to accommodate loads induced by wind and wave disturbances.

In the following, the five topics will be explained in more detail and the state of the art will be presented for each topic, indicating their shortcomings and the possibilities for further research.

### **Models of Floating Structures and Hydrodynamics**

The dynamic response of a floating wind turbine can be compared to the response of a marine craft. In [Fossen, 2011], the hydrodynamic impact on marine crafts is modelled based on empirical models of the wave spectrum which relate the significant wave height, the wind speed, and the wave frequency. Methods to estimate wave induced loads are presented based on stochastic models of the wave spectrum. The mechanics and properties of water waves, currents, and wave loads are described in [Andersen and Frigaard, 2011, Burcharth, 2002].

The shape and surface smoothness of a hull has an impact on the radiation of waves and forces which are expressed by hydrodynamics. A state-space representation of the radiation forces from the hydrodynamics is presented in [Kristiansen et al., 2005] based on frequency-dependent added masses and potential damping. The results include a computationally efficient method applicable to control design. However, the method has a disadvantage: to describe the added mass and potential damping, the model comprises several models with orders ranging from the third to the eighth, which quickly increases the complexity of the model.

The shape of the floating structure was investigated in [Berthelsen and Fylling, 2011], where three different shapes of spar buoys were compared as to their cost and dynamic response. A cost function describing the objective and algorithms were presented to minimize, e.g., steel consumption. This is a valuable method in the design of a floating wind turbine. A structural design method is a precondition for further control design, but unless a concurrent design approach is taken, it is not directly related to the control design.

Simulation code for simulating the dynamical response of a floating wind turbine is presented in [Jonkman and Sclavounos, 2006, Jonkman, 2007] and [Jonkman, 2010a, Jonkman et al., 2007, WAMIT, 2006], which presents an extensive high-fidelity model of a coupled hydro- and aerodynamic floating wind turbine including a low performance controller. The code includes a tool for model linearization, however, this is only valid for single point operation. The model was verified against other high-fidelity models in [Passon et al., 2007] which showed similar behaviour.

In [Skaare et al., 2007b], a preliminary scaled physical model of the Hywind Demo is presented to verify the dynamics of an in-house simulation model of the Hywind Demo. Based on simulated data and measurements from the scaled model, a comparison of the structural behaviour and performance is presented which is then verified against the in-house simulation model. However, the in-house simulation model and the control system are subject to confidentiality. In [Hanson et al., 2011], a similar comparison is conducted on the deployed full scale Hywind Demo, which also showed comparable results on struc-

tural behavior and performance.

In [Karimirad and Moan, 2011] and [Karimirad, 2011], the dynamic response and power production of a floating wind turbine is investigated when subject to extreme wind and wave conditions. The response to extreme wind and wave conditions were simulated using several simulation codes, which all showed similar response.

In summary:

- Coupled aeroelastic and hydrodynamic codes for dynamical simulations have been developed and validated to simulate the response of a floating wind turbine. Furthermore, the simulation codes have been verified on scaled and, later, full scale models of floating wind turbines. The presented literature consolidates the existence of advanced models and codes for floating models suitable for control design.
- In the context of control design, the hydrodynamic radiation is presented using high order models, which may be inconvenient for control design. A tool to generate a linear model of a floating wind turbine is presented for single point operation, which is insufficient to cover all possible operating points.

### **Conventional Control with Modifications**

A wind turbine control system usually has a main controller in combination with several controller designed for a series of special events of operation and disturbances. To account for the negative damping of the platform pitch, a gain-scheduled baseline control is subjected to modifications in [Jonkman, 2008]. Here, one way to address this problem is to apply an additional control loop. This is done in [Burton et al., 2001], where a method to damp fore-aft oscillations of the tower is presented, based on a tower acceleration feedback loop applied to the controller. However, in [Jonkman, 2008], the results of this method show unacceptable rotor speed excursions. Using the same method, a contradictory result is presented in [van der Veen et al., 2012], where a linear PI controller is extended by an additional tower velocity feedback loop. The PI controller is designed for a single operating point only. The linear PI controller shows reduced generator speed excursions and nacelle displacements in contrast to a linear PI controller with reduced bandwidth.

Negative damping is mostly related to the operation strategy of pitch-to-feather, since this method reduces the thrust force above the rated wind speed. Another method is to use pitch-to-stall, which is a method that increases the thrust force when conditions are above the rated wind speed. In [Jonkman, 2008, Larsen and Hanson, 2007], this method is investigated, and shows an increase in the amplitude of oscillations in the platform pitch due to the increased thrust force. The best results are achieved using pitch-to-feather and reducing the bandwidth of the baseline controller which stabilizes the system. However, the performance is far from that of an onshore wind turbine, and due to the reduced bandwidth, the blade pitch actuator becomes inadequately slow and hence not exploiting the true potential of the actuator within the fatigue lifetime of the wind turbine. This is a general problem with all results that reduce the bandwidth of the pitch system. It addresses the negative damping, by slowing down the pitch system below the bandwidth of the platform motion, and hence reduce the pitch to feather with forward motion. Unless the pitch actuator is modified, it will result in a much longer lifetime than it was designed for, which is not optimal when compared to other components.

In [Lackner, 2010], it is proposed to control the generator speed reference based on a feedback of the platform pitch velocity. The method is combined with individual blade pitch, as suggested in [Bossanyi, 2003, Bossanyi, 2005]. The results show improved performance. However, due to a constant generator torque approach, the generator speed and the electrical power show relatively large excursions. In [Skaare et al., 2007a, Skaare et al., 2011], they suggested a similar approach by manipulating the generator speed feedback loop. A modified constant power approach is suggested for improving the power performance. Based on state estimation, the rotor speed oscillations induced by the platform pitch dynamics are decoupled and subtracted from the measured rotor speed feedback. A comparison between the limited available results and conventional control shows that the method resolved the problem of the negative damped oscillations of the platform pitch at the cost of a deterioration in mean and standard deviation of the produced electrical power. However, the specific industrial controller used to achieve these results is commercially confidential.

In summary:

- Pitch-to-stall improves damping and power performance at the cost of increased rotor thrust and platform oscillations.
- Based on platform pitch velocity feedback, an additional control loop reduces the oscillations of conventional onshore control.
- The bandwidth of conventional wind turbine control has been reduced and applied to a floating wind turbine. The relatively slow controller stabilizes the system, but the production of power deteriorates, and it also causes speed excursions.
- The industry has demonstrated damped oscillations of a floating wind turbine using estimator-based feedback for conventional onshore control, however, mean and standard deviation in electrical power were deteriorated. Furthermore, the strategies and methods are commercial confidential.

## Model-Based Control and Features

Model-based control is a method which offers control of multiple input multiple output (MIMO) systems based on dynamic models. The method allows the controller gains to be found based on advanced models of the system which may not be possible using conventional control methods. Among others, the method can be used for multi-objective control for state space systems and allows the formulation of optimal control which minimizes a performance function. A floating wind turbine is indeed a MIMO system, comprising a generator torque input and three blade pitch inputs, combined with a series of sensor outputs.

In [Namik and Stol, 2008, Namik and Stol, 2009b, Namik, 2012, Stol and Zhao, 2006], model-based control is combined with periodic control of both monopile- and floating wind turbines, with focusses on cyclic blade pitch and individual blade pitch. Based on a time-varying model with respect to the azimuth angle, a linear quadratic regulator (LQR) shows improved performance in contrast to collective blade pitch. The results were further improved by controlling the blades individually using the multi blade coordinates (MBC) method. Individual blade pitch is useful for controlling the moments of the blades

and rotor. Especially the results on the control of side-side loads are improved using individual blade pitch which is achieved using asymmetric rotor loads. However, the results are based on full state feedback. In [Knudsen et al., 2011], an extended Kalman filter (EKF) is designed to estimate system states based on a deterministic model of a drivetrain and a stochastic model of the turbulence. This method can be extended to full state feedback estimation if the process is observable.

Additional actuation and control is suggested for floating system in [Luo, 2011], where a semi-active control design is applied to a tuned liquid column damper (TLCD) with a controllable valve. Wind and wave induced vibrations are reduced using an  $H_\infty$  control method to improve the structural lifetime.

In summary:

- Model-based control combined with cyclic and individual blade pitch using MBC has been applied to floating wind turbine, performing well in power and side-side motions. However, the results are based on a state feedback for single point operation of wind speed and wave frequency.
- In an model-based framework, an EKF is used to estimate the dynamic response of an onshore wind turbine.
- Structural oscillations and fatigue-lifetime can be improved using TLCD actuators in the platform by means of a semi-active control strategy which reduces static loads.

### Advanced Control Methods

Advanced control methods are investigated in [Mayne et al., 2000], where model predictive control (MPC) is presented as an attractive control method because of its ability to deal with constraints and to deal with multi-variable systems. MPC solves an optimal control problem over a finite horizon repeatedly. Given the current state of the system, an optimal control problem over a finite horizon is solved at each time step [Maciejowski, 2002]. Recently, MPC has been used with promising simulation results for the control of non-floating wind turbines in [Kumar and Stol, 2009, Kober and King, 2010].

In [Santos, 2007], model predictive control is combined with information about the future wind and a nonlinear model of the structural damage produced by repetitive loads to reduce the structural load and fatigue. In [Schlipf et al., 2012], the authors use the wind prediction information obtained from a LIDAR system in a nonlinear model predictive controller to reduce the fatigue loads on the tower and blades. In [Lindeberg et al., 2012], MPC is suggested as a full wind range control strategy. Based on the wind speed, bumpless transfer is used to switch between multi-objective controls with different objectives. The results demonstrate a smooth transition between the controllers.

In [Henriksen et al., 2010], the uncertainties regarding dynamic inflow and wind speed estimation are addressed and combined in an MPC framework. The MPC was applied to both monopile- and floating wind turbines comprising an EKF for state estimation and for supervision in a hybrid system setup. A simple static MPC reference approach were used, which might be improved using dynamic MPC reference. The method should not be too computational heavy and hence suitable for real-time applications.

In [Bakka et al., 2012], gain scheduled  $H_\infty$  control are designed to minimize a performance function, based on linear matrix inequalities (LMI) at four operating points. The combined  $H_\infty$  controller is applied to a floating wind turbine and gain-scheduled based on the assumption of known wind speed. In [Bakka and Karimi, 2012] the work was extended to consider the unknown azimuth angle in a performance function. In both [Bakka et al., 2012, Bakka and Karimi, 2012], methods of pole placements were utilized which may be difficult to relate to performance and fatigue objectives.

Another method is investigated in [Østergaard, 2008], where linear parameter varying (LPV) control is presented. Based on an LMI approach, the nonlinear disturbance from the wind is modelled as rational functions. A controller is found which is robust to the wind disturbance by minimizing an  $H_\infty$  norm. However, results are limited to onshore wind turbines.

In summary:

- Model predictive control was applied to wind turbines to predict and improve their future performance while switching between different control objectives.
- To reduce the impact of model uncertainties, LPV control offers robust performance by minimizing an  $H_\infty$  norm using LMI formulations.

### **Reducing the Impact of Wind and Wave Disturbances**

The response of a system is usually controlled and damped using feedback control. Depending on the objectives, it can also be an advantage to use feed-forward methods to address disturbances before they impact the system dynamics.

In [Johnson, 1986], a general overview is given of disturbance accommodating control (DAC), which is a method to estimate and reduce the impact of the disturbance by means of direct or indirect actuation. The method is applied to wind turbines in [Stol and Balas, 2003, Wright, 2004], where a periodic disturbance accommodating control method is used to reduce the response of a time-varying system with respect to the rotor azimuth angle. In [Namik and Stol, 2009a, Namik, 2012], a disturbance accommodating control is combined with individual blade pitch on a floating wind turbine and full state feedback. Based on known dynamic models of a single point wind speed and wave frequency, an actuator signal is estimated which reduces the impact of the disturbance induced by regular waves on the system.

In [Brown and Zhang, 2004], a periodic disturbance cancellation method was presented for a disturbance model with unknown natural frequency and gain. Based on measurements, an estimation of the unknown parameters was corrected and an actuator signal was designed to cancel the disturbance.

In summary:

- Disturbances can be reduced or canceled by direct or indirect disturbance estimation and actuation.
- Methods for reducing the disturbance from wind and waves have been suggested based on single point deterministic observer models. Only results for regular waves show a significant improvement.

- Disturbance accommodating control shows an advantage in reducing Azimuth-periodic disturbances on loads and performance.

### 1.3 Outline of the Thesis

The problem has been introduced and the state of the art and background has been presented. In the following, a summary of paper contributions are listed. The methods used in these papers are presented in Chapter 2 and the contributions of the papers are stated in Chapter 3. Conclusions are drawn in Chapter 4 and future work is presented in Section 4.1.

- **Paper A [Christiansen et al., 2011]**  
In this paper, we address the initial platform stability problem of a floating wind turbine using model-based control. The controller is designed based on a simplified model comprising a flexible drivetrain and a rotating platform. An EKF is included in the control strategy to estimate the turbulence and the mean wind speed.
- **Paper B [Christiansen et al., 2012a]**  
In this paper, we expand the simplified model and establish a basis for model-based control by presenting a linear time varying control model of a floating wind turbine. The model combine aero- and hydrodynamics as well as gyroscopic effects and the structural dynamics. A gain-scheduled LQR controller is designed for this linear time-varying model, based on estimates of the wind speed and the wave frequency.
- **Paper C [Christiansen et al., 2012b]**  
In this paper, we use the time-varying model to explore the combined freedom of the tip speed ratio and the blade pitch angle above the rated wind speed. Assuming a constant power strategy for wind speeds above the rated wind speed, we investigate the impact on power and fatigue by operating at variable rotor speed in contrast to the conventional constant rotor speed.
- **Paper D [Christiansen et al., 2012c]**  
In this paper, we address the unstable response of conventional onshore control of a floating wind turbine. An additional control loop is suggested which stabilizes the system and includes a method for reducing the impact of wave induced loads on the structure. The controller is applied as a supplement to the conventional onshore controller and thus does not require a complete redesign of the control system.
- **Paper E [Christiansen et al., 2013]**  
In this paper, we reduced the impact of wave induced loads on the structure, by using the response of the undisturbed closed-loop system as a reference for the disturbed closed-loop system. To achieve this, we use reference model-based predictive control, including models for wind and wave induced loads.



## 2 | Methodology

This chapter describes the background for the methods used in this thesis. A floating wind turbine is presented, and the properties of its structural dynamics, aerodynamics, and hydrodynamics are identified. Depending on operation and control, the wear and structural life time may differ, thus methods are presented to estimate the fatigue.

A model validation is presented by comparing the high fidelity code FAST to a linearized control model.

### 2.1 Reduced Order Model of a Floating Wind Turbine

A floating wind turbine of the spar buoy type is presented in Figure 2.1. The figure shows a standard wind turbine mounted on a spar buoy platform where the mooring system has been left out. In the following, an overview of the components and coordinate systems of a floating wind turbine is given and illustrated in Figure 2.1.

The wind turbine comprises a flexible tower, a nacelle, and a hub. The hub is connected to the gearbox by a driveshaft, and the gearbox is connected to a generator. The electrical power output of the generator is given by

$$P = \omega M_g, \quad (2.1)$$

where  $\omega$  is the generator speed and  $M_g$  is a controllable induced generator torque on the rotating shaft. The generator response can be modelled as a linear dynamical system, from the desired generator torque to the actual generator torque. This is obviously a simplification: however, in this thesis it is considered sufficient for control purposes. The wind  $v$  induces both a torque  $M_a$  and a thrust  $F_t$  on the rotor and thus the drivetrain. The aerodynamics are described in the following section, however, the aerodynamics can be controlled by altering the pitch angle of the blades. The blade pitch actuator can be modelled as a linear dynamical system. The hub and nacelle structures are supported by the tower, which is a component subject to stress. The tower is flexible and its deflections can be modelled in the directions of fore–aft  $x_t$  and in side–side  $y_t$ . The wind turbine is mounted on top of the spar buoy platform, which floats in the water, constrained only by three mooring lines. The tower and spar buoy platform interconnect just above the sea water level (SWL). In Figure 2.1, the centre of mass (COM) relates to the mass of the structure, while the centre of buoyancy (COB) relates to the volume of the displaced water. The platform is able to translate in surge, sway, and heave, and able to rotate in roll, pitch, and yaw.



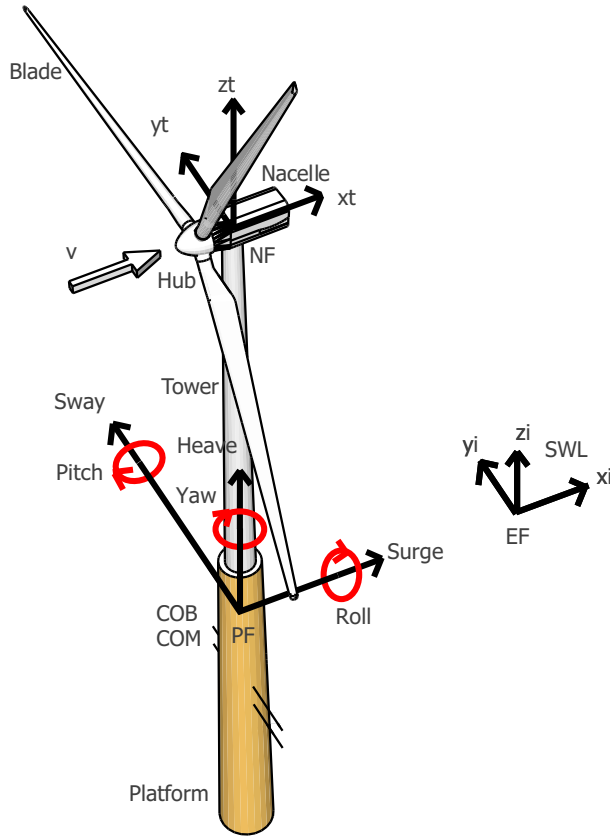


Figure 2.1: Floating wind turbine comprising a wind turbine mounted on a floating spar buoy platform (note mooring system is not shown).

Figure 2.1 presents three coordinate systems. An earth-fixed (EF) coordinate system is presented by  $(x_i, y_i, z_i)$  where the  $xy$ -plane is defined at the initial SWL-plane. The EF coordinate system is used to describe the relative position of the platform-fixed (PF) coordinate system. The PF coordinate system is described by  $(x, y, z)$  and presented by (surge, sway, heave, roll, pitch, yaw) in the figure, where translation is black and rotation is red. The origin of the PF coordinate system is located at the intersection between the tower centre line and the initial SWL-plane on the platform. A nacelle-fixed (NF) coordinate system  $(x_t, y_t, z_t)$  presents the tower deflection relative to the PF coordinate system. The origin of the NF coordinate system is located at the intersection between the tower centre line and the the rotor shaft.

The combined structure rotates about the meta centre which is located directly above the COB at a distance of  $MC = I/V$ , where  $I$  is the second moment of area of the water plane and  $V$  is the volume of the displaced water. The structure is subject to gravitational forces and buoyancy forces, which for a floating vessel are in balance at rest. To prevent the floating wind turbine from drift in translation and rotation, the platform is constrained by three mooring lines (not presented in the figure), which adds stiffness to the system.

Here, yaw stiffness is an important factor to keep the rotor–plane perpendicular to the direction of the wind.

## Dynamics of a Floating Wind Turbine

A block diagram of the dynamics and interconnections of a floating wind turbine are presented in Figure 2.2. The presented block diagram describes a model sufficient for analysis and control purposes, while a more advanced modeling framework is used for simulations.

The dynamics of a floating wind turbine consists of aerodynamics, structural dynamics, hydrodynamics and the drivetrain dynamics. However, the response of the actuators is also dynamical, thus the blade pitch dynamics and generator dynamics are also presented. The actuators control the blade pitch angle and the torque induced by the generator on the shaft. Depending on the aerodynamic torque the rotor will accelerate or decelerate. The aerodynamic torque is a function of the blade pitch angle, the rotor speed, and the relative wind speed,  $v_r$ .

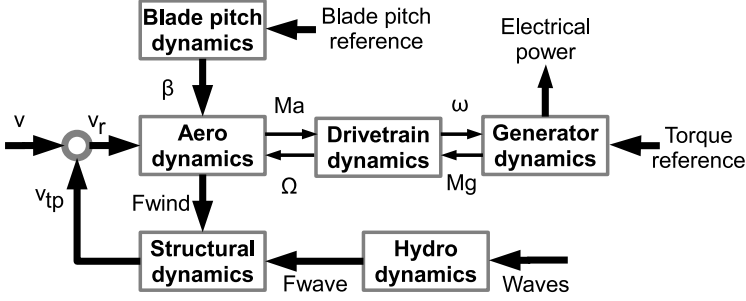


Figure 2.2: Block diagram of dynamics and interconnections of a floating wind turbine.

The wind speed experienced by the rotor is a relative wind speed which depends on the motion of the structure. The structure comprises the tower, the platform, and the mooring lines. As the wind blows, a thrust force is induced on the rotor by the wind. This thrust affects the structural dynamics, causing a translational velocity  $v_{tp}$  of the structure which, reciprocally, has an impact on the relative wind speed,  $v_r = v - v_{tp}$ , where  $v_{tp} = \dot{x} + \dot{x}_t + h\dot{\theta}$ , and  $x$  is the surge of the PF relative to the EF coordinate system,  $h$  is the height between the PF and NF coordinate systems, and  $\dot{\theta}$  is the platform pitch velocity of the PF relative to the EF. The platform is also subject to hydrodynamics and wave loads which will be explained in the following section.

In the context of model–based control, the freedoms and flexibilities can be modelled by  $\mathbf{q}$  as a linear system by means of inertia  $\mathbf{A}$ , damping  $\mathbf{B}$ , and stiffness  $\mathbf{C}$ , by

$$\mathbf{A}\ddot{\mathbf{q}} + \mathbf{B}\dot{\mathbf{q}} + \mathbf{C}\mathbf{q} = \mathbf{F}_{\text{wind}} + \mathbf{F}_{\text{wave}} + \mathbf{F}_{\text{ref}}, \quad (2.2)$$

where the forces on the right hand side of the equation are external forces induced by the wind, waves, and actuator inputs defined by  $\mathbf{F}_{\text{wind}}$ ,  $\mathbf{F}_{\text{waves}}$  and  $\mathbf{F}_{\text{ref}}$ , respectively. This model is valid for a single operation point of wind and waves.

On a standard onshore wind turbine, one can assume only a few sensor measurements are available, such as the generator speed and the acceleration of the nacelle. However, on a floating wind turbine, measurements related to the platform translation and rotation may be considered available, as well as a measure of the wave height.

### Structural dynamics

The principal freedoms of the structural dynamics are presented in Figure 2.3. The flexibilities of the tower are modelled as a second order system, comprising a single mass located in the nacelle which is connected to a damper and a spring. This mass is the sum of the three blades, the hub, the nacelle, and the tower, presented in the NF coordinate system. The tower deflection is modelled relative to the orientation of the platform centre line in the PF coordinate system.

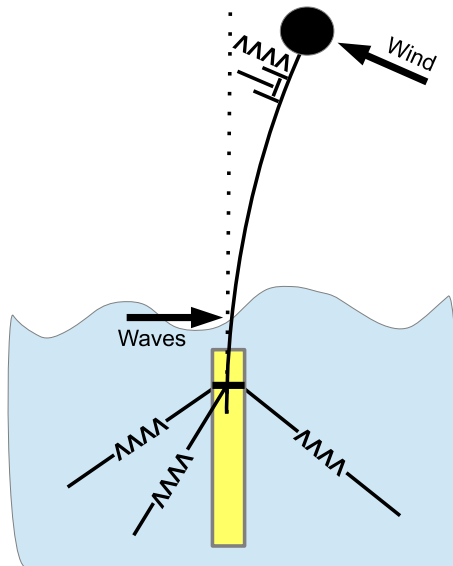


Figure 2.3: Floating wind turbine with springs and dampers.

The freedom of the platform is also modelled as a second order system comprising the mass of the rigid platform, where stiffness is added to the system from the three mooring lines which are connected to the seabed. The gyroscopic effects from the spinning rotor adds damping to the rotational freedoms in the platform pitch and yaw directions. The system is affected by aerodynamic and hydrodynamic loads. The figure shows how the wind loads are induced on the tower, while the wave loads are induced on the platform.

### Drivetrain dynamics

Figure 2.4 presents a model of a drivetrain. The drivetrain is modelled as two masses connected by a spring and a gear where both the low and the high speed shafts are subject to friction. Figure 2.4 presents the rotor inertia  $I_r$ , comprising the blades, the hub, and

the low speed drive shaft. The generator inertia  $I_g$  only models the low speed shaft of the generator. The stiffness  $K_{dr}$  is the spring constant of the shaft torsion,  $B_{dr}$  is the damping constant, and  $N$  is the gear ratio. This approach allows modelling the torsion of the rotor shaft induced by the aerodynamic torque  $M_a$  on the rotor side and the electrically induced torque on the generator side.

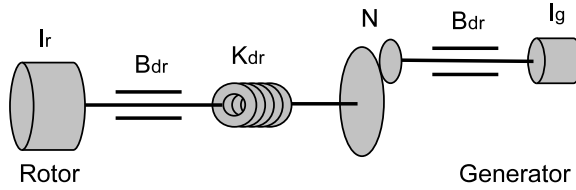


Figure 2.4: Schematic overview of a drivetrain

## Aerodynamics

The aerodynamic forces of the wind are presented as the aerodynamic rotor thrust  $F_t$  and torque  $M_a$  which have a nonlinear effect on the system, given by

$$F_t = \frac{1}{2} A \rho C_t(\lambda, \beta) v_r^2 \quad (2.3)$$

$$M_a = \frac{1}{\Omega} \frac{1}{2} A \rho C_p(\lambda, \beta) v_r^3 \quad (2.4)$$

where  $\Omega$  is the rotor speed,  $A$  is the area swept by the rotor,  $\rho$  is the air density,  $C_t$  and  $C_p$  are the thrust and power coefficients,  $\lambda = \frac{R\Omega}{v_r}$  is the ratio between the blade tip speed  $R\Omega$  and the relative wind speed  $v_r$ , and  $\beta$  is the blade pitch angle. Due to the platform pitch and tower deflection, we distinguish between the ambient and relative wind speed.

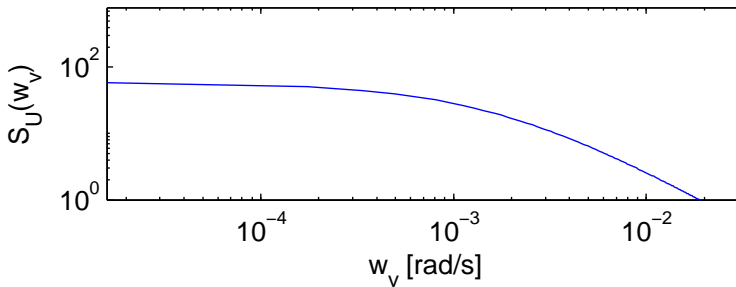


Figure 2.5: Kaimal spectrum for turbulence [Burton et al., 2001].

The blade pitch angle and the rotor speed we assume to be known, however, the ambient wind is difficult to measure. The frequency content of the ambient wind can be described using a Kaimal spectrum ([Burton et al., 2001]) as presented in Figure 2.5,

where the standard deviation of the turbulence is 1 m/s, the turbulence length scale is 150 meters and the wind speed is 10 m/s. The spectrum can be formulated as

$$S_U(f) = \sigma_K^2 \frac{4L/U_{10}}{\left(1 + 6f \frac{L}{U_{10}}\right)^{5/3}}, \quad (2.5)$$

where  $\sigma_K$  is the standard deviation of the turbulence,  $L$  is the turbulence length scale, and  $U_{10}$  is the 10-minute average of the wind speed. The spectrum provides useful information in the context of estimating the ambient wind speed.

## Hydrodynamics

To describe the hydrodynamic impact on the platform, a simple example is given which describes the response of a rigid body, when subject to hydrostatics, hydrodynamics forces and wave excitation loads represented as

$$(M_{RB} + A(w_\omega))\ddot{q} + B(w_\omega)\dot{q} + Cq = A_w X_w(w_\omega, w_\beta) e^{jw_\omega t}, \quad (2.6)$$

where  $M_{RB}$  is the inertia of the rigid body,  $A(w_\omega)$  is the hydrodynamic added mass (which depends on the wave frequency),  $B(w_\omega)$  is the hydrodynamic potential damping (which depends on the wave frequency),  $C$  is the combined buoyancy and gravity restoring stiffness,  $A_w$  is the wave amplitude,  $X_w(w_\omega, w_\beta)$  is the normalized wave excitation force (which depends on the wave frequency and direction), and  $q$  is the position. The terms are described in more detail in the following:

- **The hydrodynamic forces** include the radiation forces and the viscous forces. The radiation forces are the energy carried away by the generated surface waves, while the viscous forces are the skin friction, surge, and pitch damping. The hydrodynamics can be described using potential theory, by calculating the velocities of the fluid and the pressure at different locations along the hull of the rigid body. Based on this, the hydrodynamic forces are found by integrating the pressure over the surface of the hull. In linear wave theory, the hydrodynamic forces per unit length of a cylinder can be presented using the Morison formulation by [Frigaard and Burcharth, 1989]

$$f = \frac{1}{4} \rho \pi D^2 C_m \dot{U} + \frac{1}{2} D \rho C_d |U|U, \quad (2.7)$$

where  $D$  is the cylinder diameter,  $C_m$  is the inertia coefficient,  $U$  is the velocity, and  $C_d$  is the drag coefficient. The hydrodynamics depend on the wave frequency by the coefficients  $C_m = C_m(Re, K(w_\omega), k/D)$  and  $C_d = C_d(Re, K(w_\omega), k/D)$ , where  $Re$  is the Reynolds number,  $K(w_\omega)$  is the Keulegan–Carpenter number (which depends on the wave frequency), and  $k$  is a function of the wave length. Integrating the forces per unit length from Eq. 2.7, the link to the hydrodynamics in Eq. 2.6 are presented as  $A(w_\omega)$  and  $B(w_\omega)$  which depend on the wave frequency. Thus, the radiation dynamics comprises the added mass  $A(w_\omega)$ , and the potential damping  $B(w_\omega)$ . The added mass is related to the inertia of the displaced fluid as the rigid body is displaced, while the potential damping is related to the damping of this occurrence.

- **The hydrostatics** are the buoyancy force:  $\rho g V_{\text{dis}}$ , where  $\rho$  is the density of water,  $g$  is the acceleration due to gravity, and  $V_{\text{dis}}$  is the displaced volume of the hull at rest. The gravitational force  $mg$  where  $m$  is the mass, counteracts the buoyancy forces which restore the floating wind turbine to an upright position. The combined restoring stiffness in Eq. 2.6 related to the buoyancy and gravity is described by  $Cq = mg - \rho g(V_{\text{dis}} + V_{\text{dis}}(q))$ , where  $q$  is the displacement from rest.
- **The wave induced loads** can be expressed as a normalized time–function of the wave frequency, direction, and amplitude:  $A_w X_w(w_\omega, w_\beta) e^{jw_\omega t}$ . However, the wave induced loads can also be expressed as a sum of slowly varying drift loads and wave frequency dependent loads. In [Fossen, 2011], an empirical frequency-dependent spectrum of the waves is given by

$$S(w_\omega) = A_w w_\omega^{-5} e^{-B_w w_\omega^{-4}}, \quad (2.8)$$

where  $A_w = 4\pi^3 H_s^2 / (0.710 T_0)^4$ ,  $B_w = 16\pi^3 / (0.710 T_0)^4$ , the average wave frequency is  $\omega_0 = 2\pi / T_0$ , the significant wave height is  $H_s = 2.06 v_d^2 / g^2$ ,  $v_d$  is the developed sea wind speed, and  $g$  is the acceleration due to gravity. This spectrum is the modified Pierson–Moskowitz spectrum as presented in Figure 2.6. The figure also demonstrates how well the spectrum can be approximated by a linear function. The spectrum provides useful information in the context of estimating the wave height.

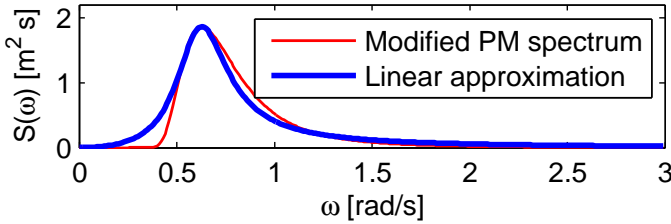


Figure 2.6: Modified Pierson–Moskowitz (PM) spectrum at  $v = 13$  m/s and  $\omega_0 = 0.8$  rad/s. The figure shows a comparison of the nonlinear and linearized spectrum related to the wave induced loads.

The hydrodynamic impact on a rigid body can be obtained using codes such as WAMIT ([WAMIT, 2006]), which return the radiation dynamics as wave frequency–dependent coefficients. Such codes can also return the hydrostatic restoring stiffness and wave load transfer functions, presented in a form suitable for control design. As in the FAST code, the data generated by WAMIT were used in this thesis to model the hydrodynamics of the spar buoy platform with respect to the added mass  $A(w_\omega)$ , potential damping  $B(w_\omega)$ , hydrostatics included in  $C$ , and the normalized wave excitation force  $X(w_\omega, w_\beta)$ .

## 2.2 Fatigue and Damage Equivalent Loads

A wind turbine is a commercial product, which is built to produce energy at a low cost. Since the cost of a wind turbine has a significant impact on the total cost of the energy, it

is of interest to reduce the fatigue on the structure. The components of a wind turbine are designed to last for a certain lifetime. However, if the wind turbine is operated regardless of fatigue, components such as the tower or the drivetrain may suffer deflections that cause undesirable long term wear or even unrecoverable damage or failure. Therefore, it is interesting to identify the critical level of fatigue of a component. Fatigue can be presented as in Figure 2.7, where a combination of stress and cycles of a material is presented in an S–N curve.

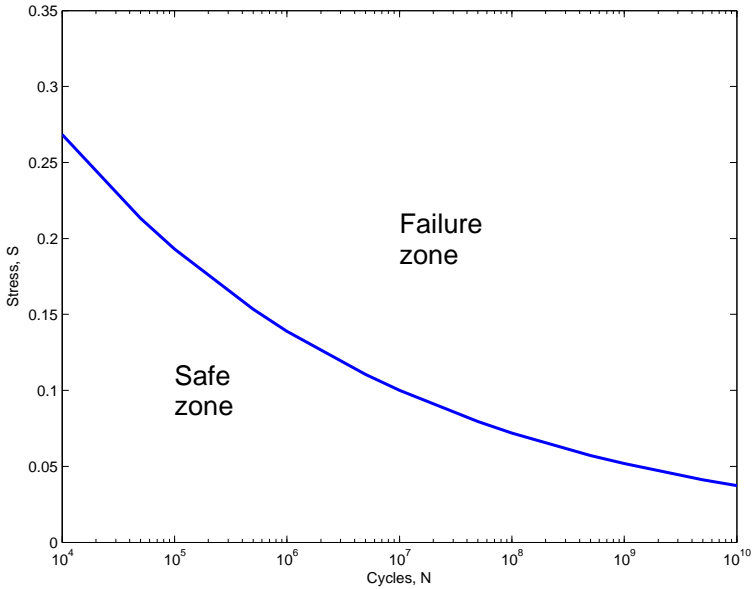


Figure 2.7: Stress and cycles of a material presented as an S–N curve.

The blue line in Figure 2.7 shows the critical level of stress as a function of the number of cycles. The area below the curve is the safe zone, where the material does not break, in contrast to the failure zone above the curve. An S–N curve of a specific material can be found using experimental data. In [Sutherland, 1999], an S–N curve is fitted to the standard S–N function:

$$S = KN^{-1/k}, \tag{2.9}$$

where  $S$  is the level of stress,  $N$  is the number of cycles to failure,  $k$  is the Wöhler coefficient, and  $K$  is a material constant. However, the S–N method can not be applied directly to a continuous time signal, since the stress levels and accumulated cycles require an analysis of the time signal. To do this, the method of rainflow counting is used, as in [Downing and Socie, 1982]. This method returns a data set of the level of stress,  $S$ , and the accumulated stress cycles  $n_i$ , where  $i$  corresponds to the specific level of stress. Based on the rainflow count, Miner’s rule [Sutherland, 1999] is applied to estimate the

accumulated damage by

$$\mathcal{D} = \sum_{i=1}^M \frac{n_i}{N_i}, \quad (2.10)$$

where  $M$  is the final stress level and  $N_i$  is the critical level of cycles for the stress level  $i$ . The damage ( $\mathcal{D}$ ), represents a ratio between the actual critical stress and the expected critical stress to failure, which in practice varies from  $\mathcal{D} = 0.79$  to  $\mathcal{D} = 1.53$  in [Sutherland, 1999], where  $\mathcal{D} = 1$  is the expected failure on average.

In this dissertation, a more complex method is used to express the damage as an equivalent fatigue load, based on the mean stress and amplitudes. First we extended the damage expression to include both the mean stress level and the stress amplitude:

$$\mathcal{D} = \int_{-\infty}^{\infty} \int_0^{\infty} \frac{n(\sigma_m, \sigma_a)}{N(\sigma_m, \sigma_a)} d\sigma_a d\sigma_m, \quad (2.11)$$

where  $\sigma_m$  is the mean stress level and  $\sigma_a$  is the stress amplitude. Based on the damage, the damage equivalent load (DEL) is defined in [Sutherland, 1999] as

$$\mathcal{F}[\sigma_m^*, \sigma_a^*] = \frac{1}{f_0} \mathcal{D} N[\sigma_m^*, \sigma_a^*], \quad (2.12)$$

where  $f_0$  is the cyclic rate for  $\mathcal{F}$ ,  $\sigma_m^*$  is an equivalent mean stress level, and  $\sigma_a^*$  is an equivalent amplitude. To determine the equivalent critical cycle  $N[\sigma_m^*, \sigma_a^*]$ , an equivalent mean stress level  $\sigma_m^*$  is chosen, while the equivalent amplitude  $\sigma_a^*$  is calculated using a power law as formulated in Equation 2.9 by

$$\sigma_a^* = \left[ \frac{\sum_i \sigma_a^k n_i}{f_0 T} \right]^{1/k}, \quad (2.13)$$

where  $T$  is the length of the time-series. The result is a single numerical value  $\mathcal{F}$ , which is the accumulated damaging equivalent load.

In this dissertation, DEL is used to compare the structural response based on different control designs. As an example in Figure 2.8 from Paper E, a comparison is presented between the essential performance indexes.

In Figure 2.8, the responses of two different controllers are compared with respect to DEL by "Tower fore-aft (DEL)" based on the time-series of the tower base moments in fore-aft. The DEL's are calculated for both time-series, and the deviation is, in percentages,

$$Z_a = \frac{z_1 - z_2}{z_1} 100\% \quad (2.14)$$

where  $Z_a$  in this case is the DEL performance index,  $z_1$  is the DEL response of the Baseline controller, and  $z_2$  is the DEL response of the MPC controller.

Figure 2.8 presents the standard deviation (std) in percentages using the same method as in Eq. 2.14. However, to present the wear in the blade pitch bearings, the absolute value (abs) of the travel blade pitch distance is a valuable performance index which is presented as

$$z_3 = \int_0^T |\dot{\beta}| dt, \quad (2.15)$$



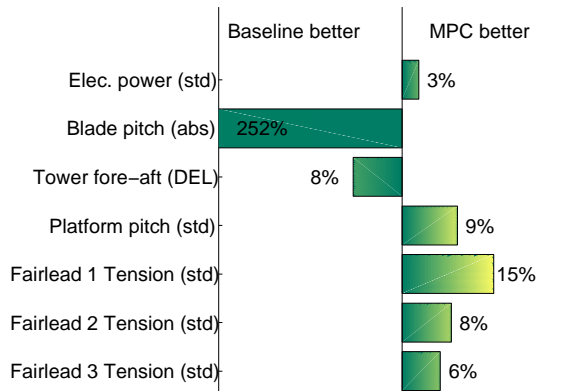


Figure 2.8: Statistical analysis of essential performance indexes.

where  $\dot{\beta}$  is the blade pitch velocity and  $T$  is the length of the time-series.

This summarizes the methods used in this thesis to evaluate the performance, which in general are methods used to emphasize the possibilities and freedoms introduced by various control methods. From an industrial point of view, the cost of the energy is essential. However, the cost of different components varies depending on the wind turbine manufacturer with respect to the financial situation, turbine type, environmental conditions, material price, stock levels etc. Thus, the results presented should be interpreted as opportunities for the industry to reduce the cost of energy. Information regarding the actual cost of components has not been available and tradeoffs between different levels of DEL are hence difficult to perform.

## 2.3 FAST and Simulation

### FAST

The models described above are supporting the control design and analysis, but in order to simulate a realistic response of the floating wind turbine system, a more advanced modelling framework has been used. Thus, to model the time-domain response of a wind turbine, a high-fidelity numerical code has been utilized throughout this dissertation, which models the fatigue, aerodynamics, structures, and turbulence (FAST) [Jonkman, 2010b, Jonkman et al., 2007]. The wind turbine comprises a flexible tower and blades with a rigid presentation of the support platform, nacelle, hub, gear, and generator. The FAST code models two- and three-bladed horizontal axis wind turbines for upwind or downwind rotors. The code offers optional foundations such as land-based or sea-based, e.g., a monopile or a floating foundation, which includes the hydrodynamics and incident wave loads on the structure. The code consists of four blocks presented in the following:

- **The fatigue** of a wind turbine can be analyzed using the time-domain output of

FAST. There exists a variety of external tools for analyzing time–series data. However, FAST can also linearize the system, and return system matrices which are suitable for analyzing the stability and damping that are significant for the fatigue. A post processing tool offers the possibility of estimating the eigenvalues and eigenvectors of a given system.

- **The aerodynamics** are handled by AeroDyn: a subroutine which is fully coupled to FAST in the sense that the motion of the wind turbine in FAST has an impact on the aerodynamic loads generated in AeroDyn. AeroDyn models the aerodynamics using blade element momentum theory. The theory allow the rotor blades to be analyzed in small sections. Depending on the wind flow, the small sections experience forces which are summed together, forming the total forces experienced by the entire rotor.
- **The structure** of a three–bladed wind turbine is modelled by an optional 24 degrees of freedom (DOF), which represents e.g., the flexibilities of the blades, the tower, and the drivetrain. However, the translational and rotational displacements of the structure are also presented. The modal representation can present both 1<sup>st</sup> and 2<sup>nd</sup> mode flexibilities of the structures.
- **The turbulence** is generated using the external tool TurbSim, which generates a time–series of wind fields. The properties of the wind are specified, e.g., the mean wind speed, turbulence intensity, and turbulence spectrum. The output is a time–series of the combined mean and turbulent wind, forming a grid of wind speeds suitable as an input to FAST.

## Control Model and Validation

In model–based control, the dynamics of the process are captured in a control model sufficiently enough to control the process and fulfill eventual objectives.

In Paper A, the FAST code response of a floating wind turbine is analyzed using the system identification methods of Lennart Ljung to establish a simple linear model suitable for control [Ljung, 2000]. To describe the method, a linear model of a system is presented as  $y_m = Gu$ , where  $y_m$  is the output of the simulation model,  $G$  is a transfer function of predefined order, and  $u$  is the input. The error between the measurement  $y$  and the model output is presented as  $v = y - y_m$ . Using the system identification method, the parameters of the transfer function  $G$  are identified such that the error  $v$  is minimized. Other formulations exist where the error is formulated based on the prediction.

In the process of model building it is relevant to validate the derived dynamics. In Paper B, a numerical parameter validation is combined with graphical validation. The FAST simulation code offers the option of linearizing the dynamics of the nonlinear response of the FAST code. Thus, for a predefined operating point, the code returns a state space model, such as

$$M\ddot{q} + C\dot{q} + Kq = Fu + F_d u_d \quad (2.16)$$

where  $M$  is an inertia matrix,  $q$  is a vector of the degrees of freedom,  $C$  is a damping matrix,  $K$  is the stiffness matrix,  $F$  is an input matrix,  $u$  is a vector of input signals,  $F_d$  is a disturbance matrix, and  $u_d$  is a vector of disturbance inputs.

However, due to the nonlinearities of the aerodynamics and hydrodynamics, the derived model to validate is presented as a system of first order nonlinear differential equations:

$$\dot{x} = f(x, u, u_d) \quad (2.17)$$

$$y = g(x, u, u_d), \quad (2.18)$$

where  $x = [q \ \dot{q}]^T$ ,  $f(x, u, u_d)$  is a nonlinear process function and  $g(x, u, u_d)$  is a nonlinear output function. To validate the nonlinear derived model, the FAST code and the derived model are linearized. However, since the operating point of the wind speed and the wave frequency change the linear dynamics, the derived model is presented as a combined linear time-varying model:

$$M(w_\omega)\ddot{q} + C(w_\omega, w_v)\dot{q} + K(w_v)q = F(w_v)u + F_d(w_\omega)u_d, \quad (2.19)$$

where  $w_\omega$  is the wave frequency and  $w_v$  is the mean wind speed. Using a similar model representation, the parameters of the linear FAST model and the derived time-varying models are compared, over a range of wind speeds and wave frequencies.

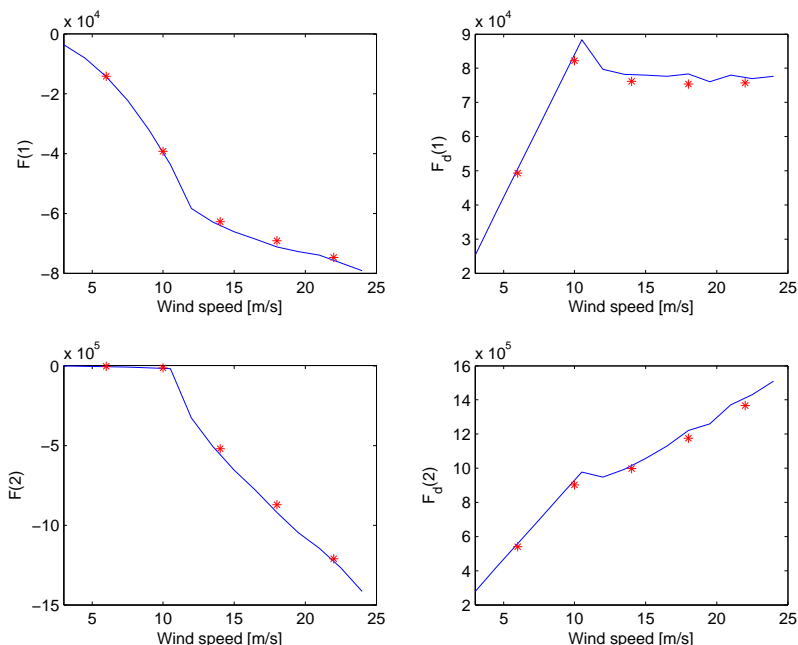


Figure 2.9: Parameter validation of the input matrix  $F$  and the disturbance matrix  $F_d$ , where blue is the linearized parameters of the derived model in Paper B and red is the linearized parameters of the FAST code.

A simple example of parameter validation related to the wind speed is presented in Figure 2.9, where the parameters of the input matrix and the disturbance matrix are compared. The comparison presents the linearization of the nonlinear aerodynamics as a

function of wind speed, where  $F(1)$  and  $F_d(1)$  are the rotor thrust parameters, and  $F(2)$  and  $F_d(2)$  are the rotor torque parameters. In the example, the control input signal is the blade pitch angle  $u = \beta$  and the disturbance input is the wind speed  $u_d = v$ . In Figure 2.9, a sudden change in the parameters is observed at 11 m/s, which is caused by the blade pitch controller to reduce produced power. Based on the wind speed, the operation trajectories for the blade pitch angle and the rotor speed are defined, which explains the change in the parameters of the process.

The result in Figure 2.9 strengthens our confidence in the derived control model with respect to the time-varying wind speed disturbance matrix and the input matrix. A similar procedure, is followed to validate the time-varying matrices of inertia, damping, stiffness, and the wave frequency-dependent disturbances.

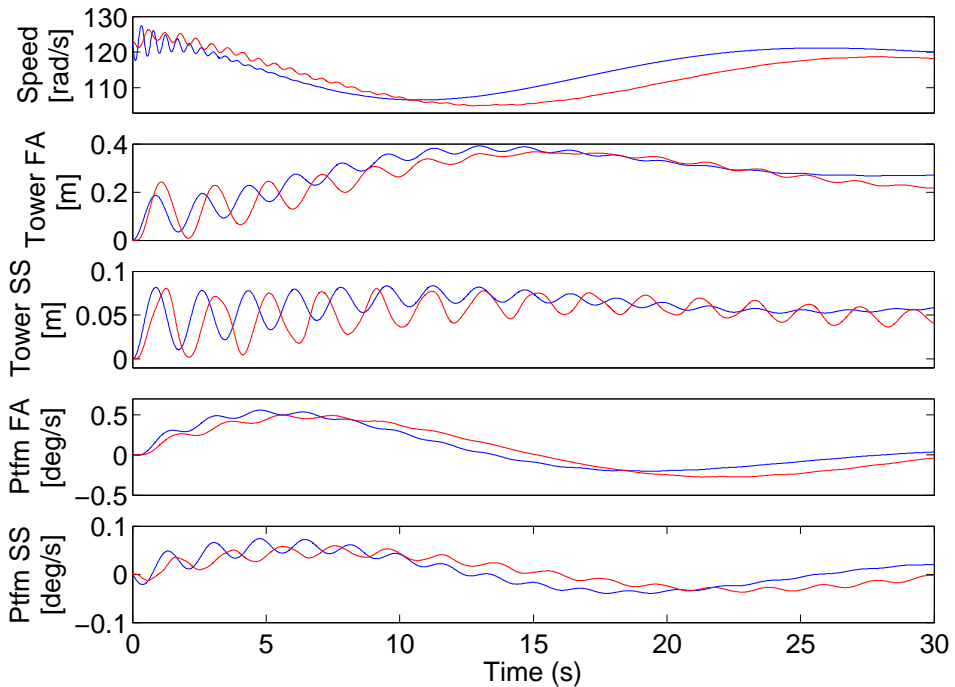


Figure 2.10: Model validation of selected states where red is the nonlinear FAST code simulation and blue is the presented control model. At time zero the floating wind turbine is released from an upright orientation in still waters at a wind speed of 14 m/s.

Figure 2.10 presents a graphical comparison. The dynamic response of a floating wind turbine is presented as a comparison between the nonlinear high-fidelity model in FAST and a the linear time-varying model. The linear time-varying model used for Figure 2.10 is presented in Paper B, which has the same structure as in Equation 2.19, however, more DOFs are included in the model of Paper B.

The figure shows the response of a floating wind turbine when released from an up-right orientation at time zero. The environmental conditions for the experimental setup are a constant wind speed of 14 m/s and still waters, thus disturbances from the turbulence of the wind and incident waves are not included in the comparison study. The rotor is spinning at rated speed, with constant generator torque and constant blade pitch angle.

The presented states are the generator speed, the tower deflection in fore-aft and side-side, and the platform rotation in fore-aft and side-side. The figure shows that the two models with different levels of complexity show similar behaviour in frequency context and amplitude levels with minor shifting in time and difference in damping. This consolidates the model validation applied throughout this thesis.

## 3 | Summary of Contributions

In the following, the progress of the contributions in this dissertation will be described. To address the problem formulation regarding negative damping, the contributions are presented within the scope of practical solutions which improve performance with respect to the objectives.

The contributions of this thesis were initiated in Paper A, where the issue of negative damping in tower fore–aft was addressed. A control model was derived using methods of system identification, and a control strategy was suggested comprising an EKF for wind speed estimation and an LQR controller. In relation to the objectives, the results showed a reduction in fatigue when compared to a baseline controller.

Due to the single operation point limitations of the linear control model in Paper A, a linear time–varying model was suggested in Paper B. Based on a new control model including variable wind speed and wave frequency, a gain–scheduled LQR was implemented which relied on estimates of the mean wind speed and the wave frequency. Thus, the EKF in Paper A for wind speed estimation was combined with an RLS filter to estimate the wave frequency.

To further fulfill the objective of reducing fatigue, a new operating strategy was suggested in Paper C. Instead of operating at constant rotor speed when above the rated wind speed, an alternative operating curve was suggested to minimize the rotor thrust force, and thus improve fatigue. The results showed a general improvement at the cost of increased actuation, when compared to the constant rotor speed approach that is normally applied above rated.

In Paper D, the disturbance of incident waves was addressed to further improve the fatigue life. Using an EKF for state estimation, the wave loads were estimated and counteracted using additional blade pitch. The unstable closed–loop system comprising a floating wind turbine and a conventional onshore controller was extended with an additional control loop which stabilized the system. This result allows a control loop to be added to the normal onshore or bottom fixed control and is thus leaning on industrial practice.

A more formal framework was suggested in Paper E, which addressed the same objective as that of Paper D. To deal with wave disturbances and improve the performance, a control strategy was suggested, comprising an EKF for state and system estimation, a dynamic reference model of the desired closed–loop response, and an MPC controller to correct the error. This result allows us to describe the desired behavior as a reference using response of a dynamical reference model of the desired closed–loop system.

This summarizes the development within reducing the negative damping on floating

wind turbines. In the following, a more detailed outline of the contributions will be given.

### 3.1 Linear Time-Varying Control Model

In paper A, a linear control model is derived using methods of system identification. Due to the nonlinear nature of the system, the model is only valid for single point operation, where the identification problem is based on the output from a simulation using FAST. In Paper B, the dynamics are analyzed and a nonlinear control model is derived. The result is based on first principles modeling as described in Chapter 2 and not system identification of a simulated response as in paper A. A linear time-varying model is presented that captures the gyroscopic effect and includes stochastic aerodynamics and hydrodynamics, and deterministic structural and actuator dynamics. The time-varying terms of the model are the mean wind speed and wave frequency. The mean wind speed determines the nonlinear aerodynamic thrust and torque, while the wave frequency determines the nonlinear hydrodynamics added mass and potential damping. The control model is

$$\mathbf{M}(w_\omega)\ddot{\mathbf{q}} + \mathbf{C}(w_\omega, w_v)\dot{\mathbf{q}} + \mathbf{K}(w_v)\mathbf{q} = \mathbf{F}(w_v)_{\text{wind}} + \mathbf{F}(w_\omega)_{\text{wave}} + \mathbf{F}_{\text{ref}}, \quad (3.1)$$

where  $w_\omega$  is the wave frequency and  $w_v$  is the mean wind speed. On the left hand side of Eq. 3.1, the model comprises structural dynamics, aerodynamics, and hydrodynamics where  $\mathbf{M}$  is the inertia,  $\mathbf{C}$  is the damping,  $\mathbf{K}$  is the stiffness and  $\mathbf{q}$  represents the degrees of freedom. On the right hand side are the external forces induced by the wind, waves, and actuators. A linear time-varying control model is presented suitable for model-based control which serves as a basis for Papers B, C, D and E.

### 3.2 Gain-Scheduled LQR control

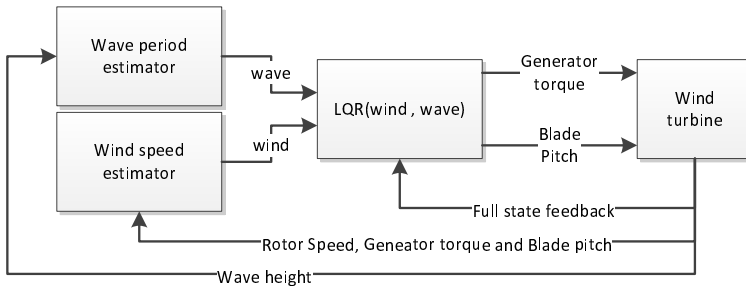


Figure 3.1: Overview of the gain-scheduled LQR control strategy.

A gain-scheduled LQR controller is presented in Paper B. The controller is based on the linear time-varying model, which depends on the mean wind speed and the wave frequency. The optimal controller gains are calculated offline, along the trajectories of the wind speeds and wave frequencies. In Figure 3.1, these controller gains are presented as  $\text{LQR}(\text{wind}, \text{wave})$ , where ‘wind’ denotes the wind speed and ‘wave’ denotes the wave

frequency. Based on estimates of ‘wind’ and ‘wave’ the controller gains are found by interpolation at each time step.

The wind speed estimator is based on the EKF presented in Paper A, while the wave frequency estimator is presented in Paper B. An important application of the presented gain–scheduled LQR controller is presented in Paper C, where it is possible to compare operation strategies such as the conventional operation strategy and the minimal thrust operation strategy.

### 3.3 Extended Onshore Control

A method to extend conventional onshore control to a floating wind turbine is presented in Paper D. Without redesigning the whole control system, the onshore controller is preserved and an additional control loop is designed. The suggested control strategy stabilizes the negative damped tower oscillations in fore–aft while reducing the impact of the wave induced loads on the structure. The strategy is presented in Figure 3.3.

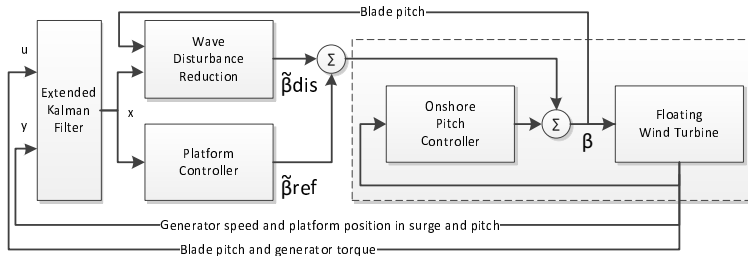


Figure 3.2: Overview of pitch control strategy. The output of the onshore controller is corrected by improved feedback and wave disturbance reduction.

The method includes an EKF to estimate the states needed for both the platform controller and the wave disturbance reduction. To achieve these estimates, stochastic models for both the wind speed and wave loads are implemented as part of the filter. The result is an additional blade pitch signal, which stabilizes the platform and accommodates the wave induced moments on the platform.

### 3.4 Reference Model–based Predictive Control

Paper E presents a method to reduce the disturbance induced by incident waves, which is based on MPC. The method is presented in Figure 3.3, where the response of an ideal undisturbed closed–loop system is estimated and then used for the control reference,  $r(n+1, n+2, n+3|n)$ . The open–loop system matrices  $A(n)$  and  $B(n)$ , and the state vector  $x(n)$ , are estimated using an EKF based on the input  $u(n)$  and output  $y(n)$  of the disturbed system.

Based on the errors between the references and the states, the MPC minimizes a performance function, in order to reduce the effect of incident waves so that the controlled system has the closest possible response to that of the undisturbed system.



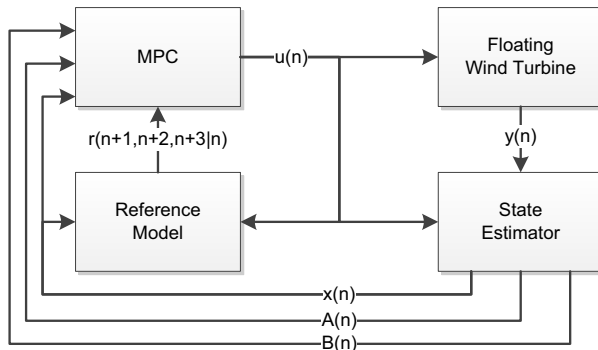


Figure 3.3: Control strategy comprising a state estimator, a reference model, and an MPC controller.

### 3.5 Paper Contributions

The objectives were addressed in Papers A to E and a summary of these contributions follows:

- **Paper A**

An LQR controller is combined with an EKF for wind speed estimation and control of a floating wind turbine. A single inertia model of the combined tower and platform dynamics is identified using methods of system identification with input from simulations in FAST. An LQR controller is designed which stabilizes the floating wind turbine and improves the performance. *This paper was published in: The Proceedings of IEEE Multi-Conference on Control Applications, (CACSD) 2011*

- **Paper B**

A linear time-varying control model of a floating wind turbine is presented which depends on the mean wind speed and the wave frequency. Combining aero-, hydro-, and structural dynamics, the model is useful for advanced control methods. Based on the model, the response of a gain-scheduled LQR controller is presented, indicating the importance of the wave frequency estimation. *This paper was submitted to: IEEE Transactions on Control Systems Technology*

- **Paper C**

A strategy is proposed to improve the fatigue lifetime of a floating wind turbine by reducing the rotor thrust force. The thrust is reduced by minimizing the thrust coefficient  $C_t$  without violating the power coefficient  $C_p$ . A new operating strategy for the rotor speed, generator torque and blade pitch is suggested, which shows an advantage when compared to the conventional strategies of constant speed. *This paper was published in: The Proceedings of IEEE Multi-Conference on Control Applications, (CCA) 2012*

- **Paper D**

An unstable closed-loop system including a conventional onshore controller is extended with additional control loops which stabilize the platform and reduces the

impact of incident waves. An EKF is implemented to estimate the states and parameters, which allows a combination of state–feedback control and disturbance accommodating control. A solution to the problem of negative damping is presented. *This paper was published in: The Proceedings of The Science of Making Torque from Wind 2012*

- **Paper E**

A framework for model–based reference control is presented using MPC. An EKF including stochastic models for the wave loads is implemented to estimate the process and the ideal closed–loop reference. Based on a dynamical reference model of the undisturbed system, the floating wind turbine is controlled using MPC to damp and reduce the impact of wave disturbance on the mooring system of the structure. *This paper was submitted to: American Control Conference 2013*



## 4 | Conclusion

The control of a floating wind turbine has been addressed in this dissertation, where the objectives have been focused on the development of a linear time-varying control model and model-based control to optimize power, reduce the impact of the disturbances and improve the fatigue. The scope has been limited to feasible controller solutions relevant for the Hywind Demo and the industrial partners of the NORCOWE project. Based on available sensor signals on a commercial Hywind Demo, the unavailable signals are estimated and controllers are designed to address the dynamics and environmental conditions of the Hywind Demo. To acknowledge industrial practice, some of the presented controllers are presented as additional loops designed for commercial wind turbine control systems.

In the context of fatigue reduction, both the process and the disturbances have been investigated. A significant portion of the fatigue is induced by load variations from turbulent wind and incident waves. The properties of these disturbances have been identified and the dynamics have been combined with the structure into a model suitable for control design purposes.

The aero- and hydrodynamics are inherently nonlinear. To support model based control design, a linear time-varying control model representation has been derived. The dynamics are presented as linear functions of the wind speed and the wave frequency. Using a generalized linear representation, the model describes a wind turbine mounted on a platform of the spar buoy type exposed to wind and waves. To our knowledge, this is the first such control model that combine aero- structural- and hydrodynamics in a consistent way.

The control of a floating wind turbine has been addressed by providing novel technological solutions, derived from commercial onshore wind turbine control systems. Based on a limited set of realistic measurements available on platforms such as the Hywind Demo, this dissertation demonstrates a practical approach, using observers to estimate the unknown states and to distinguish between signals and disturbances. The controllers were tested on high fidelity codes of a ballast stabilized spar buoy, similar to the Hywind Demo, to address a practical application.

Three controllers are presented in the dissertation which address the overall objectives, based on different methods. A gain-scheduled linear quadratic controller was presented which included both the mean wind speed and the wave frequency as scheduling variables. The controller captured the changing dynamics caused by wind and waves, demonstrating the importance of knowing the wave frequency. The wave frequency is a parameter which influences inertia, damping, and external forces in terms of the hydrodynamics, which relates to the general performance in terms of power and fatigue.

The potential of adding an additional control loop was investigated to stabilize the response of the onshore controller, while reducing the impact of incident waves. This solved the problem of negative damping fore–aft oscillations induced by the commercial wind turbine controllers and extended it to use on floating wind turbines. Instead of redesigning the entire control system, an additional control loop was simply added, which allows for well tested onshore control systems to be taken offshore and on to a floating platform.

Lastly, a model–predictive controller was presented in a framework to reduce the impact of the wave disturbances. Using a prediction of the response of the undisturbed closed–loop system as a controller reference, the results showed an improvement in disturbance accommodation.

To put results into perspectives, we choose to compare results against the response of a baseline controller from NREL which resolved the problem of negative damping by reducing the bandwidth of the controller. As a consequence of the reduced bandwidth control strategy of the NREL controller, the life-time of the pitch actuator would be extended but at the cost of reduced lifetime of other components. In our approach, the lifetime tradeoff can be made explicitly, helping in reducing the cost of the energy.

In summary, the negative damping of a floating spar buoy wind turbine has been analyzed and several control solutions have been suggested that allow the changed dynamics to be addressed. The controllers were simulated on high fidelity codes where the results successfully reached the objectives.

### 4.1 Future Work

In the following, a list of potential future work is presented which is inspired by the presented work and unresolved ideas.

- In this thesis fatigue is reduced by minimizing the amplitude of the oscillations. However, this does not truly reflect the S–N curve relation to a material subject to fatigue. To avoid violation of the S–N curves, a model predictive control method is suggested in Figure 4.1, which is extended with an S–N reference for the constraints. An S–N curve feedback is estimated based on the method of rainflow counting of the past outputs. The objectives are to correct the S–N curve error and avoid repetitive excitations at the same amplitude which cause material failure.
- The presented work is limited to the ballast–stabilized floating platform of the spar buoy type. However, the work could be extended to other floating platforms. Another interesting aspect would be to include additional actuators in the platform for stabilization. Thus, the task of platform stabilization would move from the pitch controller to a potential platform actuator controller.
- The presented time-varying control model could be extended with the rotor azimuth angle in parallel to the existing model parameters (the wind speed and wave frequency). This approach would allow individual control of the blade pitch angle, making it possible to control the loads in tower side–side and platform roll. As generator torque also induces loads in tower side–side and platform roll, optimal control laws could be formulated, where the generator torque and the blade pitch complement each other.

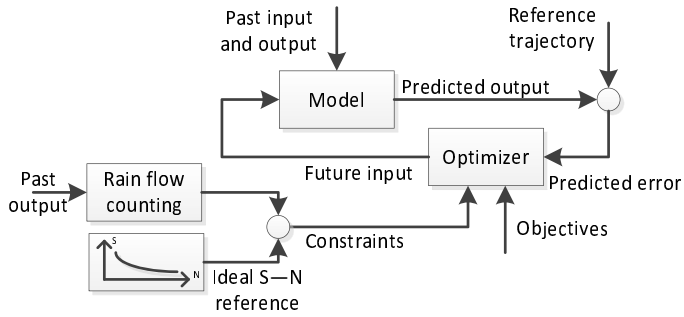


Figure 4.1: Overview of model predictive control with S–N constraints.

- It would be interesting to investigate the stability of the presented gain-scheduled linear quadratic controller, with respect to the switching of the scheduling variables.



## | References

- [Andersen and Frigaard, 2011] Andersen, T. L. and Frigaard, P. (2011). Lecture notes for the course in water wave mechanics. Technical report, Department of Civil Engineering, Aalborg University.
- [Association, 2012] Association, E. W. E. (2012). The european offshore wind industry key 2011 trends and statistics. Technical report, European Wind Energy Association.
- [Bakka and Karimi, 2012] Bakka, T. and Karimi, H. R. (2012). Robust output feedback  $h_\infty$  control synthesis with pole placement for offshore wind turbine system: An lmi approach. *IEEE International Conference on Control Applications (CCA)*, pages 1467–1472.
- [Bakka et al., 2012] Bakka, T., Karimi, H. R., and Duffie, N. A. (2012). Gain scheduling for output  $h_\infty$  control of offshore wind turbine. *The International Society of Offshore and Polar Engineers*.
- [Berthelsen and Fylling, 2011] Berthelsen, P. A. and Fylling, I. (2011). Optimization of floating support structures for deep water wind turbines. *Conference Proceedings of EWEA 2012, Copenhagen*.
- [Bossanyi, 2003] Bossanyi, E. A. (2003). Individual blade pitch control for load reduction. *WIND ENERGY*, 6:119–128.
- [Bossanyi, 2005] Bossanyi, E. A. (2005). Further load reductions with individual pitch control. *WIND ENERGY*, 8:481–185.
- [Brown and Zhang, 2004] Brown, L. J. and Zhang, Q. (2004). Periodic disturbance cancellation with uncertain frequency. *Automatica*, 40:631–637.
- [Burcharth, 2002] Burcharth, H. F. (2002). Strøm- og bølgekræfter på stive legemer. Technical report, Institutet for Vand, Jord og Miljøteknik, Aalborg University.
- [Burton et al., 2001] Burton, T., Sharpe, D., Jenkins, N., and Bossanyi, E. (2001). *Wind Energy Handbook*. Wiley.
- [Christiansen et al., 2012a] Christiansen, S., Bak, T., and Knudsen, T. (2012a). Damping wind and wave loads on a floating wind turbine. *IEEE Transactions on Control Systems Technology* – submitted.
- [Christiansen et al., 2012b] Christiansen, S., Bak, T., and Knudsen, T. (2012b). Minimum thrust load control for floating wind turbine. *IEEE Multi-Conference on Systems and Control*.



## REFERENCES

---

- [Christiansen et al., 2011] Christiansen, S., Knudsen, T., and Bak, T. (2011). Optimal control of a ballast-stabilized floating wind turbine. *IEEE Multi-Conference on Systems and Control*.
- [Christiansen et al., 2012c] Christiansen, S., Knudsen, T., and Bak, T. (2012c). Extended onshore control of a floating wind turbine with wave disturbance reduction. *The Science of Making Torque from Wind*.
- [Christiansen et al., 2013] Christiansen, S., Tabatabaeipour, S. M., Bak, T., and Knudsen, T. (2013). Wave disturbance reduction of a floating wind turbine using a reference model-based predictive control. *American Control Conference – submitted*.
- [Downing and Socie, 1982] Downing, S. D. and Socie, D. F. (1982). Simple rainflow counting algorithms. *International Journal of Fatigue*, 4:31–40.
- [Fossen, 2011] Fossen, T. I. (2011). *Handbook of Marine Craft Hydrodynamics and Motion Control*. WILEY.
- [Frigaard and Burcharth, 1989] Frigaard, P. and Burcharth, H. F. (1989). Wave loads on cylinders. CEEC COMETT Seminar on Wave and Ice Forces on offshore structures.
- [Hanson et al., 2011] Hanson, T. D., S., B., Yttervik, R., Nielsen, F. G., and Havmller, O. (2011). Comparison of measured and simulated responses at the first full scale floating wind turbine hywind. *Conference Proceedings of EWEA 2011, Brussels*.
- [Henriksen et al., 2010] Henriksen, L. C., Poulsen, N. K., and Hansen, M. H. (2010). *Model Predictive Control of Wind Turbines*. PhD thesis, Technical University of Denmark.
- [Johnson, 1986] Johnson, C. D. (1986). Disturbance-accommodating control; an overview. *American Control Conference*, pages 526–536.
- [Jonkman, 2010a] Jonkman, J. (2010a). Definition of the floating system for phase iv of oc3. Technical report, National Renewable Energy Laboratory.
- [Jonkman, 2010b] Jonkman, J. (2010b). *NWTC Design Codes*. National Renewable Energy Laboratory.
- [Jonkman et al., 2007] Jonkman, J., Butterfield, S., Musial, W., and Scott, G. (2007). Definition of a 5-mw reference wind turbine for offshore system development. Technical Report NREL/TP-500-38060, National Renewable Energy Laboratory.
- [Jonkman and Scлавounos, 2006] Jonkman, J. and Scлавounos, P. (2006). Development of fully coupled aeroelastic and hydrodynamic models for offshore wind turbines. Technical report, National Renewable Energy Laboratory.
- [Jonkman, 2007] Jonkman, J. M. (2007). *Dynamics Modeling and Loads Analysis of an Offshore Floating Wind Turbine*. PhD thesis, National Renewable Energy Laboratory.
- [Jonkman, 2008] Jonkman, J. M. (2008). Influence of control on the pitch damping of a floating wind turbine. *2008 ASME Wind Energy Symposium*.

- [Karimirad, 2011] Karimirad, M. (2011). *Stochastic Dynamic Response Analysis of Spar-Type Wind Turbines with Catenary or Taut Mooring Systems*. PhD thesis, Norwegian University of Science and Technology.
- [Karimirad and Moan, 2011] Karimirad, M. and Moan, T. (2011). Extreme dynamic structural response analysis of catenary moored spar wind turbine in harsh environmental conditions. *Journal of Offshore Mechanics and Arctic Engineering*, 133.
- [Knudsen et al., 2011] Knudsen, T., Bak, T., and Soltani, M. (2011). Prediction models for wind speed at turbine locations in a wind farm. *Wind Energy*. Submitted.
- [Kober and King, 2010] Kober, A. and King, R. (2010). Model predictive control for wind turbines. In *Proceedings of European Wind Energy Conference*.
- [Kristiansen et al., 2005] Kristiansen, E., Hjulstad, Å., and Egeland, O. (2005). State-space representation of radiation forces in time-domain vessel models. *Ocean Engineering*, 32:2195–2216.
- [Kumar and Stol, 2009] Kumar, K. and Stol, K. (2009). Scheduled model predictive control of a wind turbine. In *AIAA/ASME Wind Energy Symposium*.
- [Lackner, 2010] Lackner, M. A. (2010). Controlling platform motions and reducing blade loads for floating wind turbines. *Wind Engineering*, 33:541–553.
- [Larsen and Hanson, 2007] Larsen, T. J. and Hanson, T. D. (2007). A method to avoid negative damped low frequent tower vibrations for a floating pitch controlled wind turbine. *journal of Physics: Conference Series*, 75.
- [Lindeberg et al., 2012] Lindeberg, E., Svendsen, H. G., and Uhlen, K. (2012). Smooth transition between controllers for floating wind turbines. *Energy Procedia*, 24:83–98.
- [Ljung, 2000] Ljung, L. (2000). *System Identification Toolbox - for use with MATLAB, User's Guide*. The Mathworks, Inc. Sherborn, Mass, 5rd edition edition.
- [Luo, 2011] Luo, N. (2011). Smart structural control strategies for the dynamic load mitigation in floating offshore wind turbines. *International Workshop on Advanced Smart Materials and Smart Structures Technology*.
- [Maciejowski, 2002] Maciejowski, J. (2002). *Predictive control: with constraints*. Pearson education.
- [Mayne et al., 2000] Mayne, D. Q., Rawlings, J. B., Rao, C. V., and Sokaert, P. O. M. (2000). Constrained model predictive control: stability and optimality. *Automatica*, 36:789–814.
- [Namik, 2012] Namik, H. (2012). *Individual Blade Pitch and Disturbance Accommodating Control of Floating Offshore Wind Turbines*. PhD thesis, The University of Auckland.
- [Namik and Stol, 2008] Namik, H. and Stol, K. (2008). State-space control of tower motion for deepwater floating offshore wind turbine. *AIAA Aerpspace Sciences Meeting and Exhibit*, 46:15976–15993.

## REFERENCES

---

- [Namik and Stol, 2009a] Namik, H. and Stol, K. (2009a). Disturbance accommodating control of floating offshore wind turbines. *Proc. AIAA/ASME Wind Energy Symp.*
- [Namik and Stol, 2009b] Namik, H. and Stol, K. (2009b). Individual blade pitch control of floating offshore wind turbines. *Wind Energy*, 13 Issue 1:74–85.
- [Østergaard, 2008] Østergaard, K. Z. (2008). *Robust, Gain-Scheduled Control of Wind Turbines*. PhD thesis, Aalborg University.
- [Passon et al., 2007] Passon, P., Kühn, M., Butterfield, S., Jonkman, J., Camp, T., and Larsen, T. J. (2007). Oc3–benchmark exercise of aero-elastic offshore wind turbine codes. *The Science of Making Torque from Wind*.
- [Santos, 2007] Santos, R. (2007). *Damage mitigating control for wind turbine*. PhD thesis, University of Colorado at Boulder.
- [Schlipf et al., 2012] Schlipf, D., Schlipf, D. J., and Kühn, M. (2012). Nonlinear model predictive control of wind turbines using lidar. *Wind Energy*.
- [Shikha et al., 2003] Shikha, Bhatti, T. S., and Kothari, D. P. (2003). Aspects of technological development of wind turbines. *Journal of Energy Engineering*, 129.
- [Skaare et al., 2007a] Skaare, B., Hanson, T. D., and Nielsen, F. G. (2007a). Importance of control strategies on fatigue life of floating wind turbines. *Proceedings of 26th International Conference on Offshore Mechanics and Arctic Engineering*.
- [Skaare et al., 2007b] Skaare, B., Hanson, T. D., Nielsen, F. G., Yttervik, R., Hansen, A. M., Thomsen, K., and Hansen, T. J. (2007b). Integrated dynamic analysis of floating offshore wind turbines. Technical report, Risoe.
- [Skaare et al., 2011] Skaare, B., Hanson, T. D., Yttervik, R., and Nielsen, F. G. (2011). Dynamic response and control of the hywind demo floating wind turbine. *Conference Proceedings of EWEA 2011, Brussels*.
- [Stol and Balas, 2003] Stol, K. A. and Balas, M. J. (2003). Periodic disturbance accommodating control for blade load mitigation in wind turbines. *Journal of Solar Energy Engineering, ASME*, 125:379–385.
- [Stol and Zhao, 2006] Stol, K. A. and Zhao, W. (November 2006). Individual blade pitch control for the controls advanced research turbine (cart). *Journal of Solar Energy Engineering*, Volume 128:498 (8 pages).
- [Sutherland, 1999] Sutherland, H. J. (1999). On the fatigue analysis of wind turbines. Technical report, SAND99-0089, NM: Sandia National Laboratories.
- [UpWind, 2011] UpWind (2011). Design limits and solutions for very large wind turbines; a 20 mw turbine is feasible. Technical report, UpWind.
- [van der Veen et al., 2012] van der Veen, G., Couchman, L., and Bowyer., R. (2012). Control of floating wind turbines. *American Control Conference*, pages 3148–3153.

- [WAMIT, 2006] WAMIT (2006). *WAMIT - User Manual - The State of The Art in Wave Interaction Analysis*. WAMIT, Inc.
- [Wright, 2004] Wright, A. D. (2004). Modern control design for flexible wind turbines. Technical report, National Renewable Energy Laboratory.



# Contributions

---

<b>Paper A: Optimal Control of a Ballast–Stabilized Floating Wind Turbine</b>	<b>45</b>
<b>Paper B: Damping Wind and Wave Loads on a Floating Wind Turbine</b>	<b>61</b>
<b>Paper C: Minimum Thrust Load Control for Floating Wind Turbine</b>	<b>81</b>
<b>Paper D: Extended Onshore Control of a Floating Wind Turbine with Wave Disturbance Reduction</b>	<b>97</b>
<b>Paper E: Wave Disturbance Reduction of a Floating Wind Turbine Using a Reference Model–based Predictive Control</b>	<b>111</b>

---



# Paper A

## **Optimal Control of a Ballast–Stabilized Floating Wind Turbine**

S. Christiansen, T. Knudsen and T. Bak

This paper was published in:  
The Proceedings of IEEE Multi-Conference on Control Applications, (CACSD)  
2011



Copyright ©IEEE  
*The layout has been revised*

### Abstract

Offshore wind energy capitalizes on the higher and less turbulent wind speeds at sea. The use of floating structures for deeper waters is being explored. The control objective is a tradeoff between power capture and fatigue, especially that produced by the oscillations caused by the reduced structural stiffness of a floating installation in combination with a coupling between the fore–aft motion of the tower and the blade pitch. To address this problem, the present paper models a ballast-stabilized floating wind turbine, and suggests a linear quadratic regulator (LQR) in combination with a wind estimator and a state observer. The results are simulated using aero elastic code and analysed in terms of damage equivalent loads. When compared to a baseline controller, this controller clearly demonstrates better generator speed and power tracking while reducing fatigue loads.

## 1 Introduction

In the field of wind energy, new and promising wind turbine concept are being developed. More reliable wind turbines makes installation possible in harsher environments, such as offshore in shallow waters, where the winds are stronger and the hazard to human eyes and ears is less. In shallow water it is possible to install monopiles, but in places where water depths are greater than 30 meters, constrained floating wind turbines are economically competitive. Fig. 5.1 shows a ballast-stabilized floating wind turbine constrained by three mooring lines. The installation is light enough to float and heavy enough to be aligned in a stable upright position. The floating installation in Fig. 5.1 represents the setup for the first full size floating installation, Hywind [1].

The main objective for the control of wind turbines is to maximize power production while minimizing fatigue loads. Fatigue is the wear accumulated over time of key components such as the tower, gearbox, blades, and bearings. If a wind turbine is operated to maximize power production regardless of fatigue loads, this will significantly decrease the lifetime of its key components. This is especially important for a constrained floating wind turbine which by nature is influenced by a constant vibration caused by ocean waves and wind. Therefore a trade-off between maximized power production and minimized fatigue loads is required for optimal performance.

Applying conventional onshore control strategies to floating turbines has been shown to impose negative damped oscillations on the platform motion, [2] and [3]. The onshore controller causes the blade pitching to increase the rotor thrust as the wind speed decreases and vice versa, which causes an increase in fatigue and a possible instability.

A tower damping control strategy was introduced in [2] using a wind estimator applied to a ballast-stabilized wind turbine, and it showed reduced tower oscillation at the cost of reduced power output. In [4] a Gain Scheduled Proportional Integrating (GSPI) controller showed good performance regarding tower oscillations but overshoots rated power and generator speed, which may reduce generator lifetimes. A Linear Quadratic Regulator (LQR) was applied to a floating wind turbine in [5] which showed improved results with respect to power stability and tower oscillations compared to [4].



Figure 5.1: 5MW ballast-stabilized floating wind turbine. ©2011 by Statoil.

This paper presents a new approach to stabilization of the ballast-stabilized floating wind turbine concept from [2], the Hywind structure as seen in Fig. 5.1. Inspired by [5], an LQR controller is applied to the turbine control problem. The turbine structure addressed by [5] was based on a  $160 \text{ m}^2$  floating barge, whereas this paper addresses a ballast-stabilized floating wind turbine. We also present a more realistic control design requiring only a few sensors, in contrast to [5] where full state feedback was assumed.

The controller aims to minimize the tower oscillation while optimizing the power production at rated power with special attention to reducing overproduction in electrical power, and secondly, to reducing generator overspeed. These objectives are achieved by means of an LQR controller combined with an extended Kalman filter for wind estimation and a state observer for unavailable states. Furthermore a model of a ballast-stabilized floating wind turbine is derived. The model is based on the 5 MW ballast-stabilized floating NREL wind turbine ([6]) which resembles the Hywind structure.

In the following, a dynamical state space model of the ballast-stabilized wind turbine will be presented. Next, applied control theories will be stated, followed by the experimental setup. The results in terms of damage equivalent loads (DEL), means and standard deviations will be presented and compared to a baseline controller by NREL, [6]. The results of the comparison will be discussed and a concluding section will sum up the scientific contribution.

## 2 Methods

### Ballast-stabilized floating wind turbine model

In order to apply linear control theory, a linear model must be determined which identifies the dominant dynamic behaviour of the floating wind turbine (FWT). The dynamics of a wind turbine can be separated into those of the drive train, the structure, the actuator, and the wind.

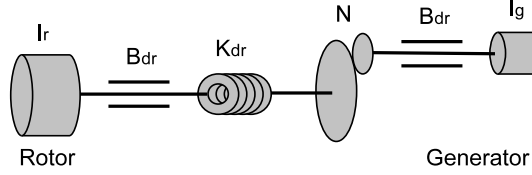


Figure 5.2: Symbolic drawing of a drivetrain consisting of two inertias, a spring, a damper and a gear.

The drivetrain is modeled as a third order system as in Fig. 5.2 where  $I_r$  and  $I_g$  are the rotor and generator shaft inertias,  $K_{dr}$  is the spring constant,  $B_{dr}$  is the damper constant, and  $N$  is the gear ratio. This approach allows modeling the torsion in the rotor shaft of the drivetrain.

The structural dynamics of the wind turbine is modeled as a second order system where the aerodynamic force on the rotor acts on a mass in connection with a spring and a damper.

The generator and the blade pitch system are modeled as first order actuators. The dynamic turbulence of the wind is modeled as a first order Gaussian white noise filter.

The ballast-stabilized FWT is modeled by a nonlinear system of differential equations  $\dot{x} = f(x, u, w)$  where

$$\dot{x} = \begin{pmatrix} \frac{-B_{dr}}{I_r} \Omega + \frac{B_{dr}}{I_r N} \omega - \frac{K_{dr}}{I_r} \phi + \frac{1}{I_r} M_a \\ \frac{B_{dr}}{I_g N} \Omega - \frac{B_{dr}}{I_g N^2} \omega + \frac{K_{dr}}{I_g N} \phi - \frac{1}{I_g} M_g \\ \Omega - \frac{1}{N} \omega \\ \dot{z} \\ \frac{-K_t}{m_t} z - \frac{D_t}{m_t} \dot{z} + \frac{F_a}{m_t} \\ \frac{1}{\tau_\beta} (\beta_c - \beta) \\ \frac{1}{\tau_g} (M_{gc} - M_g) \\ \frac{-\pi v_m v_t}{2L} + n \end{pmatrix} \quad (5.1)$$

is a function of  $x = (\Omega \ \omega \ \dot{z} \ \beta \ M_g \ v_t)^T$ , actuators  $u = (\beta_c \ M_{gc})^T$  and Gaussian white noise  $n = \epsilon$ . The elements  $x_{1,2,3}$  are devoted to the drive train, where  $\Omega$  and  $\omega$  are the angular velocities of the rotor and generator respectively, and  $\phi$  is the drive train twist angle.  $x_{4,5}$  represents the structure where  $z$  is the top tower displacement. The actuators  $x_{6,7}$  denote the blade pitch angle and generator torque respectively. The element  $x_8$  is devoted to the ambient turbulence model where  $v_t$  is the turbulence velocity.

The model output is defined as  $y = [\Omega \ \omega \ \ddot{z} \ \beta]$ . The outputs are considered realistic, resembling a standard wind turbine with tower oscillation issues hence accelerometers have been installed in the nacelle for damping tower oscillations. However, such important measurements as the wind speed are assumed not available since the nacelle anemometer reading measures the local wind speed which is very disturbed by pitching, blade passing and tower movements to such a degree that it is too uncertain for control purposes. Other measurements such as drivetrain torsion and platform pitch velocity are not standard measurements and hence not considered available.

Adding the aerodynamic rotor thrust  $F_a$  and torque  $M_g$  to Eq. 5.1 the system clearly becomes nonlinear, as follows:

$$M_a = \frac{1}{\Omega} \frac{1}{2} A \rho C_p(\lambda, \beta) v_r^3, \quad \lambda = \frac{R\Omega}{v_r} \quad (5.2)$$

$$F_a = \frac{1}{2} A \rho C_t(\lambda, \beta) v_r^2, \quad (5.3)$$

where  $v_r$  is the relative wind speed defined as  $v_r = v_t + v_m - \dot{z}$  and  $v_m$  is the static mean wind velocity.

The nonlinear model is linearized using a first order Taylor series which linearizes the plant about an expected operation point, thus the dynamics about this point is represented in state space by

$$\dot{\tilde{x}} = A\tilde{x} + B\tilde{u} + G\tilde{w}, \quad (5.4)$$

such that  $A = \frac{\partial f(\bar{x}, \bar{u}, \bar{w})}{\partial x}$ ,  $B = \frac{\partial f(\bar{x}, \bar{u}, \bar{w})}{\partial u}$  and  $G = \frac{\partial f(\bar{x}, \bar{u}, \bar{w})}{\partial w}$ , where  $\tilde{x} = x - \bar{x}$ ,  $\tilde{u} = u - \bar{u}$  and  $\tilde{w} = w - \bar{w}$  describes the deviation from the operation points.

The model is based on the 5 MW ballast-stabilized floating NREL wind turbine [6] using the same parameters of the drivetrain. However due to the complexity of the tower and platform dynamics, the equivalent spring, damper and mass constants were revealed by means of a step response in the blade pitch angle imposing large fore–aft oscillation. The results were analysed using Lennart Ljung’s system identification toolbox [7] to identify the tower parameters.

## Control design

Optimal control is suggested for achieving good performance at rated power in the sense of minimizing tower oscillation while optimizing the power production with special attention to reducing overproduction in electrical power and secondly reducing generator overspeed. A constant torque approach is used to remove the generator dynamics. In [4] this approach as shown to damp tower fore–aft oscillations. To achieve a steady power output using a constant generator torque approach it is important that the error in generator speed is removed thus a new state is introduced  $\dot{\tilde{x}}_\omega = \tilde{\omega}$ . A state observer is used to recover the unknown states.

The suggested control loop is shown in Fig. 5.3 and is combined with a wind speed estimator (WSE), a state observer for state estimation and a linear quadratic regulator (LQR) for optimal control. The output of the wind estimator is fed to the observer as an input  $\tilde{u}_w$  and to the LQR controller as a state  $\tilde{x}_w$ . Next, the three modules of the controller are chronologically explained and argued.

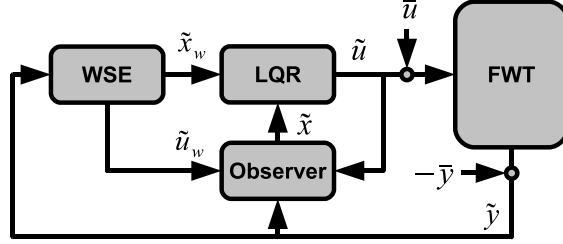


Figure 5.3: Block diagram of proposed LQR and EKF control strategy for floating wind turbines.

The wind turbine has two disturbance inputs which are wave and wind. The wind disturbance is considered the major disturbance and is observed by the wind estimator while the wave disturbance remains unmodeled. However, the wave effect on the tower can be argued as included in the measurement of the total tower acceleration and to some extent also included in the rotor speed, however, wave impact is explicitly represented in the control design. This claim is supported by [8], which states that the response of a parked ballast-stabilized floating wind turbine is excited by the coupled wind and wave impact. The response of platform pitch is dominated by the wind. Despite harsh environmental conditions no instabilities was found in the coupled wind and wave response.

### Wind speed estimator

The relative wind speed can be estimated based on measurements of the rotor velocity, blade pitch angle and the generator torque. Based on a simple model of the drive train and a turbulence model, an extended Kalman filter (EKF) is used to estimate the relative wind speed as suggested in [9].

The drive train is modeled as a first order system assuming a stiff drive train neglecting losses. The wind turbulence is modeled as a second order system.

$$J\dot{\Omega}_{dr} = M_a - M_g N \quad (5.5)$$

$$\dot{v}_t = -a(v_m)v_t + n_1 \quad (5.6)$$

$$\dot{v}_m = n_2, \quad (5.7)$$

where  $n_1, n_2$  are Gaussian white noise. The implemented EKF uses information about the linear model, disturbances and measurements to estimate the states consisting of a time update part and a measurement update part, [10]. The time update uses information about the model dynamics and the model uncertainties to estimate the states.

$$\hat{x}_k^- = A\hat{x}_{k-1} + Bu_{k-1} \quad (5.8)$$

$$P_k^- = AP_{k-1}A^T + Q \quad (5.9)$$

The measurement update uses information about the model outputs and measurement

noise.

$$K_k = P_k^- C^T (C P_k^- C^T + R)^{-1} \quad (5.10)$$

$$\hat{x}_k = \hat{x}_k^- + K_k (z_k - C \hat{x}_k^-) \quad (5.11)$$

$$P_k = (I - K_k C) P_k^- \quad (5.12)$$

### Linear State Observer

The purpose of the state observer is to estimate the drive train torsion,  $\phi$ , and the tower displacement,  $z$ . The wind speed is at this point the estimated  $\tilde{u}_w$ . Notice, however, that the uncertainty is ignored. The observer is implemented by satisfying  $\dot{\tilde{x}} = (A - LC)\tilde{x}$  where  $\tilde{x}$  is the state error and  $L$  is the observer gain. To insure stable observation the eigenvalues of  $A - LC$  are placed faster than the closed loop eigenvalues. The eigenvalues of the observer are found by shifting the eigenvalues of the closed loop system 120 to the left. The eigenvalues of the implemented state observer are

$$\lambda = [-193 \pm 47j, -140, -124, -120 \pm 0.10j, -130]. \quad (5.13)$$

### Linear Quadratic Regulator

The LQR control design is applied to the linear state space system in Eq. 5.4 except for the generator dynamics. The generator integral state is added forming a new state vector  $\tilde{x} = (\tilde{\Omega} \tilde{\omega} \tilde{\theta} \tilde{z} \tilde{\beta} \tilde{v}_t \tilde{x}_\omega)^T$  with system input  $\tilde{u} = \tilde{\beta}$ . Besides this, the design of the LQR control is straightforward: weighting the estimated states and inputs with respect to performance objectives, by minimizing the cost function

$$J = \int_0^\infty (x^T Q x + u^T R u) dt, \quad (5.14)$$

where  $Q$  is positive semi-definite and  $R$  is positive definite. Requiring full state information, the controller calculates a system input  $u = -Kx$  where the states are multiplied by the feedback gain matrix  $K$  which is found by solving the Riccati differential equation.

The implemented controller has the following properties

$$Q = \text{diag}(0, 49, 0.05, 0, 6, 0, 0, 0, 0, 500000)^{-2} \quad (5.15)$$

$$R = 10^{-2}. \quad (5.16)$$

The controller aims at limiting variations in generator speed to 49 rad/s, drivetrain torsion to 0.05 rad, top tower velocity to 6 m/s and electrical power within 500 kW by varying the blade pitch angle within 10 deg.

## 3 Experimental Setup

### Simulation Environment

The control system explained in this paper is compared to previous results under equal environmental conditions at a mean wind speed of 18 m/s with an air density of 1.225 kg/m<sup>3</sup> and a turbulence intensity in longitudinal, crosswise and vertical of  $[u \ v \ w] = [14.86\%$

10.40% 7.43%] respectively. The significant wave height of the incident waves are 6 meters simulated at water depth of 320 meters and a water density of  $1025 \text{ kg/m}^3$ . The waves are aligned with the direction of the wind, thus perpendicular wind and waves are not considered in this paper and are therefore not included in the environmental setup.

## Software

The wind turbine is a three bladed upwind 5MW reference wind turbine specified by NREL in [11], and implemented in the wind turbine simulation tool FAST which is well recognized in the OC3 code benchmark, [12]. The implementation of the wind turbine installation consist of the 5MW reference turbine mounted on a ballast-stabilized buoy to resemble an upscaled version of the 2.3MW Hywind wind turbine. The floating wind turbine has a rotor radius of 63 meters, a height of 90 meters, and six degrees of freedom.

The simulations were performed in Simulink Matlab v7.9.0 (R2009b) linked with FAST v7.00.00a-bjj and AeroDyn v13.00.00a-bjj compiled for the OC3 Hywind running Windows 7 32bit. Damage equivalent load calculations are performed using MCrunch v.100 which is an implementation of [13].

## NREL Baseline controller

To provide a baseline for assessing the performance, a GSPI baseline controller by NREL [6] has also been implemented. For all wind speeds the GSPI Baseline control strategy is shown in fig. 5.4, where PI is the proportional integrating controller, GS is the gain scheduling, Lookup is a lookup table, and FWT is the floating wind turbine.

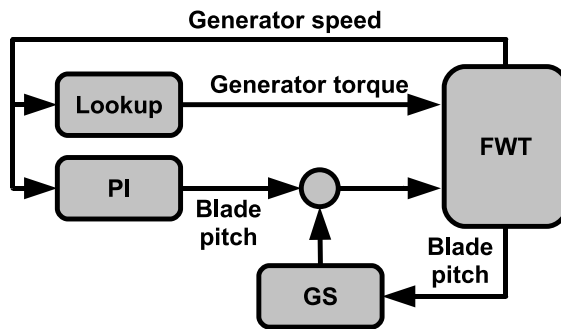


Figure 5.4: Block diagram of NREL baseline control strategy for floating wind turbines.

The lookup table translates the generator speed directly to generator torque. The blade pitch controller is a GSPI controller based on the generator speed error and blade pitch. The controller gains are scheduled as functions of the blade pitch angle, thus

$$\theta_{ref} = \left( K_P + \frac{1}{s} K_I \right) GS(\theta) (\omega - \omega_{ref}), \quad (5.17)$$

where  $K_P$  is the proportional gain,  $K_I$  is the integral gain, and  $GS(\theta)$  is a lookup table function of the current blade pitch angle. Finally the desired set point for the blade pitch



angle is defined as  $\theta_{ref}$ . The NREL Baseline controller is designed to avoid negative tower damping which has resulted in a slow varying blade pitch control.

## 4 Results

The results of the LQR controller are presented by comparing its results to those of the state-of-the-art baseline controller. The controllers are compared with respect to turbine performance and damage equivalent loads (DELs) in time-series and statistical performance. The results presented are all turbine analysis based on the same 600 second of simulations.

### Turbine Time-series Performance

The electrical power output of the two controllers are presented in Fig. 5.5 where the objective is to produce a steady 5MW of electrical power while minimizing power fluctuation.

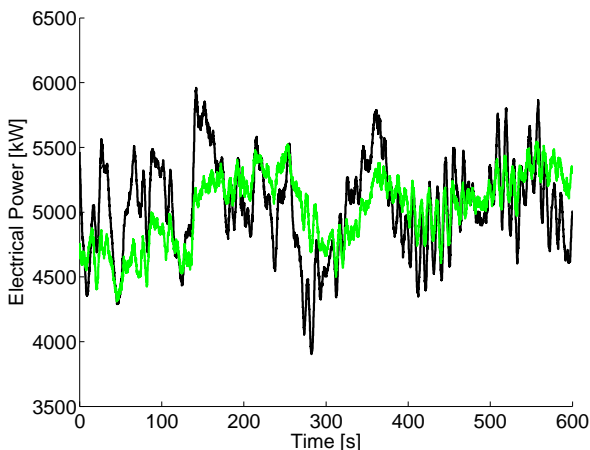


Figure 5.5: Time series of electrical power; black is the baseline, green is the LQR controller.

The generator speed performance is presented in Fig. 5.6 which, due to the constant generator torque approach, is just a scaling of the electrical power in Fig. 5.5. Indicated in the figure are the rated generator speed 1173.7 RPM and a 10% generator overspeed.

Platform pitching is presented in Fig. 5.7, showing how the two controllers induce fore-aft oscillations on the platform starting from an initial condition of 0 degrees.

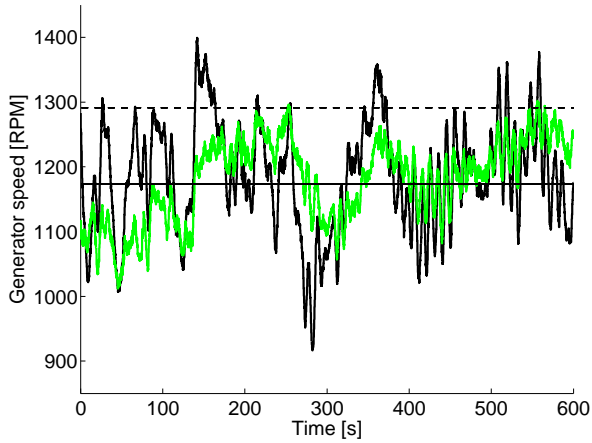


Figure 5.6: Time series of generator speed; black is the baseline and green is the LQR controller. The solid line is rated generator speed at 1173.7 RPM and the dashed line is 10% overspeed.

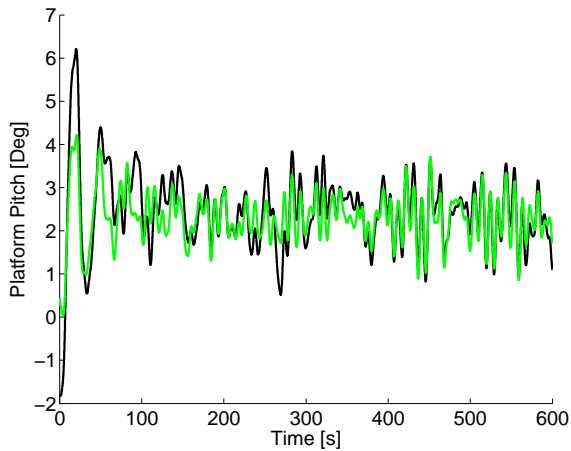


Figure 5.7: Time series of platform pitch angle; black is the baseline, green is the LQR controller.

While a constant torque approach is utilized, the only available actuator is the blade pitch system. In Fig. 5.8 activity level of the blade pitch angle is presented for the two controllers.

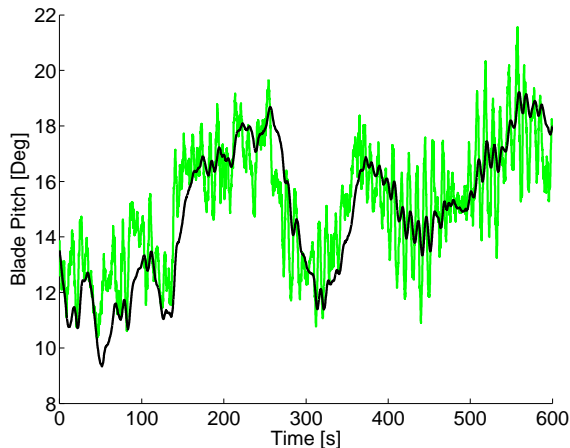


Figure 5.8: Time series of blade pitch angle; black is the baseline, green is the LQR controller.

## Turbine Statistical Performance

In Table 8.9, the two controllers are compared with respect to mean electrical power and standard deviations to reveal the effect of integral action on the generator speed error.

A selection of relevant performance measures are compared and presented in Fig. 5.9, where the bars represent the relative performance improvement of the LQR controller compared to the Baseline controller in percentage. The figure includes further perspectives of the electrical power results in Table 8.9.

	Controllers	
	Baseline	LQR
Power (MW)	5.0 [0.4]	5.0 [0.3]

Table 5.1: Electrical power: mean and standard deviation (in brackets), for baseline and LQR.

The turbine performance is analysed using a statistical approach, presenting the mean, standard deviations (std), and damage equivalent load (DEL).

## 5 Discussion

The results are discussed with respect to fatigue and maximized performance which in general are two controversial objectives. The results present a trade off between these

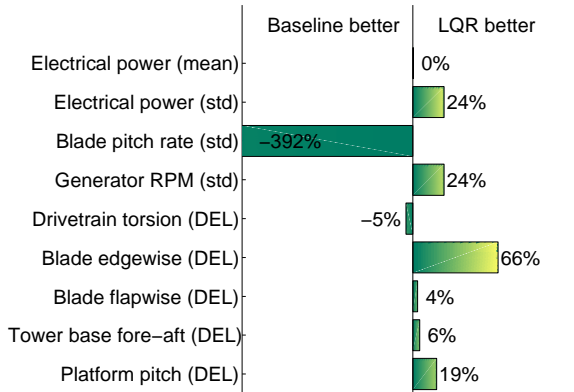


Figure 5.9: Statistical analysis of relative controller performance with respect to mean, standard deviation (std), and damage equivalent loads (DEL) in percentage, where a positive sign indicates better performance using the LQR controller.

objectives showing an increase in power performance at the cost of increased pitch activity. By means of integral action both controllers successfully reach the rated 5 MW in Table 8.9 with widely different performance. Comparing the two controllers, the LQR is able to significantly reduce the fatigue in both platform pitch moments by 19% and tower base fore-aft moments of 6% in Fig. 5.9. This has been accomplished while stability in power and generator speed has been highly improved reducing the standard deviations by 24% in Fig. 5.9. This clearly shows that the system is controllable and able to fulfill the controller objectives.

The strict LQR generator speed control results in a 5% increase in DEL of the drivetrain torsion caused by a more rapidly changing generator speed. To avoid negative tower damping, the baseline presents a conservative generator speed control approach thus allowing generator speed to reach levels higher than 10% overspeed. This puts special demands on the generator design, which normally are designed for rated speeds allowing minor fluctuations and overspeeds for only a limited period of time. In contrast, the presented LQR controller is able to limit the generator speed fluctuations to 10% of rated generator speed and reaches rated generator speed within a short time.

The increase in blade pitch rate is explained by the strict generator speed control demanding a higher level of pitch activity. However the consequence is a significant 66% reduction in edgewise blade moment and a slight reduction in flapwise blade moment of 4% compared to the baseline controller. The relatively small improvement in flapwise blade moments is explained by the fact that high levels of blade pitch activity also impose blade flapwise DEL, since lower levels of pitch angles increase the flap moments. In contrast to this, high levels of blade moments are the consequence of the conservative pitch control strategy of the Baseline controller since rapidly changing wind speeds are not accommodated by the pitch controller, causing an increase in DELs.

Electrical components on wind turbines are as well designed and optimized to rated electrical power allowing only some fluctuation. Due to the constant torque approach, the overspeed seen in the baseline generator speed is also present in the power performance with a peak electrical overproduction of 20% as well as power drops compared to only minor fluctuation of 10% for the LQR. Whether variable generator torque control can eliminate overproduction without major drawbacks in DELs remains to be investigated.

## 6 Conclusion

With respect to control design, a model of a floating wind turbine has been derived, revealing enough of the principal dynamics to damp oscillations and control the system of a floating wind turbine. Unavailable measurements have been successfully estimated using observer design. Based on an LQR controller combined with integral action, it has been shown that controller objectives are met, delivering a stable and satisfying performance in both electrical power, fatigue levels, and platform oscillations.

Despite higher drivetrain fatigue levels and an unavoidable increase in blade pitch actuation, the LQR controller is an acceptable controller based on the simple fact that the controller is able to limit generator overspeed and electrical overproduction in contrast to the Baseline controller. Whether torque control can further improve performance remains to be investigated.

Wind estimation combined with state observation in an LQR control design offers great advantage and possibilities in obtaining stability on floating wind turbines.

## References

- [1] Statoil, “Hywind facts sheet,” september 2009. [Online]. Available: <http://www.statoil.com>
- [2] B. Skaare, T. D. Hanson, and F. G. Nielsen, “Importance of control strategies on fatigue life of floating wind turbines,” *Proceedings of 26th International Conference on Offshore Mechanics and Arctic Engineering*, 2007.
- [3] T. Burton, D. Sharpe, N. Jenkins, and E. Bossanyi, *Wind Energy Handbook*. Wiley, 2001.
- [4] J. M. Jonkman, “Influence of control on the pitch damping of a floating wind turbine,” *2008 ASME Wind Energy Symposium*, 2008.
- [5] H. Namik and K. Stol, “Individual blade pitch control of floating offshore wind turbines,” *Wind Energy*, vol. 13 Issue 1, pp. 74–85, 2009.
- [6] J. Jonkman, “Definition of the floating system for phase iv of oc3,” National Renewable Energy Laboratory, Tech. Rep., 2010.
- [7] L. Ljung, *System Identification Toolbox - for use with MATLAB, User's Guide.*, 5th ed., The Mathworks, Inc. Sherborn, Mass, 2000.
- [8] M. Karimirad and T. Moan, “Extreme dynamic structural response analysis of catenary moored spar wind turbine in harsh environmental conditions,” *Journal of Offshore Mechanics and Arctic Engineering*, vol. 133, 2011.
- [9] T. Knudsen, T. Bak, and M. Soltani, “Prediction models for wind speed at turbine locations in a wind farm,” *Wind Energy*, 2011, submitted.
- [10] G. Welch and G. Bishop, “An introduction to the kalman filter,” University of North Carolina at Chapel Hill, Tech. Rep., 2006.

- [11] J. Jonkman, S. Butterfield, W. Musial, and G. Scott, "Definition of a 5-mw reference wind turbine for offshore system development," National Renewable Energy Laboratory, Tech. Rep. NREL/TP-500-38060, 2007.
- [12] P. Passon, M. Kühn, S. Butterfield, J. Jonkman, T. Camp, and T. J. Larsen, "Oc3-benchmark exercise of aero-elastic offshore wind turbine codes," *The Science of Making Torque from Wind*, 2007.
- [13] S. D. Downing and D. F. Socie, "Simple rainflow counting algorithms," *International Journal of Fatigue*, vol. 4, pp. 31–40, 1982.

# Paper B

## **Damping Wind and Wave Loads on a Floating Wind Turbine**

S. Christiansen, T. Bak and T. Knudsen

This paper was submitted to:  
Journal on IEEE Transactions on Control Systems Technology



Copyright ©IEEE  
*The layout has been revised*

## Abstract

Offshore wind energy capitalizes on the higher and less turbulent wind speeds at sea. To enable deployment of wind turbines in deep-water locations, structures are being explored, where wind turbines are placed on a floating platform. This combined structure presents a new control problem, due to the partly unconstrained movement of the platform and ocean waves excitation. If this additional complexity is not dealt with properly, this may lead to a significantly increase in the structural loads, and potentially instability of the controlled system. In this paper the wave excitation is investigated and we show the influence that both wind speed, wave frequencies and misalignment between wind and waves have on the system dynamics. A new control model is derived that extend standard turbine models to include the hydrodynamics, additional platform degrees of freedom, the platform mooring system, and tower side-side motion including gyroscopic effects. The models support a model-based design that includes estimators for wind speed and wave frequency. The design is applied to a number of examples representing different wind and wave conditions, and successfully demonstrates a reduction in the structural oscillations while improving power performance.

## 1 Introduction

In the field of wind energy, new and promising wind turbine concepts are being developed. More reliable wind turbines make it possible to install them in harsher environments, such as offshore, where the winds are stronger and the visual impact is less. In shallow waters it is possible to install monopiles, but in places where water depths are greater than 60 meters, floating wind turbines are economically competitive.

The main objective is to produce energy reliably at a competitive cost. To achieve that, maximizing the power and minimizing the fatigue is necessary. Fatigue is basically the wear accumulated over time on key components such as the tower, gearbox, blades, and bearings. If a wind turbine is operated to maximize power production regardless of fatigue loads, the lifetime of key components will significantly decrease and the cost of energy will go up. This is especially important for a floating wind turbine which by nature is influenced by a constant contribution of oscillations from wind and ocean waves. Therefore a trade-off between maximization of the power production and minimization of the fatigue loads is required for optimal performance.

Applying conventional onshore control strategies to floating wind turbines has been shown to impose negative damped oscillations on the platform motion. The onshore controller causes the blade pitching to increase the rotor thrust as the wind speed decreases and vice versa, which couples with the platform dynamics in a way that produces large oscillations in platform pitch and possibly instability. Reducing the bandwidth of the pitch controller ensure stability, but performance deteriorates.

A tower damping control strategy was introduced in [1] using a wind estimator applied to a ballast-stabilized wind turbine, and it showed reduced tower oscillation at the cost of reduced power output. In [2] a gain scheduled proportional integrating (GSPI) controller showed good performance regarding tower oscillations but overshoots rated power and generator speed, which may reduce the generator lifetime. The task of damping tower oscillations was addressed by [3], suggesting an influence of tower acceleration on blade pitch control. A linear quadratic regulator (LQR) was applied to a floating wind turbine in

[4, 5] which showed improved results in power stability and tower oscillations compared to [2]. In [4] a control strategy using individual blade pitch and generator torque reduced tower side-side oscillation in a floating structure. In [6] individual blade pitch and constant generator torque was combined with speed reference feedback from the platform pitch.

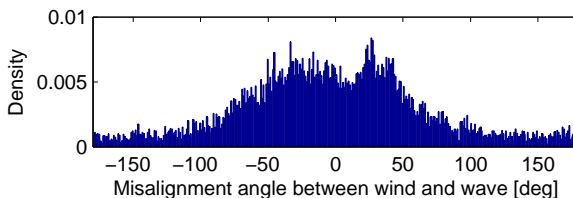


Figure 6.1: Probability density function of wave misalignment at the Hywind location sampled primary during the first five months of 2010.

In the references above, misalignment between wind and waves is not considered due to the assumption that the waves over time align with the wind.

Data from the floating wind turbine Hywind Demo (delivered by Statoil) is presented in Figure 6.1. It shows that misalignments do occur and it is hence relevant to address this in control design. Furthermore, the literature on the control strategies of floating wind turbines does not account for the frequency dependence of the hydrodynamic damping. In this paper we show that both wind speed and wave frequencies have a substantial influence on the total system damping.

In the context of model-based control, this paper contributes with a new control model of a floating wind turbine is presented, which accounts for hydrodynamics, additional platform degrees of freedom, the platform mooring system, and tower side-side motion and gyroscopic effects. This model allows us to address the topics above in the control design.

Based on the model, a new control structure is presented, which includes estimates of wind speed and wave frequency in the controller. The result is a control strategy capable of actively damping structural oscillations while fulfilling the objective of maximizing power. The control strategy allows us to operate at the designed bandwidth of the wind turbine pitch system while avoiding stability problems.

## 2 Methods

### A coupled aero- and hydro-dynamic control model

A simulation tool such as FAST [7] is able to simulate a floating wind turbine and linearize the system at some operating point. However, the model presented here is nonlinear and depends on the wind speed and the wave frequency which will prove valuable in the control design.

The forces acting on the system can be described by

$$\begin{aligned} \mathbf{M}\ddot{q} + \mathbf{F}_{\text{hydro}} + \mathbf{F}_{\text{mooring}} + \mathbf{F}_{\text{gravity}} + \\ + \mathbf{F}_{\text{gyro}} + \mathbf{F}_{\text{tower}} = \mathbf{F}_{\text{wind}} + \mathbf{F}_{\text{wave}} + \mathbf{F}_{\text{ref}}. \end{aligned} \quad (6.1)$$

The forces are both linear and nonlinear, where  $\mathbf{M}$  are the structural masses,  $q$  represents degrees of freedom (DOF),  $\mathbf{F}_{\text{hydro}}$  are the hydrodynamic added masses and damping.  $\mathbf{F}_{\text{mooring}}$  are forces from mooring lines,  $\mathbf{F}_{\text{gravity}}$  are gravitational forces,  $\mathbf{F}_{\text{gyro}}$  are gyroscopic effects, and  $\mathbf{F}_{\text{tower}}$  are tower deflection forces. The external forces are thrust force from the wind, denoted  $\mathbf{F}_{\text{wind}}$ , and wave induced loads, denoted  $\mathbf{F}_{\text{wave}}$ . The forces induced by the actuators are denoted  $\mathbf{F}_{\text{ref}}$ .

The freedom of the system can be described by

$$q = \begin{bmatrix} x \\ y \\ z \\ \theta_r \\ \theta_p \\ \theta_y \\ \hline x_t \\ y_t \\ \hline \psi \\ \phi \\ \tau \\ \beta \end{bmatrix} = \begin{bmatrix} \text{Platform surge} \\ \text{Platform sway} \\ \text{Platform heave} \\ \text{Platform roll} \\ \text{Platform pitch} \\ \text{Platform yaw} \\ \hline \text{Tower fore-aft} \\ \text{Tower side-side} \\ \hline \text{Rotor azimuth} \\ \text{Drivetrain torsion} \\ \hline \text{Generator torque} \\ \text{Blade pitch angle} \end{bmatrix}, \quad (6.2)$$

which describes platform translation  $(x, y, z)$  and rotation  $(\theta_r, \theta_p, \theta_y)$ , tower deflection  $(x_t, y_t)$ , and actuator dynamics  $(\tau, \beta)$ .

The model is based on well known wind turbine models from the literature on on-shore wind turbines comprising aerodynamics, tower dynamics, drivetrain dynamics, and actuator dynamics [8]. However, the hydrodynamic effects on the masses and friction of the platform has been included in the model [9, 10, 11]. Wind and wave loads can influence both the tower fore-aft and side-side, thus these dynamics are also included in the model. The ability of the platform to move in translational directions is closely related to the dynamics of the mooring system. This system is designed to prevent the platform for drifting away and to ensure yaw stiffness. This stiffness is important to keep the wind turbine upwind. However, an uneven wind distribution on the rotor plane can induce yaw moment on the platform. Another effect which can induce yaw moments is the gyroscopic effect of the rotor caused by fore-aft motions. Therefore both the mooring system and the gyroscopic effect are included in the model.

The combined system can be described as a nonlinear system, which depend on the wind speed and the wave frequency:

$$\mathbf{A}(w_\omega)\ddot{q} + \mathbf{B}(w_\omega)\dot{q} + \mathbf{C}q = \mathbf{F}_{\text{wind}} + \mathbf{F}_{\text{wave}} + \mathbf{F}_{\text{ref}}, \quad (6.3)$$

where  $w_\omega$  is the frequency of the propagating ocean wave. The notation of  $(\mathbf{A}(w_\omega), \mathbf{B}(w_\omega))$

is relaxed to  $(A, B)$ , thus,

$$\mathbf{A} = \begin{bmatrix} \mathbf{P}_A & \mathbf{P}T_A & \mathbf{0}_{6 \times 2} & \mathbf{0}_{6 \times 2} \\ \mathbf{T}P_A & \mathbf{T}_A & \mathbf{0}_{2 \times 2} & \mathbf{0}_{2 \times 2} \\ \mathbf{0}_{2 \times 6} & \mathbf{0}_{2 \times 2} & \mathbf{D}_A & \mathbf{0}_{2 \times 2} \\ \mathbf{0}_{2 \times 6} & \mathbf{0}_{2 \times 2} & \mathbf{0}_{2 \times 2} & \mathbf{N}_A \end{bmatrix} \quad (6.4)$$

$$\mathbf{B} = \begin{bmatrix} \mathbf{P}_B & \mathbf{P}T_B & \mathbf{0}_{6 \times 2} & \mathbf{0}_{6 \times 2} \\ \mathbf{T}P_B & \mathbf{T}_B & \mathbf{0}_{2 \times 2} & \mathbf{0}_{2 \times 2} \\ \mathbf{0}_{2 \times 6} & \mathbf{0}_{2 \times 2} & \mathbf{D}_B & \mathbf{0}_{2 \times 2} \\ \mathbf{0}_{2 \times 6} & \mathbf{0}_{2 \times 2} & \mathbf{0}_{2 \times 2} & \mathbf{N}_B \end{bmatrix} \quad (6.5)$$

$$\mathbf{C} = \begin{bmatrix} \mathbf{P}_C & \mathbf{P}T_C & \mathbf{0}_{6 \times 2} & \mathbf{P}N_C \\ \mathbf{T}P_C & \mathbf{T}_C & \mathbf{0}_{2 \times 2} & \mathbf{T}N_C \\ \mathbf{0}_{2 \times 6} & \mathbf{0}_{2 \times 2} & \mathbf{D}_C & \mathbf{D}N_C \\ \mathbf{0}_{2 \times 6} & \mathbf{0}_{2 \times 2} & \mathbf{0}_{2 \times 2} & \mathbf{N}_C \end{bmatrix}. \quad (6.6)$$

Here,  $\mathbf{A}$  represents the inertia,  $\mathbf{B}$  is the damping, and  $\mathbf{C}$  is the stiffness. These matrices include terms where  $\mathbf{P}$  represents the platform,  $\mathbf{T}$  is the tower,  $\mathbf{D}$  is the drivetrain, and  $\mathbf{N}$  is the actuator. The system properties are defined at the sea water level (SWL) about the vertical centerline of the platform.

In the following, all parameters going into  $\mathbf{A}$ ,  $\mathbf{B}$  and  $\mathbf{C}$  are referred to as inertia, damping and stiffness even though some are not in a physical sense.

## Modeling of Mass and Inertia

To model how a structure moves or rotates in water, the mass and inertia of the displaced water must be included. This mass and inertia are referred to as the added mass, and must be summed with the mass and inertia of the structure:  $\mathbf{P}_A = \text{diag}([m \ m \ m \ A_p \ A_r \ A_y]) + \mathbf{A}_{\text{hydro}}(w_\omega)$ , where the total system has a mass of  $m$ , pitch inertia of  $A_p$ , roll inertia of  $A_r$ , and yaw inertia of  $A_y$ . The frequency of the ocean waves is denoted by  $w_\omega$ , which determines the quantity of added mass from the water,  $\mathbf{A}_{\text{hydro}}(w_\omega)$ . However, note that the significant quantity of added mass for the given spar (Hywind Demo) platform only varies a few percent over frequency. The added mass matrix can be generated using a wave interaction analysis tool such as WAMIT for the platform [9, 12].

The wind turbine is mounted on top of the platform, and has a mass of  $\mathbf{T}_A = I_{2 \times 2} m_t$ , where  $\mathbf{I}$  the identity matrix and  $m_t$  comprises the mass of tower, nacelle hub, and blades. Of course the wind turbine has an impact on the platform and vice versa in both rotation and translation:  $\mathbf{T}P_A = \mathbf{P}T_A^T = [m_t \bar{\mathbf{I}}_{2 \times 2} \ \mathbf{0}_{2 \times 1} \ h_t m_t \hat{\mathbf{I}}_{2 \times 2} \ \mathbf{0}_{2 \times 1}]$ , where  $\bar{\mathbf{I}}_{2 \times 2} = [1 \ 0; 0 \ -1]$ ,  $\hat{\mathbf{I}}_{2 \times 2} = [0 \ -1; 1 \ 0]$ , and  $h_t$  is the distance from SWL to the center of mass (COM) of the tower.

The inertias of the drivetrain are defined by  $\mathbf{D}_A = [A_d \ A_t; A_t \ A_t]$ , where  $A_d$  is the inertia of the drivetrain and  $A_t$  is the inertia of the torsion in the rotor shaft. The possibility of altering the operation of the generator and rotor effectiveness is achieved using actuators. The inertias of the actuators are defined by  $\mathbf{N}_A = \text{diag}([m_b \ m_g])$ , where  $m_b$  is the inertia of the blade pitch actuator and  $m_g$  is the inertia of the generator torque actuator.

## Modeling of Damping

The damping of the platform is affected by gyroscopic effects, hydrodynamics, and linear damping:  $\mathbf{P}_B = \mathbf{B}_{\text{gyro}} + \mathbf{B}_{\text{hydro}}(w_\omega) + \mathbf{B}_{\text{viscous}}$ . The rotor causes a damping force on the platform due to the gyroscopic effect between the platform yaw and the pitch:  $\mathbf{B}_{\text{gyro}} = [\mathbf{0}_{4 \times 4} \ \mathbf{0}_{4 \times 2}; \mathbf{0}_{2 \times 4} \ 3I_B \hat{\mathbf{I}}\dot{\psi}]$ , where  $I_B$  is the inertia of one blade about the rotor axis and  $\dot{\psi}$  is speed of the rotor. The hydrodynamic damping  $\mathbf{B}_{\text{hydro}}(w_\omega)$  is caused by platform movement or rotation in the water. In contrast to the added mass, hydrodynamic damping is highly frequency dependent. Hydrodynamic damping can also be generated using a wave interaction analysis tool such as WAMIT [9, 12]. The linear damping  $\mathbf{B}_{\text{viscous}}$  is an empirical damping verified in [9] to resemble the Hywind Demo in the OC3 Hywind FAST simulator [7].

The tower deflection has a damping of  $\mathbf{T}_B = I_{2 \times 2} B_t$ , where  $B_t$  is the tower damping. However, the tower deflection has a damping effect on the platform rotation, hence  $\mathbf{P}T_B = TP_B^T = [0_{2 \times 3} \ h_t B_t \bar{\mathbf{I}}_{2 \times 2} \ \mathbf{0}_{2 \times 1}]$ .

The drivetrain has a friction defined by  $\mathbf{D}_B = \text{diag}([0 \ B_d])$ , where  $B_d$  resembles the viscous friction of the torsion in the flexible shaft of the drivetrain.

The damping of the actuators are defined by  $\mathbf{N}_B = \text{diag}([B_g \ B_p])$ , where  $B_g$  resembles the electrical damping of the generator, while  $B_p$  resembles the mechanical damping in the pitch actuator.

## Modeling of Stiffness

The stiffness of the platform is defined by  $\mathbf{P}_C = K_{\text{hydro}} + K_{\text{mooring}} + K_{\text{gravity}}$ , where  $\mathbf{K}_{\text{hydro}}$  is the hydrostatic restoring stiffness,  $\mathbf{K}_{\text{mooring}}$  is the stiffness caused by the mooring lines, and  $\mathbf{K}_{\text{gravity}}$  is the stiffness due to gravity.

The stiffness of the flexible tower is defined by  $\mathbf{T}_C = \text{diag}([K_t \ K_t])$ , where  $K_t$  is the tower stiffness. However, the flexible tower also has an impact on the platform stiffness:  $\mathbf{T}P_C = PT_C^T = [0_{2 \times 3} \ -m_t g \bar{\mathbf{I}} \ \mathbf{0}_{2 \times 1}]$ , where  $g$  is the gravitational acceleration and  $\bar{\mathbf{I}} = [0 \ 1; 1 \ 0]$ .

The stiffness related to the drivetrain is defined by  $\mathbf{D}_C = \text{diag}([0 \ K_d])$ , where  $K_d$  is the stiffness in the torsion of the drivetrain. There is also a stiffness related to the actuator, defined by  $\mathbf{N}_C = [K_g \ K_p]$ , where  $K_g$  is the stiffness related to the electrical torque generation and  $K_p$  is the mechanical stiffness in the blade pitch system. However, the generator torque also has an impact on the drivetrain:  $\mathbf{D}N_C = [N \ 0; 0 \ 0]^T$  where  $N$  is the gear ratio and also an impact on the tower's side-side deflection:  $\mathbf{T}N_C = [0 \ -N/h_h; 0 \ 0]^T$ , and since the tower deflection is only relative to the platform,  $\mathbf{P}N_C = [0_{2 \times 1} \ -N/h_h \bar{\mathbf{I}}_{2 \times 1} \ \mathbf{0}_{2 \times 1} \ -N/h_h \bar{\mathbf{I}}_{2 \times 1} \ \mathbf{0}_{2 \times 2}]^T$ , where  $\bar{\mathbf{I}}_{2 \times 1} = [1 \ 0]^T$  and  $h_h$  is the height from the SWL to the hub.

## Aerodynamic Forces

The aerodynamic force of the wind is defined by  $\mathbf{F}_{\text{wind}} = [F_t \ \mathbf{0}_{1 \times 3} \ h_h F_t \ 0 \ F_t \ 0 \ M_a \ M_a \ \mathbf{0}_{1 \times 2}]^T$ , where the aerodynamic rotor thrust  $F_t$  and torque  $M_a$  have a nonlinear effect on the system, given by  $F_t = \frac{1}{2} A \rho C_t(\lambda, \beta) v_r^2$  and  $M_a = \frac{1}{\Omega} \frac{1}{2} A \rho C_p(\lambda, \beta) v_r^3$  where  $\lambda = \frac{R\Omega}{v_r}$  is the ratio between the blade tip speed and the relative wind speed. The relative wind speed  $v_r$  is defined by  $v_r = v - \dot{x} - h_h \dot{\theta}_p - \dot{x}_t$ , where  $v$  is the ambient wind speed,  $\dot{x}$  is the

platform surge velocity,  $h_n$  is the height from SWL to hub,  $\theta_p$  is the platform pitch and  $\dot{x}_t$  is relative tower displacement. Since this expression includes some of the system states, an impact on the system damping is expected. The partial derivatives of the aerodynamic thrust force  $\partial F_t/\partial\Omega$ ,  $\partial F_t/\partial\dot{x}$ ,  $\partial F_t/\partial\dot{\theta}_p$ ,  $\partial F_t/\partial\beta$  and the aerodynamic moments  $\partial M_a/\partial\Omega$ ,  $\partial M_a/\partial\dot{x}$ ,  $\partial M_a/\partial\dot{\theta}_p$ ,  $\partial M_a/\partial\beta$ , are thus included in the damping matrix,  $\mathbf{C}$ , and the stiffness matrix,  $\mathbf{K}$ .

### Wave Excitation Force

The wave excitation force describes the impact of a single incident wave on the platform by  $\mathbf{F}_{\text{waves}} = \text{Re} \{ A_w \mathbf{X}(w_\omega, w_\beta) e^{jw_\omega t} \}$ , where  $A_w$  is the wave height,  $\mathbf{X}$  is a normalized wave excitation force vector,  $w_\omega$  is the wave frequency, and  $w_\beta$  is the wave's direction. As wave excitation force does not depend on any DOF's of the control model, the wave excitation force has no impact on the natural damping of the system.

### Inputs Reference

The system has two controllable inputs, which are defined by  $\mathbf{F}_{\text{ref}} = [\mathbf{0}_{1 \times 10} \ u_g \ u_p]^T$ , where  $u_g$  is the reference for the generator torque and  $u_p$  is the reference for blade pitch angle.

### Model Validation of Control Model

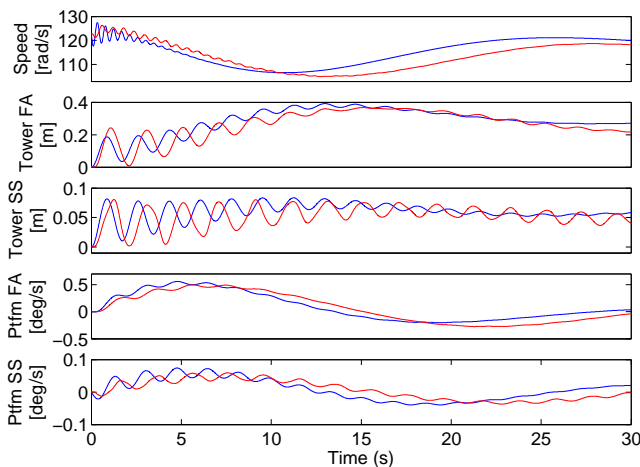


Figure 6.2: Model validation of selected states where red is the FAST code simulation and blue is the presented control model. At time zero the FWT is released from horizontal in still waters at a wind speed of 14 m/s.

To validate the presented model, a time series comparison is presented in figure 6.2 between the OC3 Hywind model of a floating wind turbine (FWT) and the presented

control model. The figure shows the response of the FWT when released from a horizontal orientation at time zero.

The presented states are generator speed, tower deflection in fore–aft and side–side, and platform rotation in fore–aft and side–side.

The rotor is spinning at rated speed, with constant generator torque and blade pitch angle. The wind speed and the wave frequency are the parameters in the presented model, thus the model is validated at a wind speed of 14 m/s in still waters. Disturbances from the turbulence of the wind and incident waves are not included in the comparison study.

The figure shows comparable behavior between the two models, in terms of the amplitude and frequency.

## Combined Aero- and Hydrodynamic Damping

To determine the combined damping of the open–loop system it is necessary to understand the aerodynamic damping. The aerodynamic damping depends on the control objectives of the wind turbine. At low wind speeds the objective is to optimize power, however at a defined rated wind speed, the objective change to limit the electrical power output. In Figure 6.3 these objectives are presented as trajectories for generator speed, blade pitch angle and generator torque.

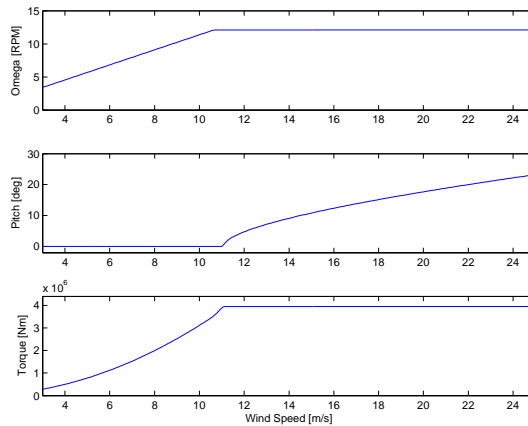


Figure 6.3: Ideal closed–loop operating strategy to maximize power below rated wind speed and reduce power above rated wind speed.

Based on these trajectories, the damping of the open loop system is presented in Figures 6.4 and 6.5, which illustrate the open loop linearized damping of the platform rotation and the relation to the wind speed and wave frequency. Due to nonlinearities (and variance in the aero- and hydrodynamics) the presented model is linearized at an interval of 0.5 m/s from 3 m/s to 25 m/s. The figure shows that the best damping of the platform rotation is achieved at a wind speed of 10.4 m/s and a wave frequency of 0.9 rad/s.



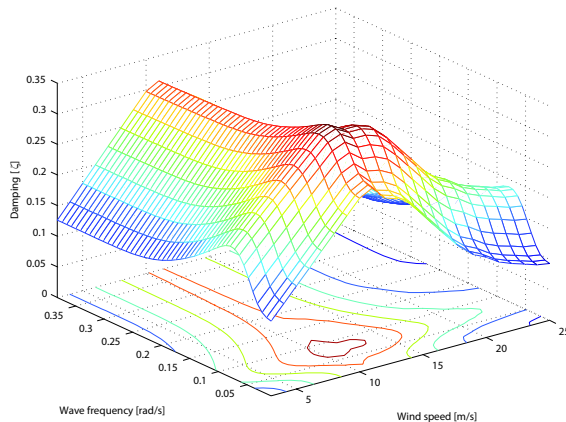


Figure 6.4: Open loop damping in platform pitch as a function of wave frequency and wind speed.

In platform roll, the wind speed has no dynamical impact. The third rotational degree of freedom is platform yaw. It is assumed that the impact of the wind and wave dynamics are insignificant on a spar buoy platform compared to other dynamics acting on the yaw, such as gyroscopic effects and the rotor yaw moments induced by the wind.

The hydrodynamic damping of the system can be explained by hydrodynamic drag, which varies over the relative wave velocity and due to the geometric and surface smoothness of the platform [13]. For deep waters, the wave velocity can be defined by  $u_\omega = a w_\omega$  at the free surface where  $a$  is the wave amplitude and  $w_\omega$  is the wave frequency. The wave amplitude is closely related to the wave spectrum which again depends on the wave frequency. Thus, the hydrodynamics damping is presented in Figures 6.4 and 6.5 as a function of wave frequency [14].

The aerodynamic damping is proportional to the aerodynamic trust force. The damping increases below the rated wind speed and decreases above the rated wind speed due to thrust reduction. In Figure 6.4 the damping seems to have a different behavior at about 10–12 m/s, which may be explained by the change in operation strategy in Figure 6.3, where constant generator speed is reached. At this point, the tip-speed-ratio goes from constant to decreasing as the wind speed increases.

### Control Strategy Above Rated Wind Speed

A model-based control strategy is chosen to control and damp the system. Despite that the control model is presented for the full wind range, a controller is designed only for wind speed above the rated wind speed to avoid transitions between objectives.

The proposed control strategy is shown in Figure 7.9, comprising a gain-scheduled LQR controller combined with wind speed and wave period estimators. Full state feedback is assumed, since the focus of this paper concerns damping, based on estimates of

wind speed and waves frequency.

The LQR controller is a linear controller which requires a linear model of the system, and several controllers are hence for various operating points of wind speeds and wave frequencies. This is achieved using the control law  $u = \bar{u}_{OP}(v_m) - \text{LQR}(v_m, w_\omega)(x - \bar{x}_{OP}(v_m))$ , where  $x = [q \dot{q}]^T$ ,  $\bar{u}_{OP}(v_m)$  and  $\bar{x}_{OP}(v_m)$  represents the operating points as functions of the mean wind speed. The controller,  $\text{LQR}(v_m, w_\omega)$ , is a gain-scheduled LQR controller which uses the slow varying mean wind speed and wave frequency as scheduling variables.

Based on the control model, the controller is designed offline and implemented as a lookup table for wind speed above the rated wind speed with a interval of 0.5 m/s and wave frequencies of 0 rad/s to 5 rad/s at an interval of 0.1 rad/s. When running online, at each time step, the controller interpolates the operating point and the controller gain.

### Wave Period Estimator

To determine the hydrodynamic contribution, the wave frequency is required. The wave period of a regular wave is straightforward to estimate. However, irregular waves are more difficult to handle. In this paper, a simple auto-regressive algorithm is implemented to estimate a model of the waves based on current wave height. The desired wave frequency is thus derived for the model as the natural frequency. The wave height is modeled as  $A(q)y(t) = e(t)$ , where  $A(q)$  is a second order system,  $y(t)$  is the wave height, and  $e(t)$  is white noise. The estimated wave height is defined by a second order model as  $\hat{y}(t, \theta) = (-y(t-1), -y(t-2))\theta$ , where  $\theta$  are the parameters of the estimation model  $\hat{A}(q)$ . The estimation error  $\epsilon(t) = y(t) - \hat{y}(t)$  is minimized using a least squares method by updating the model properties  $\theta$ . The wave frequency is determined by the natural frequency of the system  $\hat{A}(q)$ .

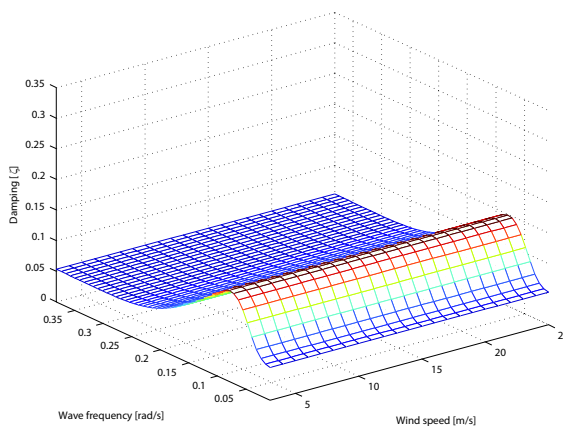


Figure 6.5: Open loop damping in platform roll as a function of wave frequency and wind speed.

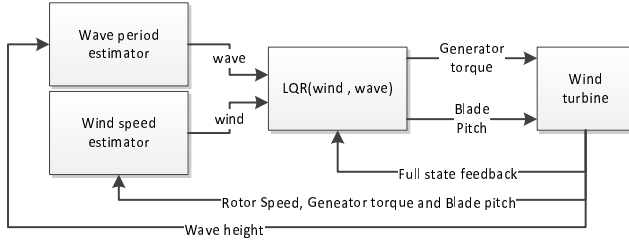


Figure 6.6: Overview of control strategy.

### Wind Speed Estimator

The wind speed can be estimated based on measurements of the rotor velocity, blade pitch angle, and the generator torque. In this study, an extended Kalman filter (EKF) is used to estimate the wind speed, as suggested in [15].

The drivetrain is modeled as a first order system assuming a stiff drive train and neglecting losses:

$$I\dot{\Omega}_{dr} = M_a - M_g N, \quad (6.7)$$

where  $I$  is the inertia of the drivetrain,  $\Omega_{dr}$  is the rotor speed, and  $N$  is the gear ratio. The wind is modeled as a second order system.

$$\dot{v}_t = -a(v_m)v_t + n_1 \quad (6.8)$$

$$\dot{v}_m = n_2, \quad (6.9)$$

where  $v_t$  and  $v_m$  are the wind turbulence and mean, respectively,  $a(v_m)$  is a wind speed dynamic parameter related to the turbulence length scale, and  $n_1$  and  $n_2$  are Gaussian white noise.

### The Linear Quadratic Regulator

In order to apply linear quadratic control methods, the model is transformed from a system of second order differential equations into a system of first order differential equations:

$$\dot{x} = \begin{bmatrix} 0 & I \\ -A^{-1}C & -A^{-1}B \end{bmatrix} x + \begin{bmatrix} 0 \\ A^{-1}F \end{bmatrix} u, \quad (6.10)$$

where  $x = [q^T \dot{q}^T]^T$ ,  $u = [M_g, \beta]^T$  and  $F$  is a reformulation of  $F_{ref}$  such that  $F = [F_1 \ F_2]$ , where  $F_1 = [\mathbf{0}_{1 \times 10} \ 1 \ 0]^T$  and  $F_2 = [\mathbf{0}_{1 \times 10} \ 0 \ 1]^T$ .

A controller is designed which minimizes the performance function:  $J = \int_0^\infty (x^T Q x + u^T R u) dt$ . The controller weighting matrices  $Q$  and  $R$ , were designed based on an initial guess of proper state weighting using Bryson's rule, followed by an iterative trial and error process. Constant  $Q$  and  $R$  were used at all wind speed above rated.

Using Bryson's rule, the LQR input weighting matrix  $R$  is handled by allowing the blade pitch angle to vary 60 deg. A constant torque approach is chosen for generator torque.

The LQR state weighting matrix  $Q$  is defined in such a way that the rotor angle,  $\psi$ , is limited to vary only 20 rad. The rotor angle can be interpreted as the integral action of the rotor speed, which can be used to reduce oscillations in mean power. In wind turbine control systems, the integral action of the rotor speed is often an interesting signal. By modeling the drivetrain as a second order system, the integral action is conveniently represented as a state.

Using Bryson's rule, the platform rotation is punished to vary only 1 deg/s for both platform pitch and roll in the weighting matrix.

Two LQR controllers are designed to demonstrate the advantage of the LQR controller. One controller, LQR1, is a controller designed for similar performance as the detuned baseline controller OC3-Hywind [9], by punishing the blade pitch rate  $\dot{\beta}$  to vary only 5 deg/s. The bandwidth of the OC3-Hywind controller is reduced compared to conventional turbine control to avoid instability as discussed in the introduction. Another controller, LQR2, is designed for a higher level of pitch activity by punishing the blade pitch rate,  $\dot{\beta}$ , to vary only 8 deg/s. This reflects the bandwidth of conventional wind turbine controllers. In contrast to the OC3-Hywind baseline controller this is possible with a more advanced control strategy as presented in this paper without stability problems. Increased bandwidth of the controller causes increased blade pitch actuation, which will reduce the actuator lifetime. However as an example, the Hywind Demo is a standard wind turbine. In the context of actuator lifetime, the actuator is designed for conventional controller bandwidth and not detuned bandwidth. Thus, we suggest to increase the bandwidth to 8 deg/s using LQR2.

## Software

The controllers are simulated on a 5 MW wind turbine mounted on a ballast stabilized buoy to resemble an upscaled version of the 2.3 MW Hywind Demo wind turbine. The floating wind turbine has a flexible tower and drivetrain, a rotor radius of 63 m, and a height of 90 m. The platform has a draft of 120 m, with six degrees of freedom in translation and rotation. The platform is constrained by three mooring lines. The wind turbine is a three bladed upwind 5 MW OC3-Hywind reference wind turbine specified by the NREL in [8], and implemented in the wind turbine high fidelity aeroelastic simulation tool FAST, which is well recognized in the OC3 code benchmark [16]. The simulations were performed in Simulink Matlab v7.9.0 (R2009b) linked with FAST v7.00.00a-bjj and AeroDyn v13.00.00a-bjj compiled for the OC3-Hywind running Windows 7 32bit.

## 3 Environmental Setup

The wind profile used in the simulations has a mean wind speed of 18.0 m/s with a turbulence intensity of 14.9%. The significant wave height is 6.0 meters, simulated with a peak wave period of 2, 5 and 10 seconds. Figure 6.7 shows three difference sequences of wave elevations. The simulation does not include the ocean current. The system is simulated at 80 Hz, while the control system operates at 10 Hz.

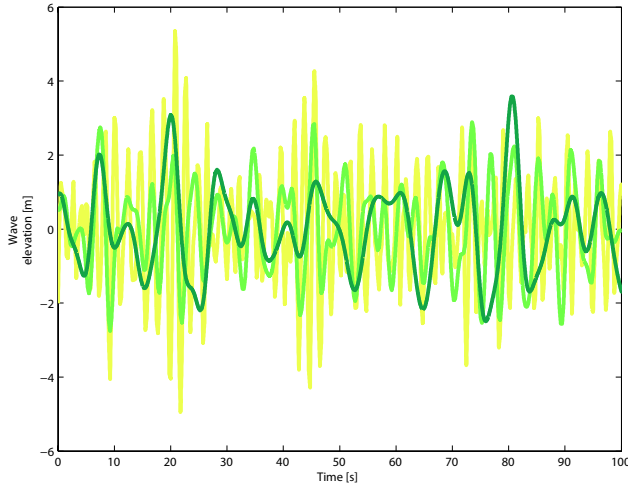


Figure 6.7: Wave height over time where yellow, light green and dark green represents peak wave periods of 2, 5 and 10 seconds respectively. The figure shows 100 seconds of the 600 seconds sequences.

## 4 Results

The performance of the suggested controllers are compared to the performance of the OC3-Hywind baseline controller [9]. The responses of the controllers are compared in a case where the waves are aligned with the wind, and in another case where the waves are perpendicular to the wind.

In Figure 6.8, the performance of the baseline controller and the LQR1 controller are compared with aligned wind–wave forces and with a peak wave frequency of 10 seconds. Figures 6.9–6.11 show the results of aligned wind and waves with a peak wave frequency of 10 seconds. Figures 6.12–6.14 make the same comparison for the case of perpendicular wind and waves.

The performances are compared in terms of blade pitch angle in Figures 6.9 and 6.12, and platform pitch in Figures 6.10 and 6.13.

An overall performance analysis is presented in Figures 6.11 and 6.14 where, also electrical power, tower deflections, and platform motions are compared. These key performance indicators are compared in terms of absolute values (abs), and standard deviations (std). The absolute values are defined by  $\int |\beta(t)| dt$ , which describes the distance traveled by the blade pitch.

## 5 Discussion

In Figure 6.8, a comparison is presented between the detuned baseline controller and the LQR1 controller. Except from platform pitch, the comparison demonstrates similar behaviors between the two controllers, with insignificant fluctuations. The purpose of this comparison is to demonstrate that the presented LQR control strategy can performance

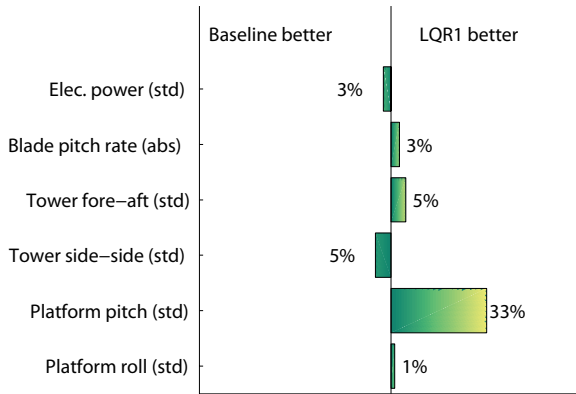


Figure 6.8: Aligned wind-wave forces with a peak wave period of 10 seconds: Statistical analysis of relative controller performance with respect to mean, standard deviation (std).

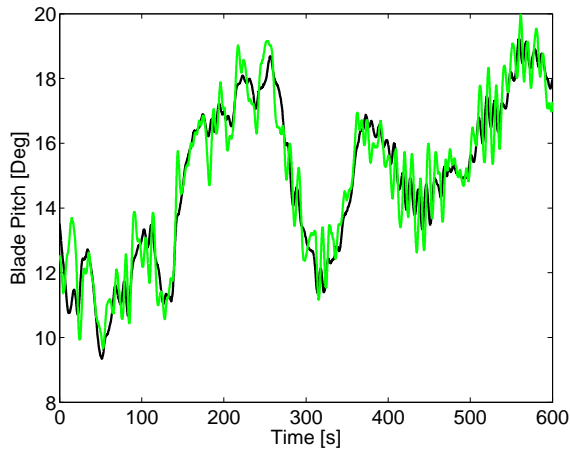


Figure 6.9: Aligned wind-wave forces with a peak wave period of 10 seconds: Blade pitch angle. The green is the LQR controller while the black is the baseline.

just as the detuned baseline controller. However, the bandwidth of these controller implementations are very slow and does not comply with conventional wind turbine standards.

The performance of the detuned baseline controller also demonstrates the limit of this controller. If the bandwidth of the detuned baseline controller was increased, the system would become unstable. However, using a model-based control strategy it is possible to operate at a conventional bandwidth while maintaining stability of the system.

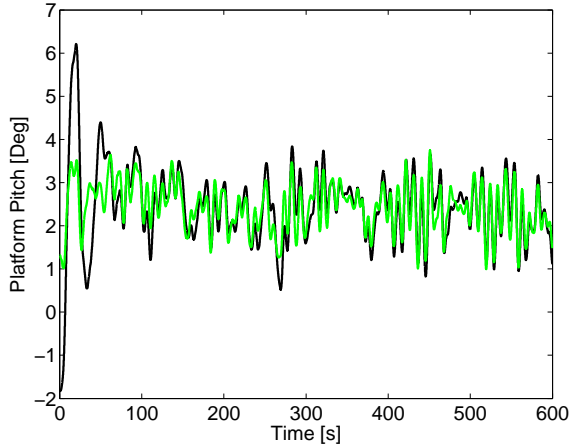


Figure 6.10: Aligned wind–wave forces with a peak wave period of 10 seconds: Platform pitch. The green is the LQR controller while the black is the baseline.

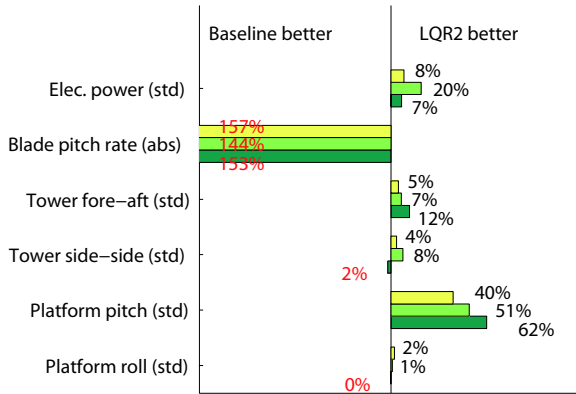


Figure 6.11: Aligned wind–wave forces: Statistical analysis of relative controller performance, where yellow, light green and dark green represents peak wave periods of 2, 5 and 10 seconds respectively.

In Figures 6.9–6.14 a comparison is presented between the detuned baseline controller and the LQR2 controller. The performance of the two controllers are compared at three different wave sequences with turbulent wind. As the buoy has the same dynamic properties in all direction, we demonstrate the two worst case scenarios; aligned forces and perpendicular forces.

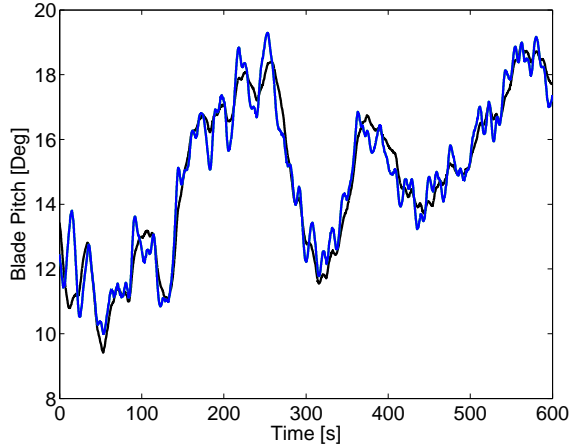


Figure 6.12: Perpendicular wind–wave forces with a peak wave period of 10 seconds: Blade pitch angle. The blue is the LQR controller while the black is the baseline.

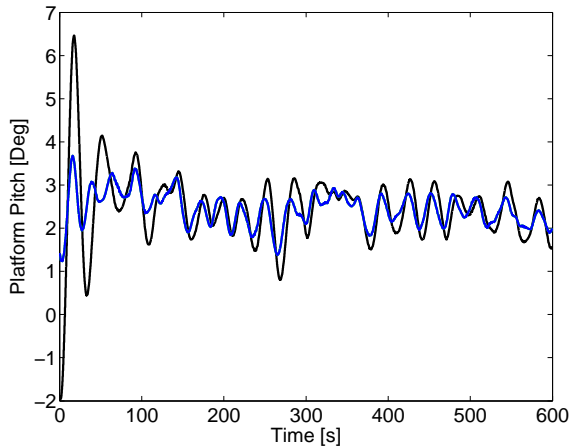


Figure 6.13: Perpendicular wind–wave forces with a peak wave period of 10 seconds: Platform pitch. The blue is the LQR controller while the black is the baseline.

The results show that it is possible to significantly improve the platform pitch oscillations by approximately 50% when forces are both aligned and perpendicular. The cost is an increase in blade pitch activity by approximately 150% when forces are aligned and approximately 100% when forces are perpendicular.

Improvements in electrical power (7-20%) and tower fore–aft deflection (5-17%) are observed, when forces are both aligned and perpendicular.



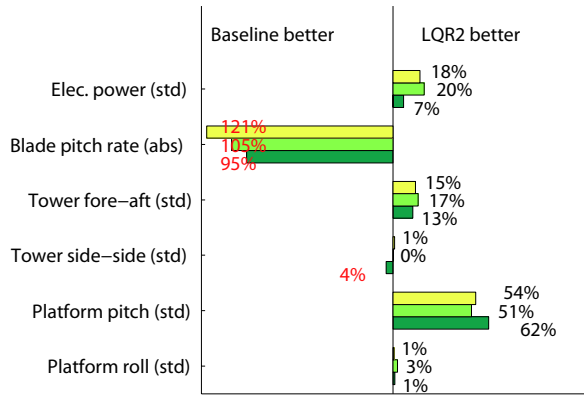


Figure 6.14: Perpendicular wind-wave forces: Statistical analysis of relative controller performance, where yellow, light green and dark green represents peak wave periods of 2, 5 and 10 seconds respectively.

Insignificant improvement are observed in platform roll and tower side-side deflection. As both control strategies uses a constant torque approach, there is only indirect actuation in both platform roll and tower side-side deflection. In the perspectives of using the generator torque for damping oscillation on the platform, the torque induced by the generator is less than 10% of the perpendicular torque induced by the rotor thrust force. Furthermore, using generator torque to damping platform roll, and tower side-side, will cause power oscillations and thus will change focus and require further research.

Comparing the results between aligned and perpendicular forces it should be noted that misaligned forces in the range of  $\pm 45$  degrees occur at much higher probability that perpendicular forces. Thus, the results on aligned forces should be weighted more importantly.

## 6 Conclusion

In the context of model-based control, a new model of a floating wind turbine is presented that captures the effect of the aerodynamics, hydrodynamics, structural dynamics, and actuator dynamics. To address the disturbance and misalignment of wind and waves, a control model is presented that requires estimates of the wind speed and the wave frequency, which offers an improved model for model-based control.

A control strategy is taken based on a gain-scheduled LQR controller. The result is a wind and wave control strategy capable of actively damping structural oscillations while fulfilling the objective of maximizing power.

Using the same bandwidth as a conventional wind turbine controller, the suggested model-based control strategy shows convincing performance in reducing platform pitch oscillations, while improving the electrical power and tower fore-aft deflections.

Misaligned wind and waves were also addressed. Worst-case wind and waves forces, has successfully been damped. While oscillations in platform pitch and tower fore-aft were actively reduced, oscillations in platform roll and tower side-side were only damped passively, due to lack of sideways controllability using the suggested strategy.

## 7 Acknowledgment

This work has been funded by Norwegian Centre for Offshore Wind Energy (NOR-COWE) under grant 193821/S60 from Research Council of Norway (RCN). NORCOWE is a consortium with partners from industry and science, hosted by Christian Michelsen Research.

## References

- [1] B. Skaare, T. D. Hanson, and F. G. Nielsen, "Importance of control strategies on fatigue life of floating wind turbines," *Proceedings of 26th International Conference on Offshore Mechanics and Arctic Engineering*, 2007.
- [2] J. M. Jonkman, "Influence of control on the pitch damping of a floating wind turbine," *2008 ASME Wind Energy Symposium*, 2008.
- [3] T. Burton, D. Sharpe, N. Jenkins, and E. Bossanyi, *Wind Energy Handbook*. Wiley, 2001.
- [4] H. Namik and K. Stol, "Individual blade pitch control of floating offshore wind turbines," *Wind Energy*, vol. 13 Issue 1, pp. 74–85, 2009.
- [5] S. Christiansen, T. Knudsen, and T. Bak, "Optimal control of a ballast-stabilized floating wind turbine," *IEEE Multi-Conference on Systems and Control*, 2011.
- [6] M. A. Lackner, "Controlling platform motions and reducing blade loads for floating wind turbines." *Wind Engineering*, vol. 33, pp. 541–553, 2010.
- [7] J. Jonkman, *NWTC Design Codes*, National Renewable Energy Laboratory, 2010. [Online]. Available: <http://wind.nrel.gov/designcodes/simulators/fast/>
- [8] J. Jonkman, S. Butterfield, W. Musial, and G. Scott, "Definition of a 5-mw reference wind turbine for offshore system development," National Renewable Energy Laboratory, Tech. Rep. NREL/TP-500-38060, 2007.
- [9] J. Jonkman, "Definition of the floating system for phase iv of oc3," National Renewable Energy Laboratory, Tech. Rep., 2010.
- [10] E. Kristiansen, Å. Hjulstad, and O. Egeland, "State-space representation of radiation forces in time-domain vessel models," *Ocean Engineering*, vol. 32, pp. 2195–2216, 2005.
- [11] E. Wayman, P. Sclavounos, S. Butterfield, J. Jonkman, and W. Musial, "Coupled dynamic modeling of floating wind turbine systems," *Offshore Technology Conference Houston, Texas*, 2006.

- [12] WAMIT, *WAMIT - User Manual - The State of The Art in Wave Interaction Analysis*, WAMIT, Inc., 2006.
- [13] H. F. Burcharth, “Strøm- og bølgekræfter på stive legemer,” Institutet for Vand, Jord og Miljøteknik, Aalborg University, Tech. Rep., 2002.
- [14] T. L. Andersen and P. Frigaard, “Lecture notes for the course in water wave mechanics,” Department of Civil Engineering, Aalborg University, Tech. Rep., 2011.
- [15] T. Knudsen, T. Bak, and M. Soltani, “Prediction models for wind speed at turbine locations in a wind farm,” *Wind Energy*, 2011, submitted.
- [16] P. Passon, M. Kühn, S. Butterfield, J. Jonkman, T. Camp, and T. J. Larsen, “Oc3–benchmark exercise of aero-elastic offshore wind turbine codes,” *The Science of Making Torque from Wind*, 2007.

# Paper C

## **Minimum Thrust Load Control for Floating Wind Turbine**

S. Christiansen, T. Bak and T. Knudsen

This paper was published in:  
The Proceedings of IEEE Multi-Conference on Control Applications, (CCA)  
2012

Copyright ©IEEE  
*The layout has been revised*

### Abstract

Offshore wind energy capitalizes on the higher and less turbulent wind at sea. Shallow water sites are profitable for deployment of monopile wind turbines at water depths of up to 30 meters. Beyond 30 meters, the wind is even stronger and less turbulent. At these depths, floating wind turbines become profitable, capable of accessing unexploited wind resources while reaching regions of new consumers. However, floating wind turbines are subject to reduced structural stiffness which results in instabilities when standard wind turbine control systems are applied. Based on optimal control, this paper presents a new minimum thrust control strategy capable of stabilizing a floating wind turbine. The new control strategy explores the freedom of variable generator speed above rated wind speed. A comparison to the traditional constant speed strategy, shows improvements in structural fore-aft oscillations and power stability when using the new control strategy.

## 1 Introduction

Floating wind turbines are the latest development in wind energy, offering installation in places where wind energy never has gone before. Wind turbines are installed in range of consumers and are economically competitive at sites of high wind and relative low roughness such as land fields and sea surface. Offshore wind turbines is an example of this trend. However, the economy in installing offshore wind turbines has been limited to shallow waters below 30 meters. The concept of floating wind turbines extend the range of wind turbines beyond 30 meters, accessing deep water sites of potentially higher wind speed while offering wind energy to consumers in new regions.

The main objectives of wind turbines are to maximize power production while minimizing fatigue loads. Fatigue is basically wear accumulated over time of key components such as tower, gearbox, blades and bearings. If a wind turbine is operated to maximize power production regardless of fatigue loads, the lifetime of key components will significantly decrease and the cost of energy will go up. This is especially important for a floating wind turbine which by nature is influenced by a constant contribution of oscillations from both wind and ocean waves. Therefore a trade-off between maximized power production and minimized fatigue loads is required for optimal performance.

A floating wind turbine resembles an onshore wind turbines in many ways, however the dynamic behavior differs. Applying conventional onshore control strategies to floating wind turbines has been shown to impose negative damped oscillations to the platform motion. Above rated wind speed, the onshore controller causes the blade pitch to increase the rotor thrust as the wind speed decreases and vice versa. Since the onshore controller is slower than the tower dynamics, but faster than the platform dynamics, instabilities only occur on floating wind turbines.

To prevent this, a tower damping control strategy was introduced in [1] using a wind estimator applied to a ballast-stabilized wind turbine, showing reduced tower oscillation at the cost of reduced power output. In [2] a gain scheduled proportional integrating (GSPI) controller showed good performance regarding platform oscillations but overshoots rated power and generator speed. The task of damping tower oscillations were addressed by [3] suggesting tower acceleration influence on blade pitch control.

However, in [2] platform oscillations were addressed using tower acceleration showing improved platform damping at the cost of relative large power drops. Active stall

control was also suggested in [2] demonstrating smooth power at the cost of increased platform oscillations. In [4], active stall control is suggested as a feasible solution on floating wind turbines.

Linear quadratic regulator (LQR) was applied to a floating wind turbine in [5, 6] which showed improved results with respect to power stability and tower oscillations compared to [2]. In [5] a control strategy utilizing individual blade pitch and generator torque reduced tower side-side oscillation on a floating structure. In [7] wind and wave estimators were combined in a full range LQR controller showing generally improved performance in power and structural oscillation.

The cited literature varies in methods, however, they all have one thing in common; they are all based on the same control strategy of constant generator speed above rated wind speed. This paper presents a new control strategy to reduce platform and tower oscillations. Instead of operating the generator at maximum speed above rated wind speeds, this paper suggests a strategy which reduces rotor thrust at higher wind speeds. The effect is reduced loads on the structure and thereby potentially a lower cost of energy. The new control strategy is implemented as an LQR control combined with wind and wave estimators. The suggested control strategy shows improved damping of structural oscillations when compared to a constant speed control strategy.

## 2 Methods

### A Dynamical model of a Floating Wind Turbine

A model for control design is needed which captures the dominant behaviors of a floating wind turbine. The control model used in this work is presented in [7]. The model represents a floating wind turbine which is able to both rotate and translate. The wind turbine tower and drivetrain are both modeled as flexible structures. Aerodynamics and hydrodynamics are modeled as functions of wind speed and wave frequency, respectively. Dynamics of actuators are also included which altogether represents a complete dynamical model of a floating wind turbine.

### Identifying Aerodynamics Impact on Structure

The damping of a floating wind turbine depends on aerodynamics and hydrodynamics [7]. The damping provided by hydrodynamics is a function of wave frequency and surface smoothness of the structure, which are uncontrollable dimensions. The damping provided by aerodynamics is a function of wind speed and the efficiency of the rotor. The wind speed is of course uncontrollable, however, the efficiency of the rotor can be controlled by altering the blade pitch angle or rotor speed.

First the aerodynamic impact on platform damping is investigated. Let us assume, a wind turbine can be modeled as a dynamical system of second order by

$$I\ddot{q} + C\dot{q} + Kq = F_{\text{ext}}, \quad (7.1)$$

where  $\dot{q} = [\dot{x}_p \ \dot{\theta}_p \ \dot{x}_t \ \Omega]^T$  and  $\dot{x}_p$  is platform translation,  $\dot{\theta}_p$  is platform rotation,  $\dot{x}_t$  is tower deflection,  $\Omega$  is generator speed. Structural properties are defined as follows;  $I$  is inertia,  $C$  is damping, and  $K$  is stiffness. The external forces are defined as  $F_{\text{ext}} =$

$[F_t \ h_t F_t \ F_t \ M_a]^T$  where  $F_t$  is the aerodynamics thrust force induced by wind,  $h_t$  is the distance from the hub to the center of buoyancy (COB), and  $M_a$  is the aerodynamics torque. In Fig. 7.1 a floating wind turbine is presented, where also surface water level (SWL) and center of mass (COM) are indicated.

The aerodynamic loads are defined as

$$F_t = \frac{1}{2} \rho A v_r^2 C_t(\lambda, \beta) \quad (7.2)$$

$$M_a = \frac{1}{2\Omega} \rho A v_r^3 C_p(\lambda, \beta), \quad (7.3)$$

where  $\rho$  is the density of air,  $A$  is the area swept by the rotor,  $C_t(\lambda, \beta)$  is the thrust coefficient of the rotor as a function of tip speed ratio,  $\lambda = \Omega R/v_r$  and blade pitch angle, respectively, and  $C_p(\lambda, \beta)$  is the power coefficient. The wind speed seen by the rotor can be defined as  $v_r = v - \dot{x}_p - h_t \dot{\theta}_p - \dot{x}_t$ , where  $v$  is the ambient wind speed.

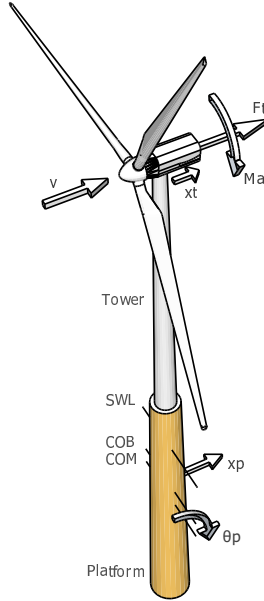


Figure 7.1: Floating wind turbine comprising of a wind turbine mounted on a floating platform.

To identify the aerodynamic damping the system is linearized by  $q = \bar{q} + \tilde{q}$ , where  $\bar{q}$  is the linearization point and  $\tilde{q}$  is small deviation. The external forces are linearized with respect to the  $\dot{\tilde{q}}$ , thus

$$\tilde{F}_{\text{ext}} \approx \frac{\partial F_{\text{ext}}}{\partial \dot{\tilde{q}}} \dot{\tilde{q}} = C_{\text{ext}} \dot{\tilde{q}}, \quad (7.4)$$

where  $C_{\text{ext}}$  are the partial derivatives of the external forces. The aerodynamics of the external forces are include in the structural model by

$$I \ddot{\tilde{q}} + (C - C_{\text{ext}}) \dot{\tilde{q}} + K \tilde{q} = 0. \quad (7.5)$$



At each wind speed a linearized system can be defined as  $\bar{q} = K^{-1}\bar{F}_{ext}$  at predefined values of tip speed ratio,  $\lambda$ , and blade pitch angle,  $\beta$ .

### Analyzing Relation Between Power and Damping

To develop a control strategy for constant power and reduced platform damping it is important to understand what  $C_p$  and  $C_t$  look like. At constant power, there exists only one correct value of  $C_p$  at a given wind speed. However, this value can be obtained

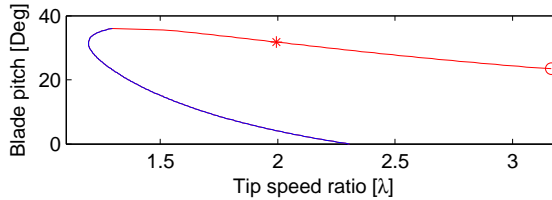


Figure 7.2: Blade pitch angle as a function of tip speed ratio at 25 m/s. The line indicates possible operating points for nominal production where red is feather and blue is stall. The circle indicates constant speed operation. The star indicates minimum thrust operation.

by numerous combinations of blade pitch angles and tip speed ratios. In reality  $C_p$  and  $C_t$  are continuous functions in the sense that there exists a smooth path of blade pitch angles and tip speed ratios which offers constant aerodynamics coefficients. In Fig. 7.2,

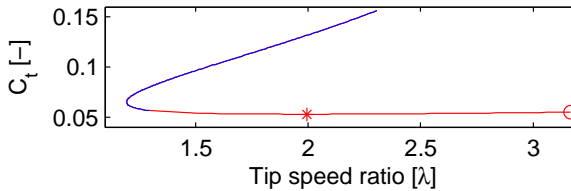


Figure 7.3: Thrust coefficient as a function of tip speed ratio at 25 m/s. The line indicates possible operating points for nominal production where red is feather and blue is stall. The circle indicates constant speed operation. The star indicates minimum thrust operation.

combinations of blade pitch angles and tip speed ratios are presented which result in nominal power production thus constant  $C_p$ . Any desired solution must be found in these set of blade pitch angles and tip speed ratios.

In Fig. 7.3 the thrust coefficient  $C_t$  is presented as a function of tip speed ratio.

The linearized system is analyzed and the natural frequency of the platform pitch,  $\theta_p$ , is identified. In Fig. 7.4, the damping of the platform pitch is presented as a function of tip speed ratio.

Fig. 7.5 represents the dynamical damping of the tower deflection,  $x_t$  as a function of tip speed ratio.

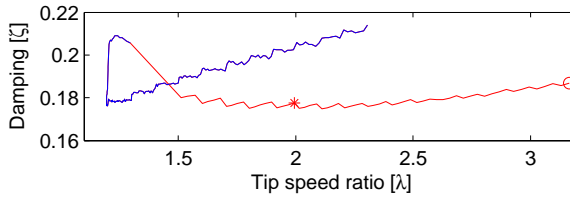


Figure 7.4: Platform damping as a function of tip speed ratio at 25 m/s. The line indicates possible operating points for nominal production where red is feather and blue is stall. The circle indicates constant speed operation. The star indicates minimum thrust operation.

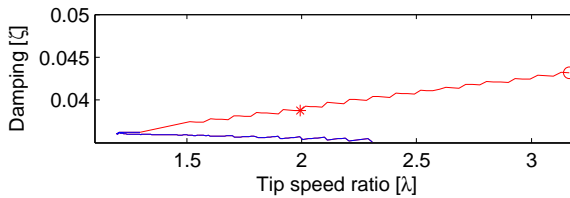


Figure 7.5: Tower damping as a function of tip speed ratio at 25 m/s. The line indicates possible operating points for nominal production where red is feather and blue is stall. The circle indicates constant speed operation. The star indicates minimum thrust operation.

### Minimum Thrust coefficient

Based on the analysis of power and damping, an operating strategy is chosen which offers a better response relative to the constant speed approach. The response of the constant speed approach is presented in Fig. 7.2-7.5 indicated by a circle.

In this paper a control strategy based on minimum thrust coefficient is chosen. This approach reduces the thrust coefficient by 3.68% at wind speed of 25 m/s compared to a constant speed approach. In Fig. 7.3 the minimum thrust coefficient is indicated by a star. However, the platform damping at this point is deteriorated by 3.76% compared to the constant speed approach as seen in Fig. 7.4. At this point, the difference in structural responses is not clear, thus structural and power performance are analyzed.

To visualize the responses of the two different systems, white noise is applied as external forces to the platform dynamics and corresponding power spectrum density for platform oscillations are presented in Fig. 7.6. The figure shows a slight frequency shifted behavior when comparing the two systems. Using the minimum thrust approach, the stationary variance is improved by minor 1.24% found by solving the Lyapunov equation.

The power is analyzed with respect to sensitivity to changes in wind speed. The power is defined as

$$P = \frac{1}{2} \rho A v_r^3 C_p(\lambda, \beta), \quad (7.6)$$

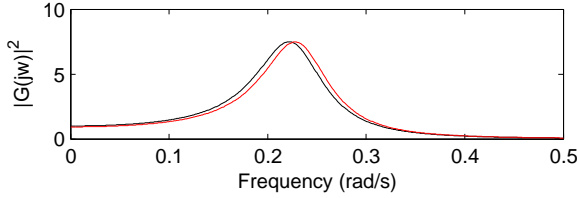


Figure 7.6: Variance of platform oscillations when white noise is applied as an external force. The black is the constant speed approach and the red is the minimum thrust approach.

with partial derivative

$$\frac{\partial P}{\partial v_r} = \frac{1}{2} \rho A \left( 3\bar{v}_r^2 C_p(\bar{\lambda}, \bar{\beta}) + \bar{v}_r^3 \frac{\partial C_p(\bar{\lambda}, \bar{\beta})}{\partial \lambda} \frac{\partial \lambda}{\partial v_r} \right), \quad (7.7)$$

where  $\frac{\partial \lambda}{\partial v_r} = \frac{-\bar{\Omega} R}{\bar{v}_r^2}$  and  $\frac{\partial C_p(\bar{\lambda}, \bar{\beta})}{\partial \lambda}$  are found numerically. The sensitivity is analyzed at 25 m/s where the deviation in control strategies is largest. The two strategies are analyzed showing a potential decrease of 8.27 % in power sensitivity,  $\frac{\partial P}{\partial v_r}$ , to changes in wind speeds using minimum thrust approach.

## Control Trajectories

In Fig. 7.7 the suggested minimum thrust approach is compared to the constant speed approach. The proposed strategy is only relevant above rated wind speed since there only exists one operating point for optimal power below rated wind speed. In Fig. 7.8 the rotor thrust force is shown together with the improvement in deviation by minimum thrust approach. It is expected that the suggested minimum thrust approach causes an increase in actuator activity due to the extended range of the actuator trajectories.

## LQR Control Design

A model based control strategy is chosen to control and damp the system. The proposed control strategy is shown in Fig. 7.9 comprising a LQR controller combined with wind speed and wave period estimators.

As the system is nonlinear several controllers are designed for various operating points (OP's) of wind speeds and wave frequencies. Stability studies regarding transition between these controllers are not included in this work. To determine the operating point the controller requires two estimated schedule parameters which are wind speed and wave frequency.

The wind speed estimator is an extended Kalman filter which uses the wind turbine as wind speed sensor based on tip speed ratio, blade pitch angle and generator torque. The implemented wind estimator is presented in [8].

The wave frequency estimator is estimated based on measured wave height. A simple auto regressive algorithm is implemented to estimate a model of the wave height. The desired wave frequency is thus derived for the model as the natural frequency. The wave frequency estimator is documented in [7].

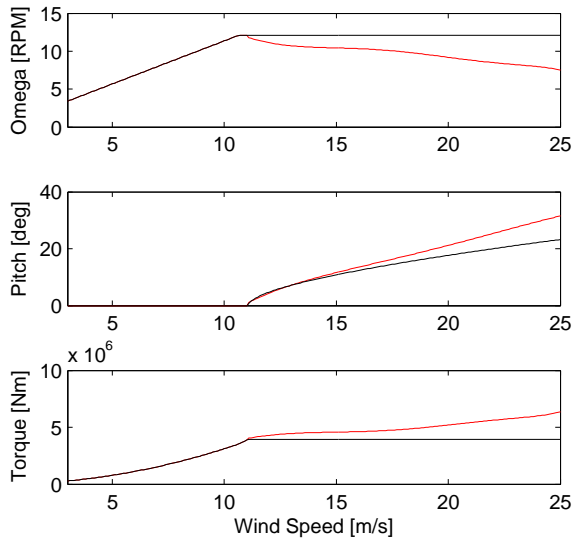


Figure 7.7: Operation strategy. The black is the constant speed approach and the red is the minimum thrust approach.

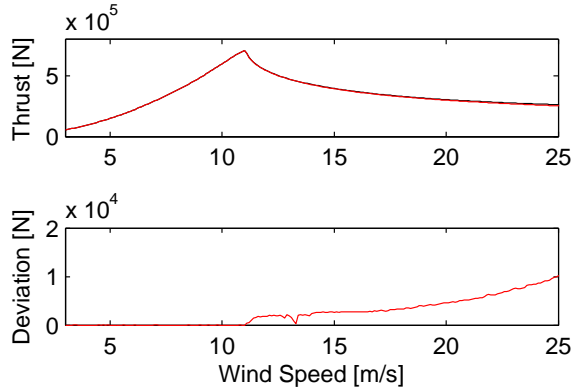


Figure 7.8: The upper shows aerodynamic thrust while the lower shows the improvement achieved using minimum thrust strategy. The black is the constant speed approach and the red is the minimum thrust approach.

A series of linearized LQR state feedback controllers are designed at wind speeds above rated power at intervals of 0.5m/s and wave frequencies of 0 rad/s to 5 rad/s at an interval of 0.1 rad/s.

In the introduction, four degrees of freedom (DOF) are presented related to the aerodynamics, however, the controller is designed based on further eight DOF which are actuator and structural dynamics as presented in [7].

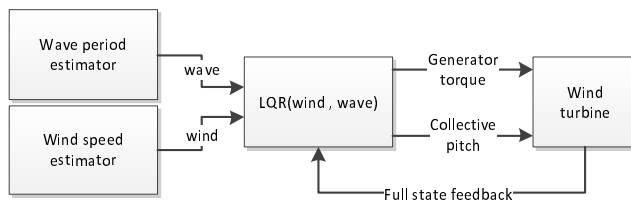


Figure 7.9: Overview of control strategy.

A state space system is presented in the classical form as  $\dot{x} = Ax + Bu$  and  $y = Cx$ . The feedback control is defined as  $u = -L(v, w_\omega)x$ , where  $v$  is estimated wind speed and  $w_\omega$  is estimated wave frequency indicating estimator dependencies.

The controller weighting matrices are designed based on Bryson's rule by an initial guess of proper state weighting followed by an iterative trial and error process.

The LQR input weighting matrix  $R$  is handled by allowing the blade pitch actuator reference to vary 90 deg, and the generator torque reference to vary 20000 Nm at all OP's.

The LQR state weighting matrix  $Q$  is defined such that rotor angle is punished to vary only 10 rad. The rotor angle can be interpreted as integral action of the rotor speed. In wind turbine control systems the integral action of the rotor speed is often an interesting state. Conveniently, by modeling the drivetrain as a second order system the integral action is represented as a state. The state can be used to damp fluctuations in generator speed.

In constant torque operation this state is also proportional to power, however, this is not the case when torque is varying. Thus, a power state is introduced in the system equations. In minimum thrust strategy, the integrated electrical power state was punished to vary only 300 kW. However in the constant speed strategy, the state was relaxed to 2 MWs since the punishing of the generator speed already of this effect.

To avoid unnecessary fast actuator activity the blade pitch rate is punished to vary only 8 deg/s. The tower deflection in fore-aft is punished to vary only 5 m/s in translation at hub height while platform rotation is punished to vary 0.5 rad/s.

### 3 Experimental Setup

#### Simulation Environment

The control strategy suggested in this paper is compared to a constant speed control strategy under equal environmental conditions at a mean wind speed of 25 m/s with an air density of 1.225 kg/m<sup>3</sup> and a turbulence intensity of 10%.

To reveal system damping ability, at time zero the floating wind turbine is released from upright alignment and forced backward by wind and waves resembling a step response.

The relative high wind speed is selected to demonstrate the large deviations in control strategies. Waves are simulated as irregular waves with a JONSWAP/Pierson-Moskowitz spectrum [9]. The significant wave height of the incident waves are 6 meters with a wave frequency of 10 seconds. The environmental conditions are at water depth of 320 meters

and a water density of  $1025 \text{ kg/m}^3$ . The waves are aligned with the direction of the wind, thus perpendicular wind and waves are not considered in this paper and are therefore not included in the environmental setup.

## Software

The wind turbine is a three bladed upwind 5MW reference wind turbine specified by NREL in [10], and implemented in the wind turbine simulation tool FAST which is well recognized in the OC3 code benchmark, [11]. The implementation of the wind turbine installation consists of a 5MW wind turbine mounted on a ballast-stabilized buoy to resemble an upscaled version of the 2.3MW Hywind wind turbine. The floating wind turbine has a rotor radius of 63 meters, a tower height of 90 meters, and six degrees of freedom.

The simulations were performed in Simulink Matlab v7.9.0 (R2009b) linked with FAST v7.00.00a-bjj and AeroDyn v13.00.00a-bjj compiled for the OC3 Hywind running Windows 7 32bit. Damage equivalent load calculations are calculated using MCrunch v.100 which is an implementation of [12].

## 4 Results

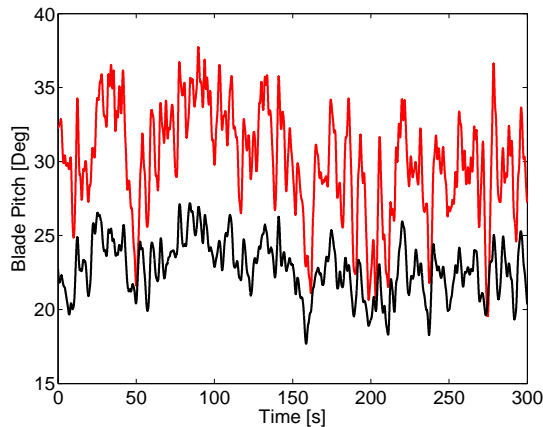


Figure 7.10: Blade pitch angle at 25 m/s. The black line is constant speed strategy and red line is suggested minimum thrust strategy.

In Fig. 7.10-7.14, time-series of the two control strategies are compared with respect to blade pitch, generator speed, platform pitch, tower deflection and electrical power.

Based on Fig. 7.10-7.14 and some additional performance indexes, a statistical analysis is presented in Fig. 7.15. In the figure, the performances of the two control strategies are compared.

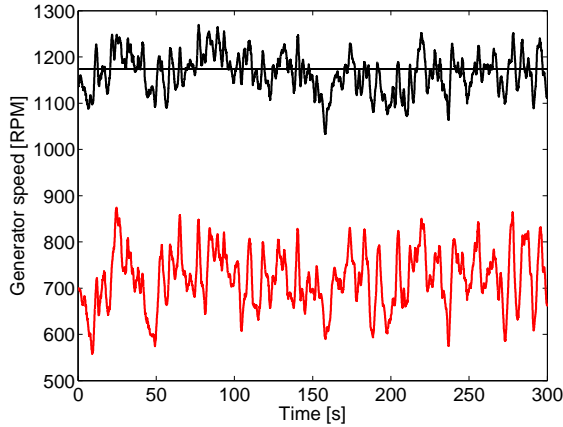


Figure 7.11: Generator speed at 25 m/s. The black line is constant speed strategy and red line is suggested minimum thrust strategy.

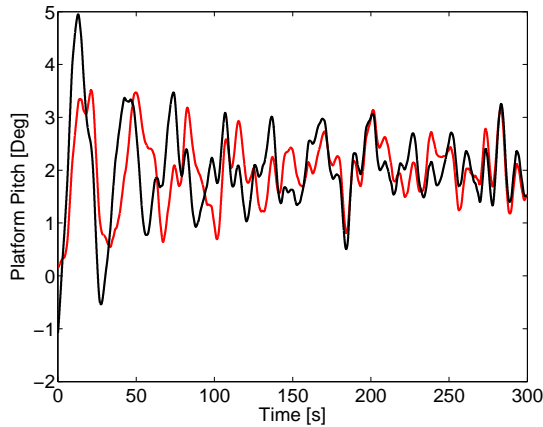


Figure 7.12: Platform pitch angle at 25 m/s. The black line is constant speed strategy and red line is suggested minimum thrust strategy.

## 5 Discussion

The results show that the suggested minimum thrust strategy offers reduced structural fore-aft oscillations in both tower and platform as indicated in the analysis. The strategy was designed to reduce fore-aft oscillation, however, side-side oscillation suffers in both tower and platform due to increased generator torque actuation.

Due to increased aerodynamic torque and generator torque, drive train torsion has unavoidably increased. However, the low speed shaft should be dimensioned to withstand the increased level of torsion. An advantage of the minimum thrust strategy is the reduced generator speed which will reduce viscous wear in bearing along the drive train

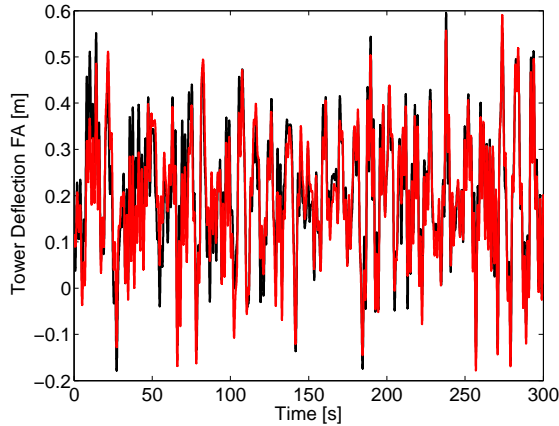


Figure 7.13: Tower fore-aft deflection at 25 m/s. The black line is constant speed strategy and red line is suggested minimum thrust strategy.

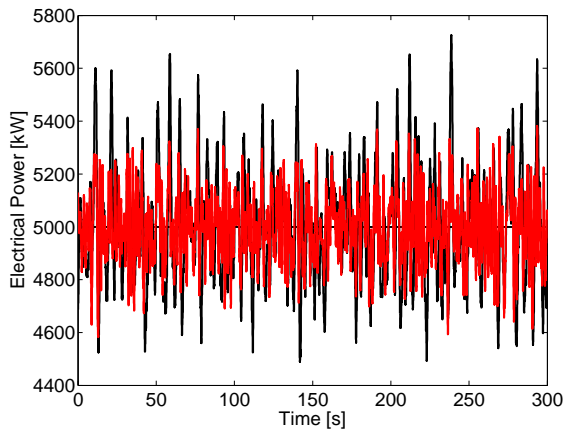


Figure 7.14: Power performance at 25 m/s. The black line is constant speed strategy and red line is suggested minimum thrust strategy.

and generator.

Actuator activity in blade pitch and generator torque shows increased operation. As expected, the minimum thrust strategy causes a range-extension in both blade pitch and generator torque. The constant speed strategy demands constant generator torque, however, the suggested strategy demands varying generator torque which explains the increased actuator activity.

The power performance in mean level and standard deviation is improved by 60 per cent compared to the constant speed strategy as indicated in the analysis. However due to the differences in the strategies, it is difficult to determine if this improvement in perfor-



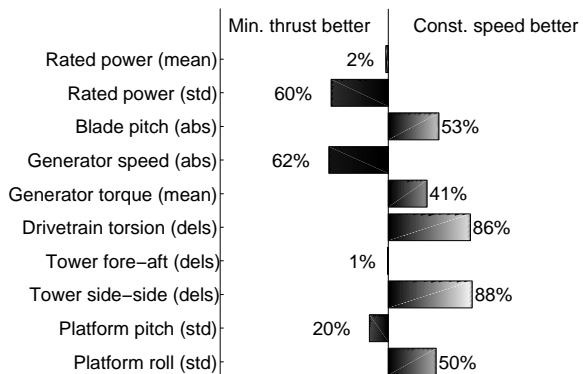


Figure 7.15: Statistical analysis of relative controller performance with respect to mean, standard deviation (std), travel distance (abs) and damage equivalent loads (dels).

mance is just caused by a generally increase in actuator usage.

## 6 Conclusion

The coupling of aerodynamics and structural dynamics was analyzed. Based on this, a minimum thrust strategy was proposed to improve structural oscillations and power stability to changes in wind speeds. LQR controllers based on estimates of wind speed and wave frequency was designed for minimum thrust strategy and constant speed strategy.

The results show improvements in power and structural oscillations in fore-aft. However, the constant generator speed strategy shows significantly better performance in side-side oscillations. The two strategies show widely different results with pros and cons, however, the best solution could potentially be a combined strategy which offers reduced thrust at a constant and reduced generator speed.

Based on simulations of a wind turbine, a new operating strategy is suggested which offers better fore-aft damping and power performance exploring the freedom of variable generator speed and torque in contrast to the traditional constant speed strategy.

## 7 Acknowledgment

This work is supported by the Norwegian centre for offshore wind energy (NORCOWE).

## References

- [1] B. Skaare, T. D. Hanson, and F. G. Nielsen, "Importance of control strategies on fatigue life of floating wind turbines," *Proceedings of 26th International Conference on Offshore Mechanics and Arctic Engineering*, 2007.
- [2] J. M. Jonkman, "Influence of control on the pitch damping of a floating wind turbine," *2008 ASME Wind Energy Symposium*, 2008.
- [3] T. Burton, D. Sharpe, N. Jenkins, and E. Bossanyi, *Wind Energy Handbook*. Wiley, 2001.
- [4] T. J. Larsen and T. D. Hanson, "A method to avoid negative damped low frequent tower vibrations for a floating pitch controlled wind turbine," *journal of Physics: Conference Series*, vol. 75, 2007.
- [5] H. Namik and K. Stol, "Individual blade pitch control of floating offshore wind turbines," *Wind Energy*, vol. 13 Issue 1, pp. 74–85, 2009.
- [6] S. Christiansen, T. Knudsen, and T. Bak, "Optimal control of a ballast-stabilized floating wind turbine," *IEEE Multi-Conference on Systems and Control*, 2011.
- [7] S. Christiansen, T. Bak, and T. Knudsen, "Damping wind and wave loads on a floating wind turbine," *IEEE Transactions on Control Systems Technology – submitted*, 2012.
- [8] T. Knudsen, M. Soltani, and T. Bak, "Prediction models for wind speed at turbine locations in a wind farm," *Wind Energy*, vol. 14, pp. 877–894, 2011, published online in Wiley Online Library (wileyonlinelibrary.com). DOI: 10.1002/we.491.

- [9] J. M. Jonkman, “Dynamics modeling and loads analysis of an offshore floating wind turbine,” Ph.D. dissertation, National Renewable Energy Laboratory, 2007.
- [10] J. Jonkman, S. Butterfield, W. Musial, and G. Scott, “Definition of a 5-mw reference wind turbine for offshore system development,” National Renewable Energy Laboratory, Tech. Rep. NREL/TP-500-38060, 2007.
- [11] P. Passon, M. Kühn, S. Butterfield, J. Jonkman, T. Camp, and T. J. Larsen, “Oc3–benchmark exercise of aero-elastic offshore wind turbine codes,” *The Science of Making Torque from Wind*, 2007.
- [12] S. D. Downing and D. F. Socie, “Simple rainflow counting algorithms,” *International Journal of Fatigue*, vol. 4, pp. 31–40, 1982.

# Paper D

## **Extended Onshore Control of a Floating Wind Turbine with Wave Disturbance Reduction**

S. Christiansen, T. Knudsen and T. Bak

This paper was published in:  
The Proceedings of The Science of Making Torque from Wind 2012

Copyright ©IEEE  
*The layout has been revised*

### Abstract

Reaching for higher wind resources beyond the water depth limitations of monopile wind turbines, there has arisen the alternative of using floating wind turbines. But the response of wave induced loads significantly increases for floating wind turbines. Applying conventional onshore control strategies to floating wind turbines has been shown to impose negative damped oscillations in fore–aft due to the low natural frequency of the floating structure. Thus, we suggest a control loop extension of the onshore controller which stabilizes the system and reduces the wave disturbance. The results shows that when adding the suggested control loop with disturbance reduction to the system, improved performance is observed in power fluctuations, blade pitch activity, and platform oscillations.

## 1 Introduction

As the interest in renewable energy increases, the means of harvesting and capturing wind energy have been continuously developed and improved. More reliable wind turbines make installation possible in harsher environments, such as offshore in shallow waters, where winds are stronger and hazards to human eyes and ears are less.

Floating wind turbines (FWT) are one of the latest developments in wind energy. The concept of a floating wind turbine extends the range of wind turbines beyond the limitations of monopile water depths, accessing deep water sites with potentially higher wind speeds and may offer wind energy to consumers in new regions.

A wind turbine installation has one simple objective: to produce cheap energy. However, if a wind turbine is operated to maximize power production regardless of fatigue loads, the lifetime of key components will significantly decrease and the cost of the energy will go up. This is especially important for a floating wind turbine, which by nature is influenced by a constant contribution of oscillations from wind and ocean waves. Therefore, a trade-off between maximum power production and minimum structural oscillation is required to minimize the total cost of the energy.

Applying conventional onshore control strategies to floating wind turbines has been shown to impose negative damped oscillations on the platform motion. The control must hence be adapted to the dynamic response of the floating structure. This can in principle be done by redesigning the entire control system or by adding control loops that extend the existing control system to handle the dynamics of a floating installation.

A number of results are available that redesign the control system. In [1], a tower damping control strategy was introduced using a wind estimator showing reduced tower oscillation at the cost of reduced power output. In [2] a detuned gain scheduled proportional integrating controller was applied. Linear quadratic control was applied in [3]. In [4, 5] wind and wave estimators were combined in a full range controller. In [6] a disturbance accommodating control was applied to reduce the wind disturbance.

All these results mentioned above rely on a redesigned control system. This paper takes a different approach, by suggesting a control loop extension to the onshore control without modifying the onshore controller. This provides potential benefits to manufacturers, as it simplifies the changes required in the control system to handle the floating installation. The strategy is presented in Fig. 9.2. Note that the onshore pitch controller is left untouched, and the control redesign is merely an additional loop which acts on

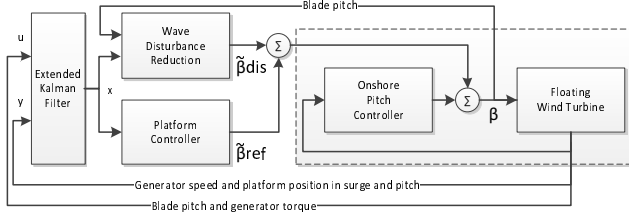


Figure 8.1: Overview of pitch control strategy. A Kalman filter is used to estimate the states and disturbance. The output of the onshore controller is corrected by improved feedback and wave disturbance reduction.

the onshore controller’s output and stabilizes the system. Furthermore, disturbances from 1st and 2nd order wave induced moments are reduced by means of contrary blade pitch induced moments.

In Section 2, the closed loop stability of the onshore controller is investigated. In Section 2, a controller is designed to stabilize the system. In Section 2, a strategy is presented for reducing the wave disturbance in platform fore–aft. However, measuring wave disturbance is difficult. Thus, in Section 2, an estimate is made by designing an observer which models the wave induced moments as a stochastic process using an extended Kalman filter (EKF) [7]. In Sections 4 and 5, the results are presented and discussed. In Section 6, the contributions are concluded.

## 2 Methods

### Closed Loop Stability of the Onshore Controller

The dynamics of a floating wind turbine is analyzed to determine the stability in platform pitch when applying onshore control. Only the wind is assumed to have a substantial impact on the dynamics. A model of platform translation and rotation in fore–aft is constituted by

$$\dot{\mathbf{x}}_s = A_s x_s + B_s F_t, \tag{8.1}$$

where  $\mathbf{x}_s = [x_p \dot{x}_p \theta_p \dot{\theta}_p]^T$  represents the platform translational velocity  $\dot{x}_p$  and rotational velocity  $\dot{\theta}_p$ . The aerodynamic thrust is defined by  $F_t = \frac{1}{2} \sigma A v^2 C_t(\lambda, \beta)$ , where  $\sigma$  is the density of air,  $v$  is the wind speed,  $C_t$  is the thrust coefficient,  $\lambda$  is the tip speed ratio, and  $\beta$  is the blade pitch angle. The tip speed ratio is defined by  $\lambda = \Omega R/v$ , where  $\Omega$  is the rotor speed and  $R$  is the rotor radius.

The drivetrain is modeled by the first order system

$$I \dot{\omega} = -M_g + \frac{1}{N} M_a, \tag{8.2}$$

where  $\omega$  is the generator speed,  $N$  is the gear ratio,  $M_g$  is the generator torque, and the aerodynamic torque is defined by  $M_a = \frac{1}{2\Omega} \sigma A v^3 C_p(\lambda, \beta)$ , where  $C_p$  is the power coefficient.

The available onshore controller is designed for systems with neglectable actuator dynamics, assuming that the dynamics of the actuators are insignificant in the closed loop system.

The onshore controller consist of a blade pitch controller and a generator controller. The pitch controller is a gain scheduled PI controller modeled by

$$\beta = \frac{1}{1 + \frac{\beta}{\beta_k}} PI(\omega_{\text{ref}} - \omega), \quad (8.3)$$

where  $\beta$  is, as before, the blade pitch angle,  $\beta_k$  is a constant, and  $\omega_{\text{ref}}$  is the generator speed reference. The onshore torque controller is modeled by

$$M_g = P_{\text{ref}}/\omega, \quad (8.4)$$

where  $P_{\text{ref}}$  is the power reference. The properties of these two controllers are specified in [8, 9].

Disregarding disturbances from the wind and waves, the combined dynamics of the platform, drivetrain, and controller is given by

$$\dot{\mathbf{x}} = f(\mathbf{x}, v), \quad (8.5)$$

where  $\mathbf{x} = [\mathbf{x}_s^T \ \omega \ x_i]^T$ , and  $x_i$  is an internal control state for integral control of the generator speed.

To determine its stability, the system is linearized by

$$\dot{\tilde{\mathbf{x}}} = \mathbf{A}\tilde{\mathbf{x}} = \frac{\partial f(\mathbf{x}, v)}{\partial \mathbf{x}} \tilde{\mathbf{x}}, \quad (8.6)$$

where  $\tilde{\mathbf{x}} = x - \bar{x}$  describes the dynamics about an operating point  $\bar{\mathbf{x}}$ . The poles of the system are shown in Fig. 8.2, which show three conjugate pole pairs. The fastest closed loop poles are mostly related to the drivetrain, while the slowest are mostly related to translation of the platform and the unstable pair are mostly related to platform rotation.

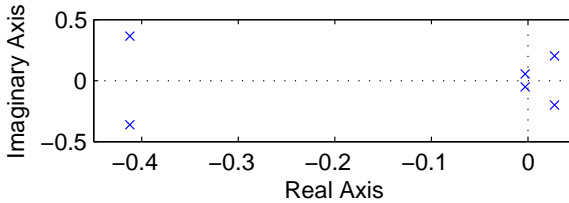


Figure 8.2: Closed loop poles of the FWT controlled by the onshore controller at 13 m/s.

## Platform Controller

A platform controller is designed to stabilize the system by moving the unstable poles of the platform rotation in Fig. 8.2 to the left half plane. A new control signal  $\beta_{\text{ref}}$  is added to the output of the onshore controller as shown in Fig. 9.2, and the new system becomes

$$\dot{\tilde{\mathbf{x}}} = \mathbf{A}\tilde{\mathbf{x}} + \mathbf{B}\tilde{\beta}_{\text{ref}}. \quad (8.7)$$



The controller is based on state feedback by

$$u = -\mathbf{K}\tilde{x}, \quad (8.8)$$

where  $u = \tilde{\beta}_{\text{ref}}$ . An LQ approach is used for stabilization and minimization of the perturbations of the system. The controller gain,  $\mathbf{K}$ , is found by minimizing the quadratic cost function

$$J = \int_0^{\infty} (\mathbf{x}^T \mathbf{Q} \mathbf{x} + u^T \mathbf{R} u) dt, \quad (8.9)$$

where  $\mathbf{Q}$  and  $\mathbf{R}$  are weights to trade-off states and input perturbations.

The LQ controller is designed for the system in (8.7) for a wind speed of 13 m/s. Bryson's rule is used to determine the weights:  $\mathbf{R} = 1/90^2$  and  $\mathbf{Q} = [0 \ 0 \ 0 \ 1/.03^2 \ 1/\bar{\Omega}^2]$ , which state that the blade pitch is allowed to vary by up to 90 degrees, while the platform rotational velocity is allowed to vary by up to 0.03 rad/s and the rotor speed is allowed to vary by up to  $\bar{\Omega} = 12.1$  RPM.

In Fig. 8.3, the damping of the platform pitch is presented with and without the platform controller. The sudden dip in damping at 11.4 m/s is caused by the activation of the blade pitch controller. The platform controller is activated in the same region as the onshore controller, that is, above the rated wind speeds ( $v > 11.4$  m/s). The response of the linearized onshore controller shows that the platform rotation stabilizes beyond 14 m/s. However, simulations using the nonlinear controller show that stability occur beyond 20 m/s. The mismatch is most likely caused by insufficient linearization of the gain-scheduled onshore controller.

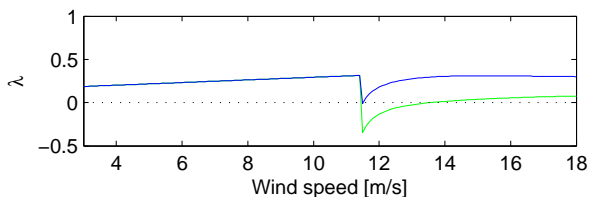


Figure 8.3: Comparison of damping ratio on platform rotation where green is the onshore controller and blue is the onshore controller with the platform controller.

The tuning of the platform controller is a matter of moving the green curve in Fig. 8.3 upward until the damping at all wind speeds is positive.

## Wave Disturbance Reduction

The dynamical model of the combined system in (8.7–8.8) is extended to include the disturbance of hydrodynamic loads by

$$\dot{\tilde{x}} = (\mathbf{A} - \mathbf{BK})\tilde{x} + \mathbf{B}_d \tau_{\text{waves}}, \quad (8.10)$$

where  $\tau_{\text{waves}}$  is the wave induced load on the platform. A blade pitch signal,  $\beta_{\text{dis}}$ , is designed to reduce the wave disturbance. This signal is added to the output of the onshore controller as shown in Fig. 9.2, and the system can be presented as

$$\dot{\tilde{x}} = (\mathbf{A} - \mathbf{BK})\tilde{x} + \mathbf{B}_d \tau_{\text{waves}} + \mathbf{B}_p \tilde{\beta}_{\text{dis}}, \quad (8.11)$$

where  $\mathbf{B}_p$  translates the blade pitch to platform torque using the partial derivative of the aerodynamic thrust with respect to the blade pitch. The blade pitch signal,  $\beta_{\text{dis}}$ , is designed to reduce the wave disturbance by a factor of  $\alpha$ , thus

$$\tilde{\beta}_{\text{dis}} = -\alpha \mathbf{B}_p^{-1} \mathbf{B}_d \hat{\tau}_{\text{waves}}, \quad (8.12)$$

where  $\hat{\tau}_{\text{waves}}$  is the estimated wave disturbance.

## State Estimation Using Extended Kalman Filter

The combined platform controller and wave disturbance reduction strategy requires full state feedback. However, wind speed and wave loads can be difficult to measure. Thus we suggest an EKF for estimating all states based on three outputs, which are

$$y = [ x_p \quad \theta_p \quad \omega ]^T. \quad (8.13)$$

The wind speed and wave loads are modeled by stochastic processes.

The wave induced loads can be presented as  $\tau_{\text{waves}} = \tau_{\text{waves1}} + \tau_{\text{waves2}}$  which are, respectively, the wave frequency dependent loads and the slowly varying drift loads. In [10], an empiric frequency dependent spectrum of the waves was presented as

$$S(\omega) = A\omega^{-5} e^{-B\omega^{-4}}, \quad (8.14)$$

where  $A = 4\pi^3 H_s^2 / (0.710T_0)^4$ ,  $B = 16\pi^3 / (0.710T_0)^4$ , the average wave frequency is  $\omega_0 = 2\pi/T_0$ , the significant wave height is  $H_s = 2.06v_d^2/g^2$ ,  $v_d$  is the developed sea wind speed, and  $g$  is the acceleration due to gravity. This spectrum is the modified Pierson–Moskowitz spectrum. Assuming the spectrum is constant, a linear stochastic model can be used to describe the combined wave induced loads by

$$\dot{\mathbf{x}}_w = \mathbf{A}_w \mathbf{x}_w + \mathbf{B}_w [w_1 \ w_2]^T \quad (8.15)$$

$$\tau_{\text{waves}} = \tau_{\text{waves1}} + \tau_{\text{waves2}} = \mathbf{C}_w \mathbf{x}_w, \quad (8.16)$$

where  $w_{1,2}$  are Gaussian white noise processes and

$$\mathbf{A}_w = \begin{bmatrix} 0 & 1 & 0 \\ -\omega_0^2 & -2\lambda_w \omega_0 & 0 \\ 0 & 0 & 0 \end{bmatrix} \quad (8.17)$$

$$\mathbf{B}_w = \begin{bmatrix} 0 & 0 \\ K_w & 0 \\ 0 & 1 \end{bmatrix} \quad \mathbf{C}_w = [ 0 \quad X_i(\omega_0) \quad X_i(\omega_0) ], \quad (8.18)$$

where  $X_i(\omega_0)$  is a wave frequency dependent constant which transforms the wave height to the wave induced load.

To determine the unknown parameters  $K_w$ ,  $\lambda_w$ , and  $\omega_0$ , the modified Pierson–Moskowitz spectrum is linearized and in Fig. 8.4 a comparison is shown of the linearization and the original. Depending on the purpose, constant values for  $\omega_0$  and  $\lambda_w$  are suggested in [10]. From (8.14), it is acknowledged that the modified Pierson–Moskowitz spectrum depends on the developed sea wind speed and average wave frequency, which could be estimated by the EKF. However, variations of these are not considered in this paper.

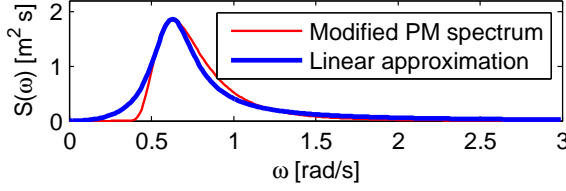


Figure 8.4: Modified Pierson–Moskowitz (PM) spectrum at  $v = 13$  m/s and  $\omega_0 = 0.8$  rad/s. The figure shows a comparison of the nonlinear and linearized spectrum related to the wave induced loads,  $\tau_{\text{waves1}}$ .

The wind speed is  $v = v_m + v_t$  where  $v_t$  is for turbulent wind and  $v_m$  is a slowly varying mean wind speed. These are modeled by

$$\dot{v}_t = \frac{-\pi v_m}{2L} v_t + w_3 \quad (8.19)$$

$$\dot{v}_m = w_4 \quad (8.20)$$

where  $t_i$  is the turbulence intensity and  $L$  is the turbulence length scale.

The EKF is designed to estimate the dynamics of the platform, drivetrain, waves, and wind, forming the state vector  $\mathbf{x}_{\text{EKF}} = [\mathbf{x}_s^T \ \omega \ \mathbf{x}_w^T \ v_t \ v_m]^T$ . The EKF is implemented as described in [7]. The total system is defined by

$$\dot{\mathbf{x}}_{\text{EKF}} = f(\mathbf{x}_{\text{EKF}}, \mathbf{u}) + \mathbf{w} \quad (8.21)$$

$$\mathbf{y} = [x_p \ \theta_p \ \omega]^T, \quad (8.22)$$

where  $\mathbf{u} = [M_g \ \beta]^T$ .

The EKF consists of a time update part and a measurement update part, [11]. The time update uses information about the dynamics of the model and covariance to estimate the process.

$$\hat{x}_k^- = A\hat{x}_{k-1} + Bu_{k-1} \quad (8.23)$$

$$P_k^- = AP_{k-1}A^T + Q \quad (8.24)$$

Based on the time update, the measurement update corrects the estimated states taking into account the uncertainties in the states and the measurements.

$$K_k = P_k^- C^T (C P_k^- C^T + R)^{-1} \quad (8.25)$$

$$\hat{x}_k = \hat{x}_k^- + K_k (z_k - C\hat{x}_k^-) \quad (8.26)$$

$$P_k = (I - K_k C) P_k^- \quad (8.27)$$

### 3 Experimental Setup

#### Simulation Environment

The wind is simulated with a mean wind speed of 13 m/s, an air density of  $1.225 \text{ kg/m}^3$ , and a turbulence intensity of 10%.

The waves are simulated as irregular waves with a JONSWAP/Pierson–Moskowitz spectrum [12]. The significant wave height of the incident waves is 3.6 meters with a wave frequency of 10 seconds. The environmental conditions are simulated at a water depth of 320 meters and a water density of  $1025 \text{ kg/m}^3$ .

The waves are aligned with the direction of the wind. In Fig. 8.5, the wind speed and wave elevation used in the simulations are presented.

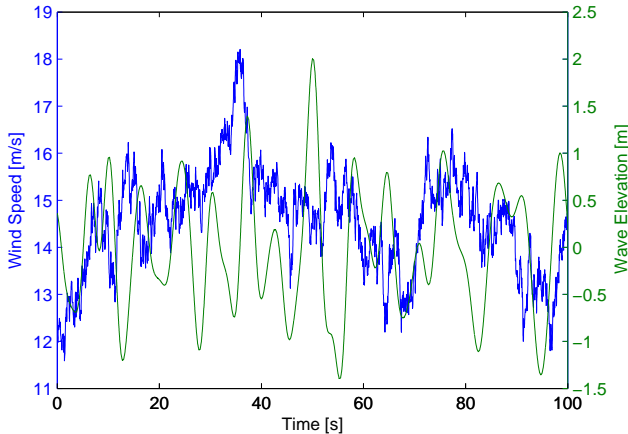


Figure 8.5: Wind speed and wave elevation used for the simulations. Wind and waves are aligned in the downwind direction.

To reveal the system damping, the simulations were initialized at time zero in such a way that the floating wind turbine is released from an upright position and shortly after is forced backward by the wind and waves.

## Software

The wind turbine is a three bladed upwind 5MW reference wind turbine specified by the NREL in [9], and implemented in the wind turbine simulation tool FAST, which is well recognized in the OC3 code benchmark, [13]. The implementation of the wind turbine installation consist of a 5 MW wind turbine mounted on a ballast-stabilized buoy, to resemble an upscaled version of the 2.3 MW Hywind wind turbine. The floating wind turbine has a rotor radius of 63 meters, a tower height of 90 meters, and six degrees of freedom.

The simulations were performed in Simulink Matlab v7.9.0 (R2009b) linked with FAST v7.00.00a-bjj and AeroDyn v13.00.00a-bjj compiled for the OC3 Hywind running Windows 7 32bit.

## 4 Results

Based on the wind and wave environment in Fig. 8.5, the response of the onshore controller is presented with and without the platform controller. Furthermore, the result of

adding wave disturbance reduction is presented. The disturbance is reduced by scaling factors of 0, 0.1, and 0.2, where a factor of 0 refers to the case of no disturbance reduction.

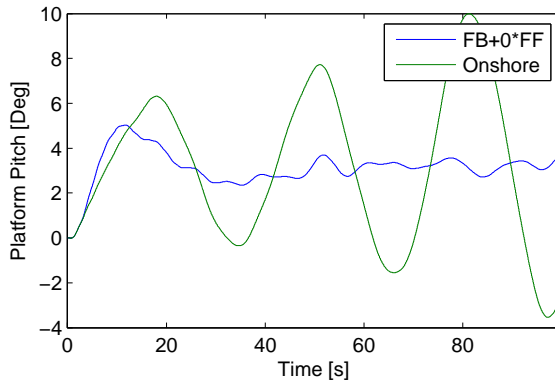


Figure 8.6: Comparing platform pitch responses using the onshore controller with platform controller (FB) without wave disturbance reduction (0\*FF) and the onshore controller (Onshore). The mean wind speed is 13 m/s.

During these simulations the EKF estimate among others wind and wave induced moments on the platform which are presented in Fig. 8.7.

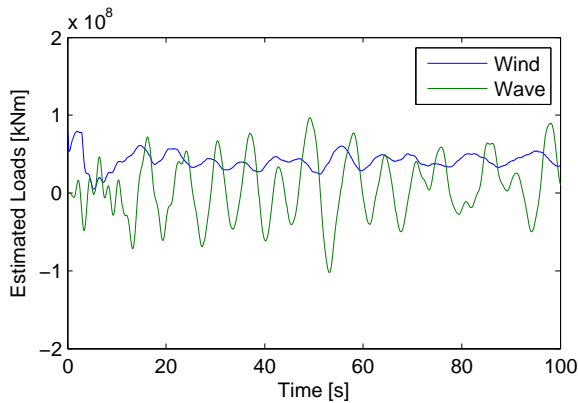


Figure 8.7: Torque induced by wind and waves, estimated during the simulation using the EKF.

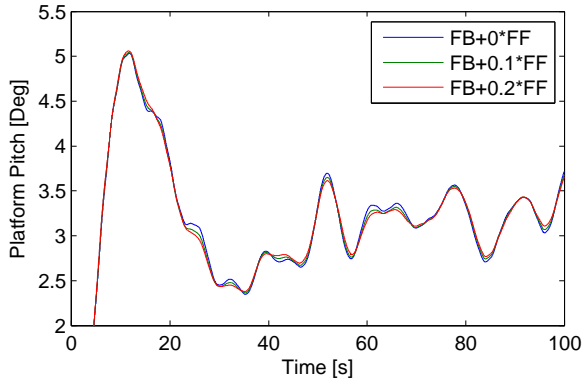


Figure 8.8: Comparing platform pitch response using onshore controller with platform controller (FB) including wave disturbance reduction (FF) scaled with factors of 0, 0.1, 0.2.

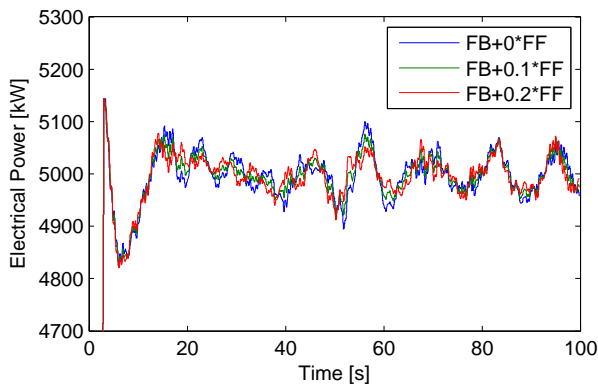


Figure 8.9: Comparing electrical power response using onshore controller with platform controller (FB) including wave disturbance reduction (FF) scaled with factors of 0, 0.1, 0.2.

## 5 Discussion

As expected from the analysis in Fig. 8.3, the response of the onshore controller shows an instability in the platform pitch in Fig. 8.6. However, when the platform controller is included, the system is stabilized. In Figs. 8.8–8.11, the disturbance reduction is added to the control system to reduce the wave disturbance. The results show that when adding disturbance reduction to the system, a reduction in power fluctuations, blade pitch activity, and platform oscillations is observed, improving the performance. Surprisingly, a reduction in actuation is achieved while improving performance in power and platform pitch. This can be explained by the fact that the disturbance reduction uses more information about the system. However, using a multi-objective control strategy is a trade-off

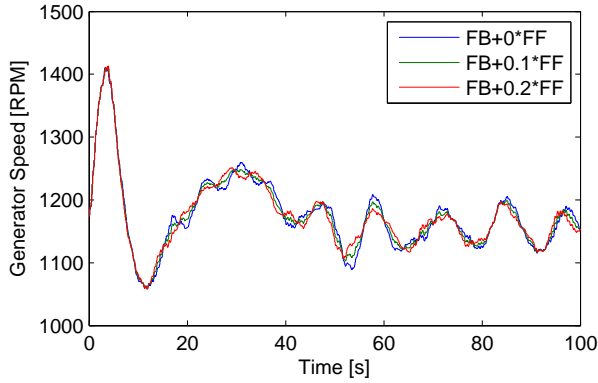


Figure 8.10: Comparing generator speed response using onshore controller with platform controller (FB) including wave disturbance reduction (FF) scaled with factors of 0, 0.1, 0.2.

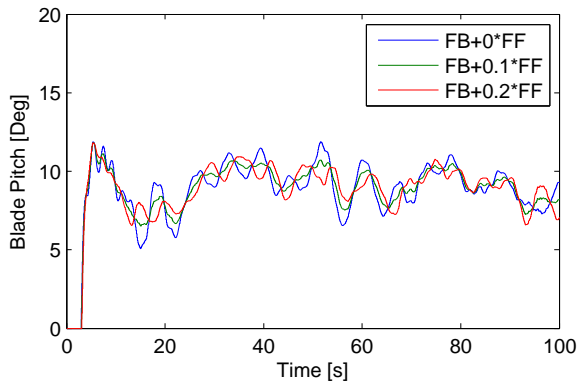


Figure 8.11: Comparing blade pitch response using onshore controller with platform controller (FB) including wave disturbance reduction (FF) scaled with factors of 0, 0.1, 0.2.

between input and state perturbations.

Instead of manipulating the blade pitch output of the onshore controller, it might be more feasible to manipulate the existing speed reference to the onshore controller. This would leave a cleaner interface between the onshore controller and the platform controller.

## 6 Conclusion

The stability problem arising when onshore control is applied to a floating wind turbines has been addressed. The system has been analyzed and a platform controller has been suggested which stabilizes the system.

To accommodate wave disturbances, the wave induced moments on the platform were estimated, and the disturbance was reduced by using contrary blade pitch actuation. An

extended Kalman filter was implemented to estimate the states, as is necessary for both the platform controller and the wave disturbance reduction. To achieve these estimates, Stochastic models for both the wind speed and the waves was implemented as a part of the filter.

Without redesigning the whole control system, the onshore controller has been preserved and an additional control loop was successfully designed to stabilize the system and reduce wave disturbance on a floating wind turbine.

## 7 Acknowledgment

This work was supported by the Norwegian Centre for Offshore Wind energy (NOR-COWE).

## References

- [1] B. Skaare, T. D. Hanson, and F. G. Nielsen, "Importance of control strategies on fatigue life of floating wind turbines," *Proceedings of 26th International Conference on Offshore Mechanics and Arctic Engineering*, 2007.
- [2] J. M. Jonkman, "Influence of control on the pitch damping of a floating wind turbine," *2008 ASME Wind Energy Symposium*, 2008.
- [3] S. Christiansen, T. Knudsen, and T. Bak, "Optimal control of a ballast-stabilized floating wind turbine," *IEEE Multi-Conference on Systems and Control*, 2011.
- [4] S. Christiansen, T. Bak, and T. Knudsen, "Damping wind and wave loads on a floating wind turbine," *IEEE Transactions on Control Systems Technology – submitted*, 2012.
- [5] —, "Minimum thrust load control for floating wind turbine," *IEEE Multi-Conference on Systems and Control*, 2012.
- [6] H. Namik and K. Stol, "Disturbance accommodating control of floating offshore wind turbines," *Proc. AIAA/ASME Wind Energy Symp.*, 2009.
- [7] T. Knudsen, M. Soltani, and T. Bak, "Prediction models for wind speed at turbine locations in a wind farm," *Wind Energy*, vol. 14, pp. 877–894, 2011, published online in Wiley Online Library (wileyonlinelibrary.com). DOI: 10.1002/we.491.
- [8] J. Jonkman, "Definition of the floating system for phase iv of oc3," National Renewable Energy Laboratory, Tech. Rep., 2010.
- [9] J. Jonkman, S. Butterfield, W. Musial, and G. Scott, "Definition of a 5-mw reference wind turbine for offshore system development," National Renewable Energy Laboratory, Tech. Rep. NREL/TP-500-38060, 2007.
- [10] T. I. Fossen, *Handbook of Marine Craft Hydrodynamics and Motion Control*. WILEY, 2011.



- [11] G. Welch and G. Bishop, "An introduction to the kalman filter," University of North Carolina at Chapel Hill, Tech. Rep., 2006.
- [12] J. M. Jonkman, "Dynamics modeling and loads analysis of an offshore floating wind turbine," Ph.D. dissertation, National Renewable Energy Laboratory, 2007.
- [13] P. Passon, M. Kühn, S. Butterfield, J. Jonkman, T. Camp, and T. J. Larsen, "Oc3–benchmark exercise of aero-elastic offshore wind turbine codes," *The Science of Making Torque from Wind*, 2007.

# Paper E

## **Wave Disturbance Reduction of a Floating Wind Turbine Using a Reference Model-based Predictive Control**

S. Christiansen, S. M. Tabatabaeipour, T. Bak and T. Knudsen

This paper was submitted to:  
American Control Conference 2013

Copyright ©IEEE  
*The layout has been revised*

### Abstract

Floating wind turbines are considered as a new and promising solution for reaching higher wind resources beyond the water depth restriction of monopile wind turbines. But on a floating structure, the wave-induced loads significantly increase the oscillations of the structure. Furthermore, using a controller designed for an onshore wind turbine yields instability in the fore-aft rotation. In this paper, we propose a general framework, where a reference model models the desired closed-loop behavior of the system. Model predictive control combined with a state estimator finds the optimal rotor blade pitch such that the state trajectories of the controlled system tracks the reference trajectories. The framework is demonstrated with a reference model of the desired closed-loop system undisturbed by the incident waves. This allows the wave-induced motion of the platform to be damped significantly compared to a baseline floating wind turbine controller at the cost of more pitch action.

## 1 Introduction

In the demand for cheaper energy, the development in wind energy has gone from onshore to bottom-fixed wind turbines in shallow water where wind speeds are stronger and more steady. Previously, the bottom-fixed wind turbine has been installed in water depths of up to 50 meters. However, a new and promising development in wind energy reaches deep water locations of even higher wind speeds, based on the concept of a floating wind turbine (FWT). In Fig. 9.1 a sketch of a floating wind turbine is shown. The principle components, are a platform (yellow), the tower, the nacelle and the blades.

A wind turbine installation has one simple objective: to keep the lifetime cost of energy as low as possible. This involves a trade-off between power production and turbine lifetime.

The FWT is different from the onshore wind turbine, in the sense of structural degrees of freedom (DOF's) and the presences of waves. The response of a FWT is highly affected by the relatively slow hydrodynamics, causing a low natural frequency of the fore-aft rotation of the FWT. Although conventional onshore control is designed such that it does not excite the tower oscillations, applying the conventional onshore control strategies to FWT's has been shown to impose negative damped oscillations on the fore-aft rotation of the FWT.

To resolve this, in [1], a tower damping control strategy was introduced using a wind estimator showing reduced tower oscillations at the cost of reduced power output. In [2] a detuned gain scheduled proportional integrating controller was applied. A Linear quadratic control was applied in [3], [4, 5] where the two latter included wind and wave estimation combined in a full range control strategy. In [6] a disturbance accommodating control was applied to reduce the wind disturbance. In [7] a strategy for reducing the impact of waves was presented.

Model Predictive Control (MPC) is an attractive control method because of its capability to deal with constraints and to deal with multi-variable systems [8]. MPC solves an optimal control problem over a finite horizon repeatedly. Given the current state of the system, an optimal control problem over a finite horizon is solved at each time step. The optimal input sequence is found and only the first element of the sequence is applied to the system. At the next time step, a new optimal control problem is solved based on the

new measurements from the system and the same procedure is repeated [9]. Recently, MPC is used with promising simulation results for control of non-floating wind turbines, see [10], [11], [12]. [13] uses model predictive control with the information about the future wind and a nonlinear model of the structural damages produced by repetitive loads to reduce the structural load and fatigue. In [14], the authors have used the wind prediction information obtained from a LIDAR system in a nonlinear model predictive controller to reduce fatigue loads on the tower and blades.

This paper presents a framework for specifying the desired closed-loop behaviour of the controlled system based on a control strategy including a reference model. Using model-based predictive control (MPC) the FWT is controlled to adapt to the behavior of a reference model. As an example, a reference model is presented which models the behavior of a FWT in still water without the disturbance of the waves. This allows us to reduce wave induced platform motion and loads on e.g. mooring system. The controller structure, allows other reference models, and as such is generally applicable to shaping the desired structural behavior.



Figure 9.1: Sketch of a ballast stabilized floating wind turbine.

This paper consist of a principle model presented in Section 2. In Section 2, stochastic models of wind and waves are presented. In Section 2, a strategy for reference model-based predictive control is presented. In Section 2, an extended Kalman filter (EKF) is used to estimate the unmeasured states and system matrices. In Section 2, a closed-loop reference model is presented. In Sections 4 and 5, the results are presented and discussed. In Section 6, the contributions are concluded.

## 2 Methods

### Principle Model of Floating Wind Turbine

The dynamics of a floating wind turbine depends on the structural-, aero- and hydrodynamics as described in [4]. The hydrodynamics is a function of the wave frequency and surface smoothness of the structure. The aerodynamics is a function of wind speed and the efficiency of the rotor. The wind speed is obviously uncontrollable, however, the efficiency of the rotor can be controlled by altering the blade pitch angle and/or the rotor speed.

First, the aerodynamic impact on the FWT is investigated. Let us assume, a wind turbine can be modeled as a second order dynamical system by:

$$I\ddot{q} + C\dot{q} + Kq = F_{\text{wind}} + F_{\text{waves}}, \quad (9.1)$$

where  $\dot{q} = [\dot{x}_p \ \dot{\theta}_p \ \Omega]^T$  and where  $\dot{x}_p$  is the platform translational velocity in fore-aft,  $\dot{\theta}_p$  is the platform rotational velocity in fore-aft, and  $\Omega$  is the rotor speed. Structural dynamics including the added mass of displaced water and hydrodynamic damping are defined as follows;  $I$  is the inertia,  $C$  is the damping, and  $K$  is the stiffness. The external forces from wind and waves are  $F_{\text{wind}}$  and  $F_{\text{waves}}$ , respectively.

The external forces from the waves are modeled as  $F_{\text{waves}} = [0 \ M_w \ 0]^T$ , where  $M_w$  is the induced moment by the incident wave. The external forces from the wind are  $F_{\text{wind}} = [F_t \ h_t F_t \ M_a]^T$  where  $F_t$  is the aerodynamics thrust force induced by the wind,  $h_t$  is the distance from the hub to the center of buoyancy (COB), and  $M_a$  is the aerodynamics torque. The aerodynamic loads are modeled as

$$F_t = \frac{1}{2} \rho A v_r^2 C_t(\lambda, \beta) \quad (9.2)$$

$$M_a = \frac{1}{2\Omega} \rho A v_r^3 C_p(\lambda, \beta), \quad (9.3)$$

where  $\rho$  is the density of air,  $A$  is the area swept by the rotor,  $C_t(\lambda, \beta)$  is the thrust coefficient of the rotor as a function of tip speed ratio  $\lambda = \Omega R / v_r$ , and  $\beta$  which is blade pitch angle.  $C_p(\lambda, \beta)$  is the power coefficient. The wind speed seen by the rotor can be defined as  $v_r = v - \dot{x}_p - h_t \dot{\theta}_p$ , where  $v$  is the ambient wind speed.

### Stochastic Wind and Wave Models

The wind speed is modeled as  $v = v_m + v_t$  where  $v_t$  is the turbulent wind and  $v_m$  is a slowly varying mean wind speed as described in [15]. These are modeled as

$$\dot{v}_t = \frac{-\pi v_m}{2L} v_t + w_1 \quad (9.4)$$

$$\dot{v}_m = w_2 \quad (9.5)$$

where  $L$  is the turbulence length scale and  $w_{1,2}$  are Gaussian white noise process, and  $w_{1,2} \in W(V_v)$ . The covariance of the Wiener process is modeled as

$$V_v = \begin{bmatrix} \pi v_m^3 t_i^2 / L & 0 \\ 0 & V_{v2} \end{bmatrix}, \quad (9.6)$$

where  $t_i$  is the turbulence intensity and  $V_{v2}$  is the covariance of the slow varying mean wind speed,  $v_m$ .

The wave induced loads can be presented as  $M_w = X_i(a_{w1} + a_{w2})$  where  $X_i$  is a wave frequency dependent constant which transforms the wave height into wave induced load.  $a_{w1}$  is a wave frequency dependent wave height and  $a_{w2}$  is a slowly varying drift height. In [16], an empiric modified Pierson–Moskowitz spectrum is presented. The wave spectrum can be linearized at a given wind speed and wave frequency. Assuming the spectrum is constant, a linear stochastic model can be used to describe the combined wave height by

$$\dot{a}_w = a_{w1} \quad (9.7)$$

$$\dot{a}_{w1} = -w_0^2 a_w - 2\lambda_0 \omega_0 a_{w1} + k_0 w_3 \quad (9.8)$$

$$\dot{a}_{w2} = w_4 \quad (9.9)$$

where  $w_0$ ,  $\lambda_0$  and  $k_0$  are parameters of the linearized wave spectrum concerning the wave frequency, the damping factor, and the gain, and where  $a_w$  is an internal state and  $w_{3,4} \in W(V_a)$ . The covariance of the Wiener process is modeled as

$$V_a = \begin{bmatrix} V_{a1} & 0 \\ 0 & V_{a2} \end{bmatrix}, \quad (9.10)$$

where  $V_{a1}$  is the covariance of the frequency dependent wave height,  $a_{w1}$ , and  $V_{a2}$  is the covariance of the slow varying drift height,  $a_{w2}$ .

## Reference Model–Based Predictive Control

In the search to reduce the structural oscillation induced by the incident waves, we suggest a control strategy which will counteract the wave loads using blade pitch. The blade pitch is controlled using a model predictive controller which as an example is based on a reference model of the closed–loop system without disturbance from incident waves. The reference model produces the state trajectory of the controlled undisturbed system as a reference for the MPC. Using the blade pitch, the MPC will counteract the disturbance from the waves and will try to track the closed–loop trajectory of the undisturbed reference model.

MPC is optimal, however, using a reference model of the closed–loop system does not guarantee optimal performance of the process. It only guarantees optimal performance in the sense of tracking the state trajectories of the desired closed–loop system. The controller included in the reference model is a classical PI controller, which is not an optimal design.

In figure 9.2 the general control framework is presented as a block diagram. To capture the nonlinear behavior of the systems at different operating points, at each sample time the nonlinear model is linearized at the current state. Therefore, a state estimator is implemented, since the MPC requires knowledge of the current states and the open–loop system matrices of the process. Using a reference model–based predictive control also requires a closed–loop model of the desired response of the system. A closed–loop reference model is implemented which estimates the closed–loop response three samples ahead. The overall control strategy is as follows. The state estimator estimates the current

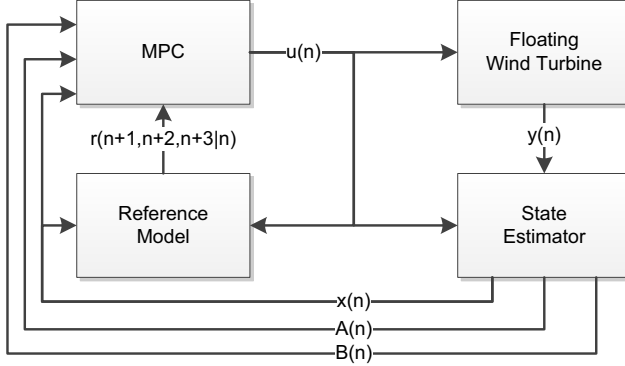


Figure 9.2: Control strategy comprising of a state estimator, a reference model and an MPC controller.

state of the system. Then, the nonlinear model of the FWT is linearized at the current operating point and the open-loop matrices of the system are calculated. These matrices are assumed to be constant in the prediction horizon. Then, the closed-loop reference model generate state trajectories of the undisturbed system as a reference for the states of the disturbed system. Given these references, the MPC will control the system by manipulating the blade pitch such that the states of the system tracks the trajectories produced by the reference model as close as possible.

In the following, the state estimator, the reference model, and the MPC will be described in details.

### Model Predictive Controller

The goal of the model predictive controller in the example discussed in this paper is to reduce the effect of incident waves such that the controlled system has the closest possible response to that of the undisturbed system without violation of constraints. Assume that the general model of the disturbed open-loop system is given as:

$$\begin{aligned} x(k+1) &= A_w x(k) + B_w u(k), \\ y(k) &= C_w x(k). \end{aligned} \quad (9.11)$$

where the disturbance is included in the state vector and the open-loop model of the undisturbed plant is given by:

$$\begin{aligned} x_r(k+1) &= A_r x_r(k) + B_r u_c(k), \\ y_r(k) &= C_r x_r(k), \end{aligned} \quad (9.12)$$

where the pre-designed controller for the undisturbed plant is described by:

$$\begin{aligned} x_c(k+1) &= A_c x_c(k) + B_c y_r(k) + E_c r(k), \\ u_c(k) &= C_c x_c(k) + D_c y_r(k) + F_c r(k), \end{aligned} \quad (9.13)$$

where  $r$  is an internal reference signal. Here, the controller is a classical PI which will be explained later. We assume that the states and input must be bounded in a given compact



polyhedral set given respectively by  $\mathcal{X}$  and  $\mathcal{U}$ . Then, the model predictive controller solves the following optimization problem at each step:

$$\min_{\{u(k), \dots, u(k+T-1)\}} \sum_{k=k_0}^T \|x(k) - x_r(k)\|_Q^2 + \|u(k)\|_R^2 \quad (9.14)$$

$$s.t. \begin{cases} x(k_0) = x_0 \\ x_r(k_0) = x_{r0} \\ x(k+1) = A_w x(k) + B_w u(k), \\ y(k) = C_w x(k), \\ x_r(k+1) = A_r x_r(k) + B_r u_c(k), \\ y_r(k) = C_r x_r(k), \\ x_c(k+1) = A_c x_c(k) + B_c y_r(k) + E_c r(k), \\ u_c(k) = C_c x_c(k) + D_c y_r(k) + F_c r(k), \\ x(k) \in \mathcal{X}, \\ u(k) \in \mathcal{U}, \\ k = k_0, \dots, k_0 + T, \end{cases} \quad (9.15)$$

and finds the input sequence  $\{u(k), \dots, u(k+T-1)\}$ . The first element of the sequence i.e  $u(k)$  is applied to the system and the whole procedure is repeated in the next iteration. In the above optimization problem the initial state of the system as well as the initial states of the reference model are updated at each iteration using a state estimator in form of an EKF. Also, to update the matrices of the model with respect to the current states, the nonlinear system is linearized at each iteration around the current state. The system is considered as time invariant during the prediction horizon which means that these matrices are the same for the whole prediction horizon.

## State Estimation

Since the states related to the wind and waves are not always available on a wind turbine, stochastic models of wind and waves are used to estimate these states.

The system outputs which are assumed to be measured are  $y = [x_p \ \theta_p \ \Omega]^T$ , where  $x_p$  is the platform translational velocity in fore-aft,  $\theta_p$  is the platform rotational velocity in fore-aft, and  $\Omega$  is the rotor speed.

Based on the available measurements, an EKF is implemented to estimate the unmeasured states as described in [15]. The deterministic model in Eq. (9.1–9.3) and the stochastic model in Eq. (9.4–9.9) are combined in the estimator.

The output of the state estimator is a state vector and the system matrices of the linearized open-loop system at the current state.

## Reference Model

The reference model resembles the dynamics of the closed-loop system of a floating wind turbine described in Sec. 2 augmented with a baseline controller designed for a floating wind turbine as described in [17, 18].

The baseline controller consists of a blade pitch controller combined with constant generator torque. The pitch controller is a gain scheduled PI controller modeled by

$$\beta = \frac{1}{1 + \frac{\beta}{\beta_k}} PI(\omega_{\text{ref}} - \omega), \quad (9.16)$$

where  $\beta$  is the blade pitch angle,  $\beta_k$  is a constant, and  $\omega_{\text{ref}}$  is the generator speed reference. The constant generator torque is implemented by

$$M_g = P_{\text{rated}}/\omega_{\text{rated}}, \quad (9.17)$$

where  $P_{\text{rated}}$  is the rated power and  $\omega_{\text{rated}}$  is rated generator speed.

The stochastic wave model is not included in the closed-loop reference model since this is an undesired disturbance that we wish to compensate for. Thus, for the closed-loop system, the wave model in Eq. (9.7–9.9) is modeled as

$$\dot{a}_w = 0 \quad (9.18)$$

$$\dot{a}_{w1} = 0 \quad (9.19)$$

$$\dot{a}_{w2} = 0, \quad (9.20)$$

where the initial conditions are  $a_w = a_{w1} = a_{w2} = 0$ .

### 3 Experimental Setup

#### Simulation Environment

The wind is simulated with a mean wind speed of 18 m/s, an air density of 1.225 kg/m<sup>3</sup>, and a turbulence intensity of 15%.

The waves are simulated as irregular waves with a JONSWAP/Pierson–Moskowitz spectrum [19]. The significant wave height of the incident waves is 6.9 meters with a wave frequency of 7.8 seconds. The environmental conditions are simulated in waters, with a depth of 320 meters and a water density of 1025 kg/m<sup>3</sup>. The waves are aligned with the direction of the wind.

#### Model-Based Predictive Control

The parameters of the optimization problem of the MPC are chosen as follows  $R = (20\text{deg})^{-2}$  and  $\mathbf{Q} = \text{diag}([\mathbf{0}_{1 \times 3} \ \mathbf{Q}_s \ \mathbf{0}_{1 \times 2}])$ . The weighting of the structural states,  $\mathbf{Q}_s$ , are based on Bryson's rule where the initial guesses are 20% of the steady state operating points while using trail and error with respect to the integrated rotor speed. Thus we choose  $\mathbf{Q}_s = [(0.2\bar{x}_p)^{-2} \ (0.2\theta_p)^{-2} \ (0.07\Omega)^{-2} \ \mathbf{0}_{1 \times 2} \ (0.2\Omega)^{-2}]$ , where the steady state operation points are  $\bar{x}_p = 12.1\text{m}$ ,  $\theta_p = 2.55\text{deg}$  and  $\Omega = 12.1\text{RPM}$ .

#### Software

The wind turbine is a three bladed upwind 5MW reference wind turbine specified by the NREL in [18], and implemented in the wind turbine simulation tool FAST, which is well recognized in the OC3 code benchmark, [20]. The implementation of the wind

turbine installation consists of a 5 MW wind turbine mounted on a ballast-stabilized buoy, to resemble an upscaled version of the 2.3 MW Hywind wind turbine. The floating wind turbine has a rotor radius of 63 meters, a tower height of 90 meters, six degrees of platform freedom, and flexible tower, blades and drivetrain.

The simulations were performed in Simulink Matlab v7.9.0 (R2009b) linked with FAST v7.00.00a-bjj and AeroDyn v13.00.00a-bjj compiled for the OC3 Hywind running Windows 7 -32bit.

### 4 Results

The results shows the response of the FWT when applying the baseline controller and the MPC controller. In all cases the wind turbine is released from an upright position and forced backward by the wind and waves.

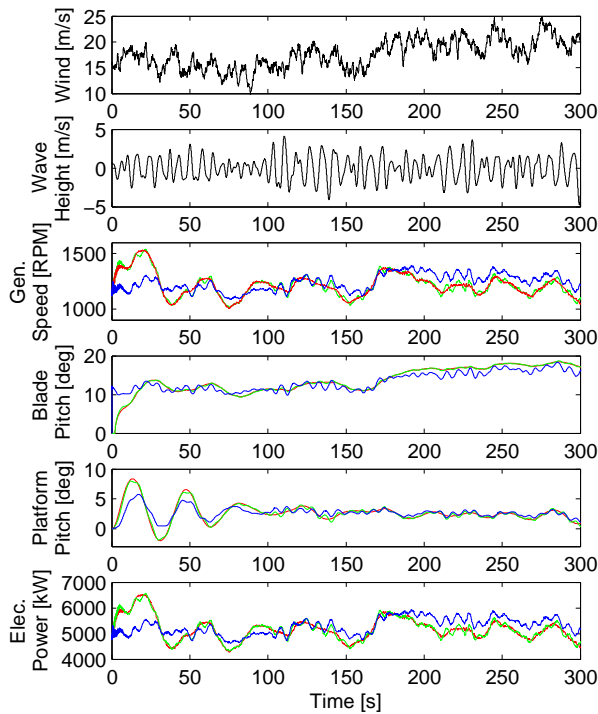


Figure 9.3: Initial comparison of performance between the baseline controller without waves (red), the baseline controller with waves (green) and the MPC controller with waves (blue).

In figure 9.3 and 9.4, both of the controlled systems are simulated for 600 seconds with incident waves. Furthermore the baseline controller is simulated without incident waves which demonstrate the optimal reference for the MPC controller.

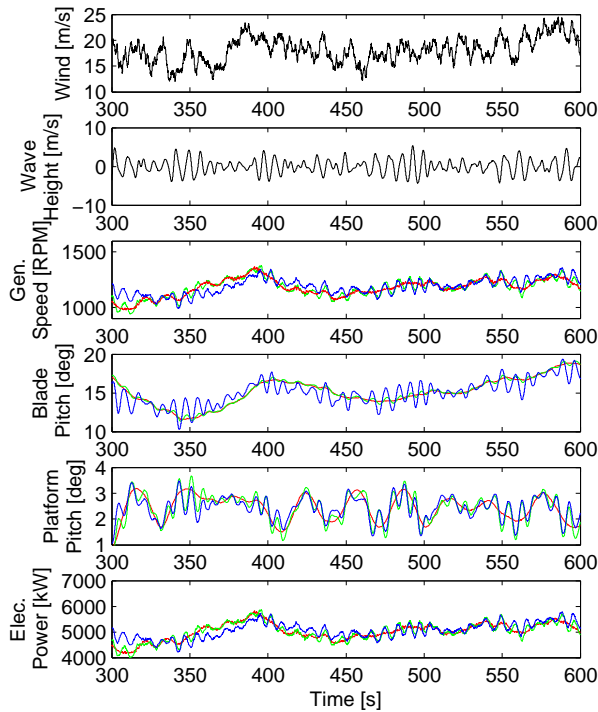


Figure 9.4: Comparison of performance between the baseline controller without waves (red), the baseline controller with waves (green) and the MPC controller with waves (blue).

The FWT is constrained by three anchors. A mooring system connects the anchors to three fairleads on the FWT. In figure 9.5, the tension on the three fairleads are presented. The fairleads are located on the platform with 120 degrees in between, where fairlead 1 is located at 180 degrees in relation to the incoming wind and waves.

In figure 9.6 a statistical analysis is presented, where the performance of the two controllers are compared. In relation to the results in figure 9.3–9.5, the analysis is performed on the time interval 100–600 seconds to neglect the initial behavior.

## 5 Discussion

When comparing the time-series performances in figure 9.3 and 9.4, the similarities in performances are noticeable. The similar behavior is caused by the almost similar objectives, except for the desire to reduce wave disturbance.

In figure 9.4, it is clear that the blade pitch of the baseline controller only correlates to the mean of the wind speed, while the blade pitch of the MPC controller correlates with both the mean wind speed and wave height. As expected, this causes an increase in blade

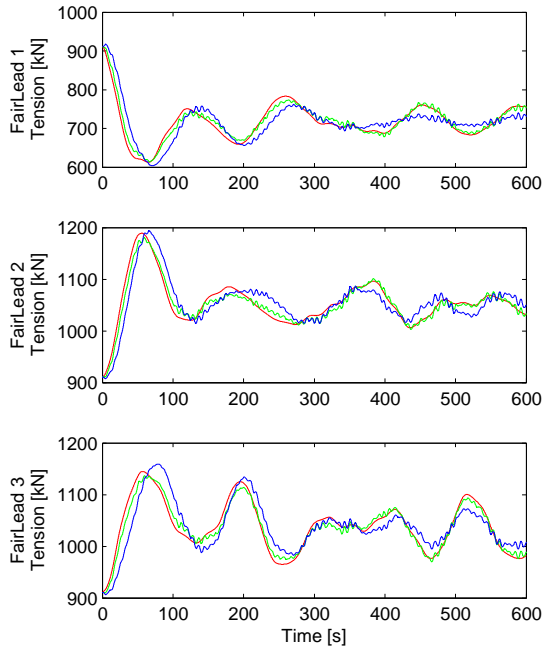


Figure 9.5: Comparison of loads on the three fairleads between the baseline controller without waves (red), the baseline controller with waves (green) and the MPC controller with waves (blue).

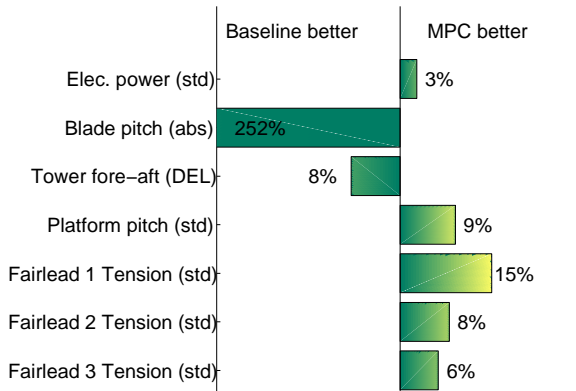


Figure 9.6: Statistical analysis of essential performance indexes.

pitch activity by the MPC controller. However, the benefit is observed as a reduction in platform pitch.

A reduction in platform pitch reduces the variations in tension on the mooring system. In figure 9.5, the tension of the three fairleads are presented. The figure shows a general reduction in load oscillations on the fairleads, where the tension of fairlead 1 is aligned with the direction of the wind and waves. This explains the reduced mean load on fairlead 1. The fairleads are connected to the anchors by the mooring lines.

In figure 9.6, the time-series are analyzed with respect to the standard deviation (std) and the distance travel by the blade pitch (abs) defines as  $\int |\dot{\beta}| dt$  and damage equivalent load (DEL). The figure shows that the MPC performs better in the power, platform pitch and fairlead tensions. As expected, the blade pitch activity has increased which explains the increase in DEL of the tower in fore-aft. In other words, the controller uses not only the blade pitch and rotor thrust to reduce the wave disturbance, but also the tower experiences higher levels of loads in the combined effort to reduce the wave disturbance.

## 6 Conclusion

A framework for reducing the wave disturbances in a FWT based on MPC combined with a reference model and a state estimator has been presented. The presented state estimator is based on a principle model of a FWT, including stochastic models for wind and waves. The reference model represents a closed-loop model of the FWT, including a baseline controller, discarding the wave disturbances. The MPC controller find the optimal control input such that the state trajectory of the FWT tracks the reference trajectory generated by the reference model. As a result, the behavior of the FWT would be close to the behavior of the system in still water without considering the wave disturbances.

As expected, an increase in the blade pitch activity is necessary to reduce the wave disturbance. Besides a slight power improvement, the results shows that oscillations on the platform pitch are effectively reduced, which result in reduced oscillations of the loadings on the fair leads. A disadvantage in the application example is the increase in tower fore-aft deflection. The generality of the proposed framework with a reference model allow such concerns to be addressed by modifying the reference model. This will of course have a cost back on the blade pitch activity or the loadings on the fairleads and as such clearly demonstrate the trade-off between pitch activity, tower deflection and load oscillations.

## 7 Acknowledgment

This work has been funded by Norwegian Centre for Offshore Wind Energy (NOR-COWE) under grant 193821/S60 from Research Council of Norway (RCN). NORCOWE is a consortium with partners from industry and science, hosted by Christian Michelsen Research.

## References

- [1] B. Skaare, T. D. Hanson, and F. G. Nielsen, "Importance of control strategies on fatigue life of floating wind turbines," *Proceedings of 26th International Conference*

- on Offshore Mechanics and Arctic Engineering*, 2007.
- [2] J. M. Jonkman, "Influence of control on the pitch damping of a floating wind turbine," *2008 ASME Wind Energy Symposium*, 2008.
  - [3] S. Christiansen, T. Knudsen, and T. Bak, "Optimal control of a ballast-stabilized floating wind turbine," *IEEE Multi-Conference on Systems and Control*, 2011.
  - [4] S. Christiansen, T. Bak, and T. Knudsen, "Damping wind and wave loads on a floating wind turbine," *IEEE Transactions on Control Systems Technology* – submitted, 2012.
  - [5] —, "Minimum thrust load control for floating wind turbine," *IEEE Multi-Conference on Systems and Control*, 2012.
  - [6] H. Namik and K. Stol, "Disturbance accommodating control of floating offshore wind turbines," *Proc. AIAA/ASME Wind Energy Symp.*, 2009.
  - [7] S. Christiansen, T. Knudsen, and T. Bak, "Extended onshore control of a floating wind turbine with wave disturbance reduction," *The Science of Making Torque from Wind* - submitted, 2012.
  - [8] D. Q. Mayne, J. B. Rawlings, C. V. Rao, and P. O. M. Scokaert, "Constrained model predictive control: stability and optimality," *Automatica*, vol. 36, pp. 789–814, 2000.
  - [9] J. Maciejowski, *Predictive control: with constraints*. Pearson education, 2002.
  - [10] L. C. Henriksen, "Model predictive control of a wind turbine," Master's thesis, Technical University of Denmark, 2007.
  - [11] K. Kumar and K. Stol, "Scheduled model predictive control of a wind turbine," in *AIAA/ASME Wind Energy Symposium*, 2009.
  - [12] A. Kober and R. King, "Model predictive control for wind turbines," in *Proceedings of European Wind Energy Conference*, 2010.
  - [13] R. Santos, "Damage mitigating control for wind turbine," Ph.D. dissertation, University of Colorado at Boulder, 2007.
  - [14] D. Schlipf, D. J. Schlipf, and M. Kühn, "Nonlinear model predictive control of wind turbines using lidar," *Wind Energy*, 2012.
  - [15] T. Knudsen, T. Bak, and M. Soltani, "Prediction models for wind speed at turbine locations in a wind farm," *Wind Energy*, 2011, submitted.
  - [16] T. I. Fossen, *Handbook of Marine Craft Hydrodynamics and Motion Control*. WILEY, 2011.
  - [17] J. Jonkman, "Definition of the floating system for phase iv of oc3," National Renewable Energy Laboratory, Tech. Rep., 2010.

- [18] J. Jonkman, S. Butterfield, W. Musial, and G. Scott, "Definition of a 5-mw reference wind turbine for offshore system development," National Renewable Energy Laboratory, Tech. Rep. NREL/TP-500-38060, 2007.
- [19] J. M. Jonkman, "Dynamics modeling and loads analysis of an offshore floating wind turbine," Ph.D. dissertation, National Renewable Energy Laboratory, 2007.
- [20] P. Passon, M. Kühn, S. Butterfield, J. Jonkman, T. Camp, and T. J. Larsen, "Oc3–benchmark exercise of aero-elastic offshore wind turbine codes," *The Science of Making Torque from Wind*, 2007.